Fermilab

TM-1075
2750.000

DESIGN REPORT FOR A CRYOSTABLE 3m DIAMETER SUPERCONDUCTING SOLENOID FOR THE FERMILAB COLLIDER DETECTOR FACILITY

R. Fast, J. Grimson, R. Kephart, E. Leung, M. Mruzek
D. Theriot, R. Wands, and R. Yamada

October 1981
(First revision, November 16, 1981)

TABLE OF CONTENTS

		PAGE
CHAPTER I.	INTRODUCTION	1
	Operational Guidelines	3
CHAPTER II.	COIL DESIGN	7
	General Features	7
	Conductor Design and Stability	7
	Electrical Insulation	13
	Conductor Joints	15
	Discharge Analysis	17
	Eddy Current Losses in Coil Bobbin and Helium Vessel	21
	Transient Field Losses in Conductor	22
	Coil Winding and Banding	22
	Axial Load Analysis	23
CHAPTER III.	YOKE DESIGN	27
	General Features	27
	End Cap Hadron Calorimeter	31
	Magnetic Field Calculations	33
	Electromagnetic Forces on Detector Components	37
	Decentering Forces on Coil	44
	Testing of Coil Without Yoke	45
	Interaction of Yoke and Coil Upon Fast Coil Discharge	46
CHAPTER IV.	CRYOSTAT DESIGN	47
	General Features and Descriptions	47
	Helium Vessel	47
	Support System	52
	Radiation Shields and Thermal Intercepts	56
	Vacuum Vessel	61
	Power Chimney	63
	Liquid Helium System	65
	Support of Central Tracking Chamber	66
CHAPTER V.	COOLING CONSIDERATIONS	69
	System Description	69
	Summary of Heat Load	69
	Cool Down and Warm Up	69
CHAPTER VI.	POWER SUPPLY AND INSTRUMENTATION	73
	Magnet Power Supply	73
	Interlock System	73
	Instrumentation	74
	Bus Circuit	74
CHAPTER VII.	CONCLUSION	77
ACKNOWLEDGMENTS		77

PAGE

APPENDIX A. SYSTEM PROPERTIES 79

APPENDIX B. MATERIAL PROPERTIES 85

APPENDIX C. COIL DISCHARGE ANALYSIS 87

APPENDIX D. EDDY CURRENT LOSSES IN HELIUM VESSEL 89

APPENDIX E. TRANSIENT FIELD LOSSES IN CONDUCTOR 95

APPENDIX F. COIL WINDING AND BANDING 101

APPENDIX G. AXIAL LOAD ANALYSIS 109

APPENDIX H. MAGNETIC FORCES ON DETECTOR COMPONENTS 111

APPENDIX I. STRESS ANALYSIS OF HELIUM VESSEL 121

APPENDIX J. MECHANICAL ANALYSIS OF SUPPORTS 139

APPENDIX K. THERMAL ANALYSIS OF RADIATION SHIELDS AND INTERCEPTS . 149

APPENDIX L. CODE DESIGN OF VACUUM VESSEL 155

APPENDIX M. DESIGN OF POWER CHIMNEY. 169

APPENDIX N. DESIGN OF LOCAL LHE STORAGE DEWAR 173

APPENDIX O. HEAT LOAD TO LHE AND LIN SYSTEMS 181

APPENDIX P. MAGNET COOLDOWN 187

APPENDIX Q. VENTING OF HELIUM VESSELS IN FAULT MODES 195

CHAPTER I. INTRODUCTION

The Fermilab Collider Detector Facility (CDF) is a large detector system designed to study $\bar{p}p$ collisions at very high center of mass energies. The central detector for the CDF* [shown in Fig. I(1)] employs a large axial magnetic field volume instrumented with a central tracking chamber composed of multiple layers of cylindrical drift chambers and a pair of intermediate tracking chambers. The purpose of this system is to determine the trajectories, sign of electric charge, and momenta of charged particles produced with polar angles between 10 and 170 degrees. The magnetic field volume required for tracking is approximately 4 m long and 3 m in diameter. To provide the desired $\Delta p_T/p_T \leq 15\%$ at 50 GeV/c using drift chambers with $\sim 200\mu$ resolution the field inside this volume should be 1.5 T. This field should be as uniform as is practical to simplify both track finding and the reconstruction of particle trajectories with the drift chambers.

Such a field can be produced by a "cylindrical current sheet" solenoid with a uniform current density of 1.2×10^6 A/m (1200 A/mm) surrounded by an iron return yoke. For practical coils and return yokes, both central electromagnetic and central hadronic calorimetry must be located outside the coil of the magnet. This geometry requires that the coil and cryostat

*"Design Report for the Fermilab Collider Detector Facility," Fermilab, Batavia, Illinois (August 1981).

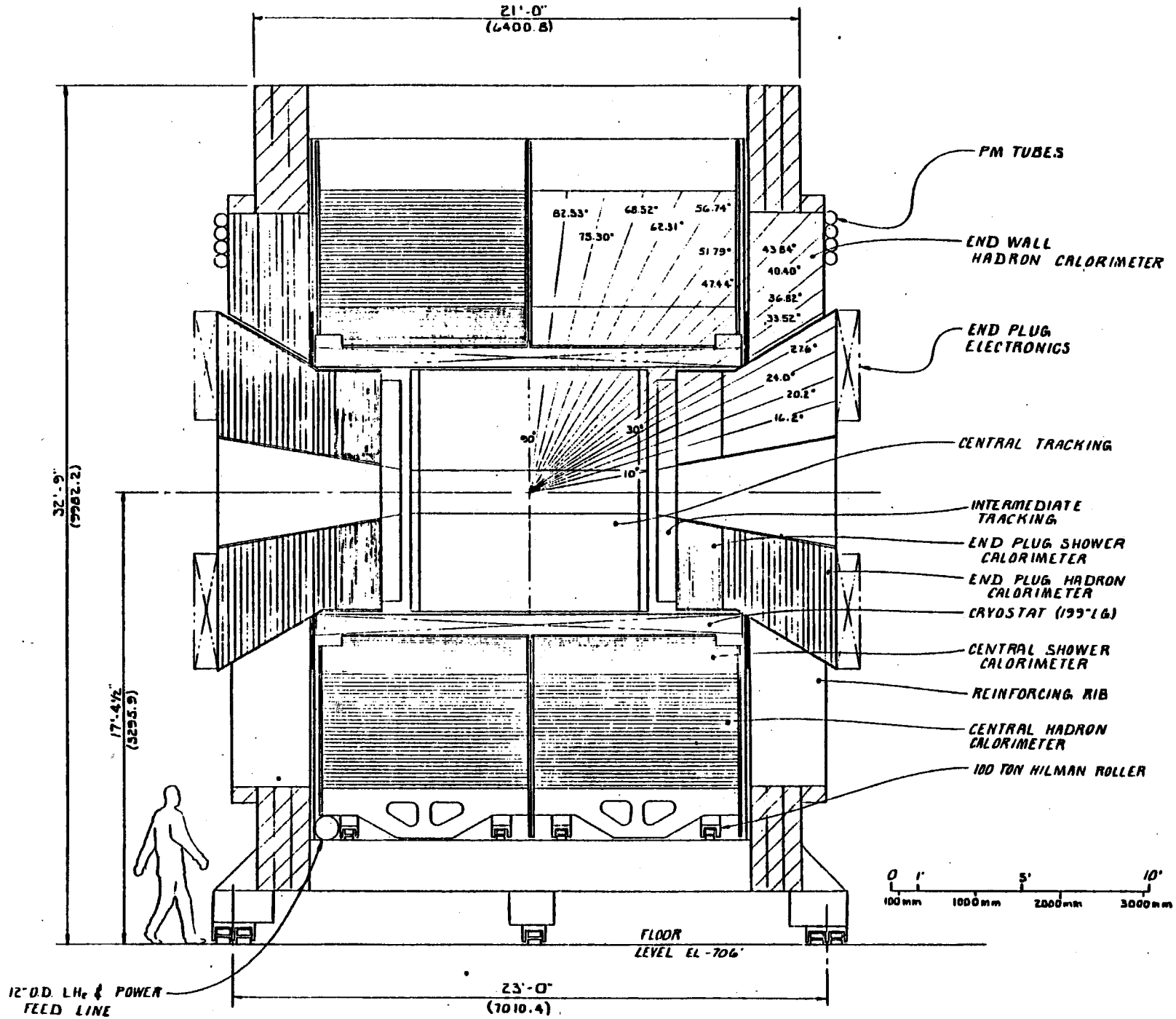

Fig. I(1). Side view of detector

be "thin" both in physical thickness and in radiation and absorption lengths. This dual requirement of high linear current density and minimal coil thickness can only be satisfied using superconducting technology. In this report we describe a design for a cryostable superconducting solenoid intended to meet the requirements of the Fermilab CDF.

The components of the magnet system are discussed in the following chapters, with a summary of parameters listed in Appendix A. Additional operational guidelines used for the design are discussed below.

Operation Guidelines. The central detector weighs 2400 short tons (2.18×10^6 kg). It must be capable of operation in either of two locations; the Collision Hall or an adjacent Assembly Hall*, with a moving time between the two areas of approximately 16 hours. The move is a straight-line translation of 98.25 ft (30 m). The superconducting magnet will be mounted in the detector and must be capable of isolated operation for up to two days (giving a factor of three time cushion to accommodate unforeseen difficulties during a move.) The detector rolls on recirculating machinery rollers using hydraulic cylinders as prime movers. The areas are shown in Fig. I(2).

Power supply and refrigeration systems must be located outside the radiation area at 743 ft elevation along the east

*W. Nestander, et al., "Colliding Beam Experimental Area at B0 Straight Section," Title 1 Design Report, Fermilab, Batavia, Illinois (August 28, 1981).

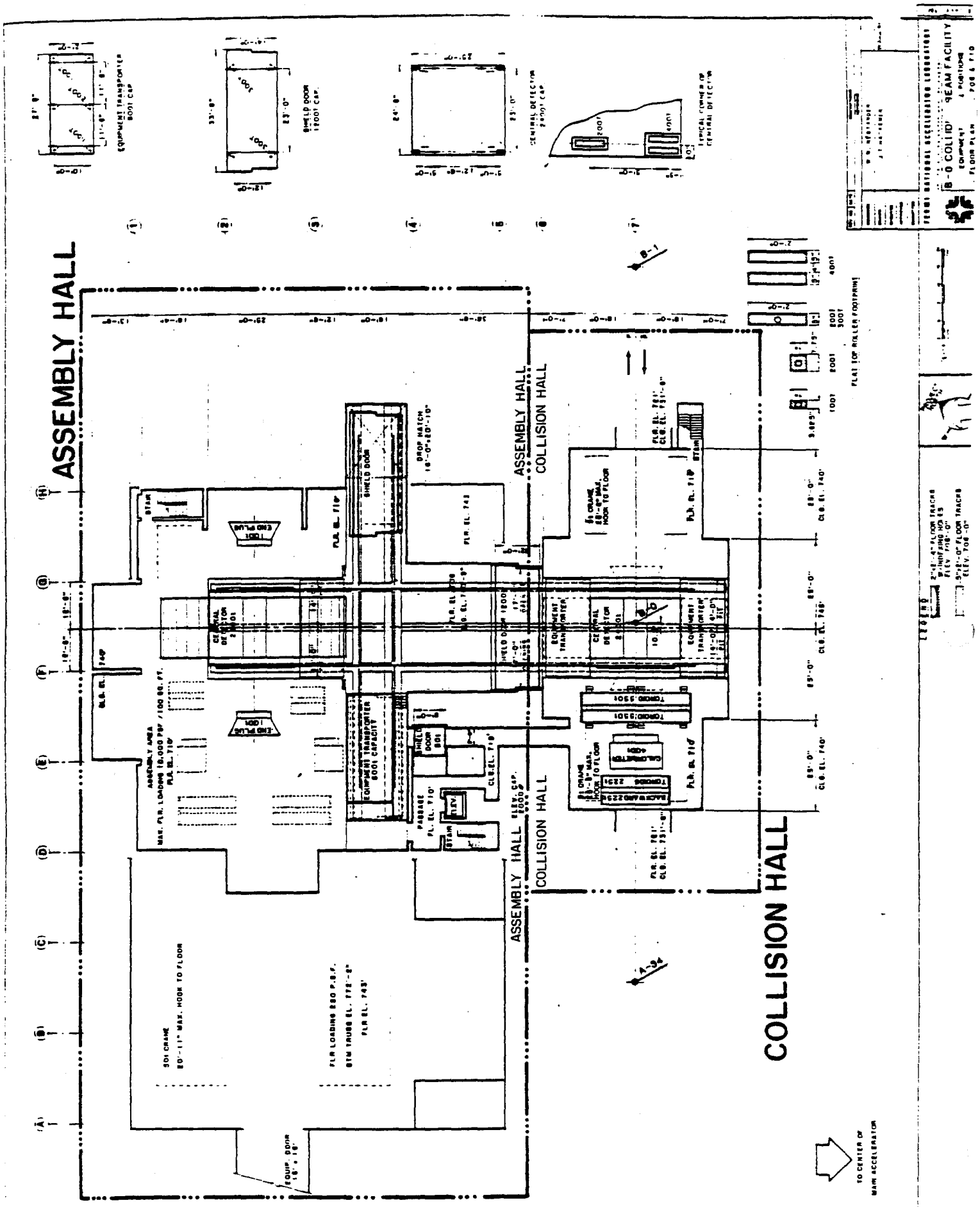

Fig. I(2). Plan view of facility

wall of the Assembly Hall. The power bus (104 ft, 31.7 m) and cryogenic transfer line (120 ft) will enter the Collision Hall via an 18 in. (457 mm) duct. Liquid nitrogen will be force fed via this line, and there will be no reserve dewar in the Collision Hall or mounted on the central detector. A separate transfer line and power bus will exist for testing and operation of the magnet in the Assembly Hall.

During normal operation, the magnet must be capable of being charged to full field or discharged in approximately 15 minutes. Under fault conditions, it must be possible to remove the large stored magnetic energy (~ 31 MJ) without damage to the magnet or detector and in a manner that insures the safety of personnel. Moreover, the magnet and all of its auxilliary cryogenic and electrical systems must meet Fermilab and DOE safety requirements.

Auxiliary equipment necessary for operation or installation of the magnet, such as dewars, dump resistors, transfer lines, etc., must be compatible with other parts of the detector. In particular, the magnet system must not interfere with the central hadron and EM shower calorimeters and their removal for service, the mounting of the central tracking chamber and its service, end plug removal, intermediate tracking chambers, end wall calorimeters, and forward and end wall muon chambers.

The coil support structure must be designed to safely handle the large electromagnetic forces which act on the coil. Finally since the coil is an essential component of the only general

purpose detector that will in the forseeable future investigate $\bar{p}p$ collisions at center-of-mass energies of 2 TeV, it is crucial that the design goals are met, and that it be as trouble free and reliable in operation as possible.

CHAPTER II. COIL DESIGN

General Features

In view of the considerations just outlined our goal was to design a solenoid coil based upon well proven superconducting technology. The coil should be simple and forgiving thus involving low risk, and able to operate reliably for long periods of time in an area with limited personnel access.

We describe below one design solution to these problems based upon a cryostable, aluminum stabilized coil cooled by a bath of liquid helium boiling at atmospheric pressure. A number of large cryostable pool boiling magnets have been built and operated successfully in recent years and numerous others are currently under construction. These include the 12 foot, 15 foot, and BEBC bubble chamber magnets, analysis magnets such as AVIS, the Multiparticle Spectrometer Magnet, and the Chicago Cyclotron Magnet (Fermilab), the Michigan State superconducting cyclotron, and plasma confinement magnets such as the Mirror Fusion Test Facility (LLNL) and the Large Coil Project (ORNL).

Conductor Design and Stability

A superconducting composite conductor in a large coil can be subjected to a sudden and local energy release such that the local conductor temperature rises well above the critical temperature. If this occurs, the superconductor will make a transition to the normal, i.e., nonsuperconducting state and the current will flow through the conductor stabilizer generating ohmic (joule) heat. The time evolution of the normal zone thus

created depends on competition between joule heating in the normal zone and heat removal from the zone by the helium environment. If sufficient heat can be removed from the normal zone, the zone will collapse and the entire conductor will return to the superconducting state. If not, the normal zone will grow in size and the coil will quench. The design must insure that in this event the coil will not be damaged by high local conductor temperatures.

"The full recovery current is the current below which the whole length of the conductor in the normal state recovers to the superconducting state simultaneously, i.e., there is recovery independent of longitudinal thermal conduction. It corresponds to what is generally referred to as Stekly criterion."* Although recovery is possible at higher currents than the full recovery current via conduction of joule heat to at least one end of the conductor which is cold and superconducting, we prefer to use the more conservative Stekly criterion. The Stekly parameter α is defined to be the ratio of the resistive heating to the available cooling power at the conductors critical current.

$$\alpha = \frac{\rho I_c^2}{h\ AP}$$

*B. Turck, Cryogenics, 20(3):146(1980). Also see: Stekley, Z.J.J., and Zar, J.L., IEEE Transaction in Nucl. Sc., NS12:367 (1965).

where

ρ = resistivity of the stabilizer including magnetoresistivity. (We use an experimental value for high purity aluminum (RRR=1200) at B = 1.75 T of $\rho = 0.7 \times 10^{-8}$ Ω-cm

I_c = critical current at 1.5 T and 4.2 K

p = average perimeter of the conductor in contact with the He bath

A = cross sectional area of the aluminum stabilizer (we neglect the contribution from the copper matrix)

h = maximum heat flux for nucleate boiling in 1.25 mm wide and 33.8 mm high vertical channels* = 0.6 W/cm^2

If we define a parameter α' such that $\alpha' = \alpha\left(\frac{I_{op}}{I_c}\right)^2$,

(where I_{op} is the operating current of the magnet), then the Stekly criterion is the requirement that $\alpha' \leq 1$.

The conductor and coil geometry we propose to satisfy this criterion is shown in Fig. II(1). The conductor is a copper/superconductor matrix co-extruded with a high purity

* Martin Wilson, Heat Transfer to Boiling He in Narrow Vertical Channel, in "Pure and Applied Cryogenics," Vol. 5, Pergamon Press, Oxford, England (1966), p. 109.

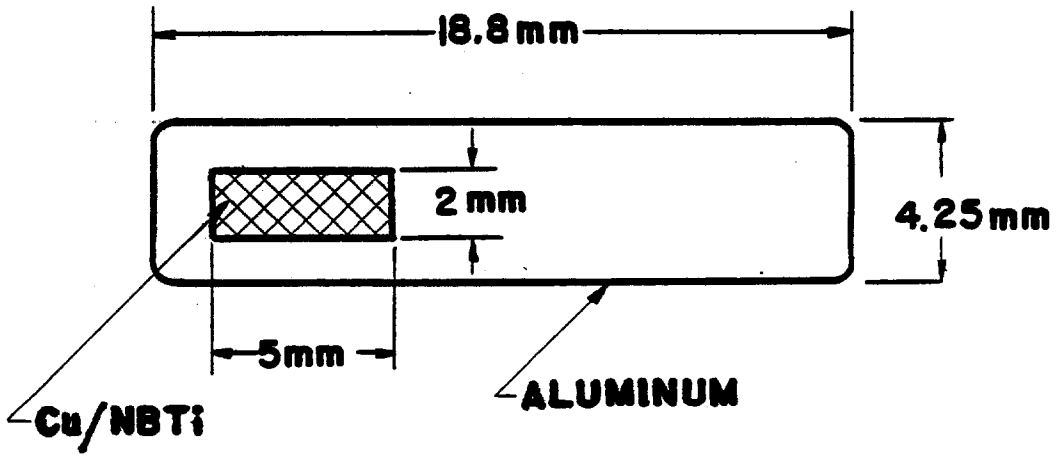

Fig. II(1).a). Proposed Cu/NbTi/Al conductor

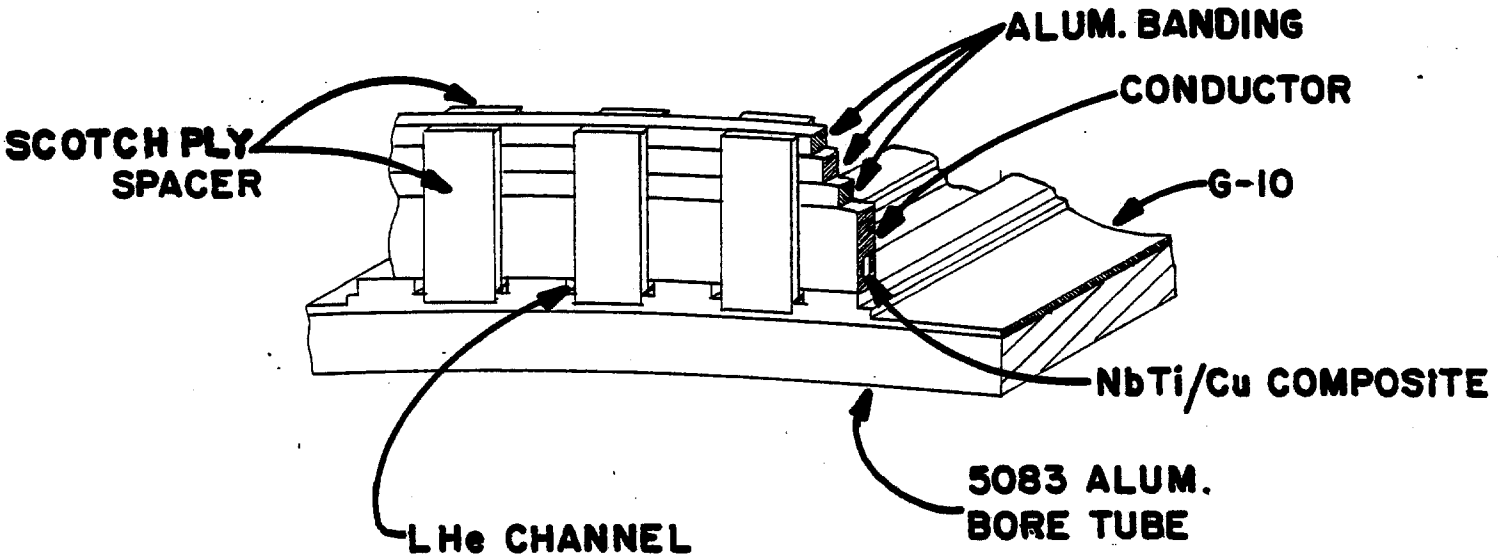

Fig. II(1).b). Proposed coil geometry

aluminum stabilizer.* The turn-to-turn insulation consists of epoxy fiberglass laminate spacers arranged so that ~50% of the conductor surface is exposed to the He bath. Similarly the thickness of these insulators was chosen to insure good heat transfer properties in the cooling channels. With these choices and selecting a desired value of α the operating current of the magnet can be optimized to minimize the required stabilizer. As a result of this procedure, we selected an operating current, I_{op}, of 6600 A, and a critical current, I_c, of 13200 A [see Fig. II(2)]. These choices correspond to

$$\alpha = \frac{(0.7 \times 10^{-8}\ \Omega\text{-cm})(13200\ \text{A})^2}{(0.6\ \text{w/cm}^2)(0.70\ \text{cm}^2)(2.3\ \text{cm})}$$

$$= 1.26$$

and $\alpha' = 1.26(6600/13200)^2 = 0.32$ thus meeting the Stekly criterion. In addition we note that B. Turck** estimates that the full recovery current I_F is bounded by the following expression:

$$\frac{-1 + \sqrt{1 + 4}}{2\alpha} < \frac{I_F}{I_c} < \frac{1}{\sqrt{\alpha}}$$

*There are several manufacturers capable of co-extruding such conductor. The numbers used for resistivity, etc., in this report was based upon test results of conductor made by Hitachi, Ltd., Japan using their EFT method (extrusion with front tension).

**B. Turck, op cit.

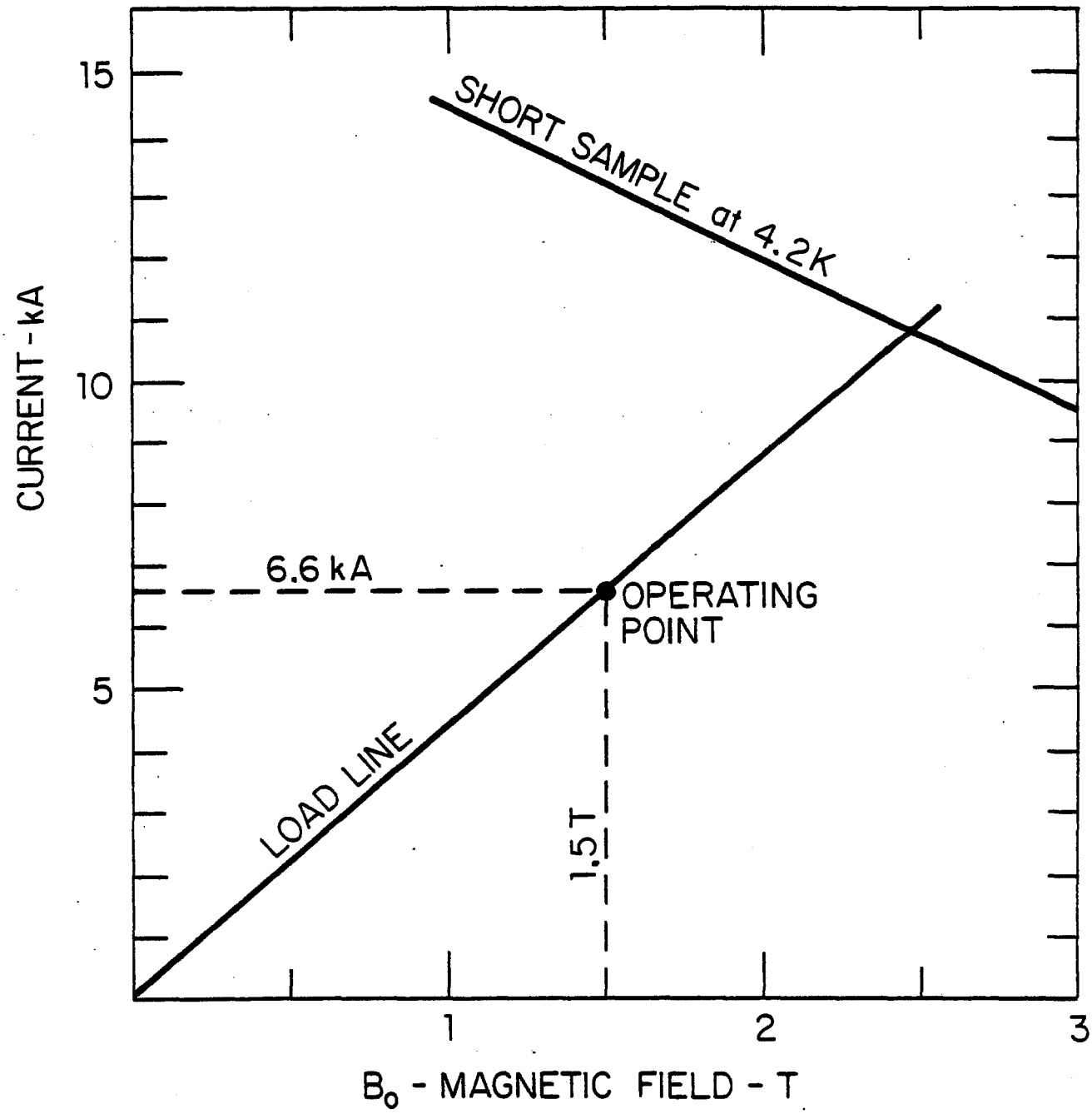

Fig. II(2). Solenoid excitation curve

For our values of I_C = 13200 A and α=1.26,

$$7630 < I_F < 11747 \text{ and so}$$

we are operating between 56% and 86% of the full recovery current.

Turck also gives an expression for the cold-end recovery current,

I_{CE}, as

$$\frac{-1 + \sqrt{1 + 2\alpha}}{\alpha} < \frac{I_{CE}}{I_C} < \frac{-1 + \sqrt{1 + 8\alpha}}{2\alpha}$$

which in our case becomes

$$9174 \text{ A} < I_{CE} < 12189 \text{ A.}$$

Even if we use the worst case film boiling heat flux of $h = 0.2\ w/cm^2$ (α= 3.78) with Turck's "accurate" equation for cold-end recovery we get I_{CE} = 8013 A and it can be seen that the coil will return to the superconducting state via cold end recovery. Thus we conclude that with this conductor and geometry, as long as the coil remains immersed in the LHe bath, it should not be possible for the coil to quench.

Electrical Insulation

There are several requirements for the coil insulation. It must provide coil to ground insulation for the voltages that exist when the magnet is charged or discharged. It must also provide both turn to turn insulation and He cooling channels

between adjacent conductors. Finally it must transmit the electromagnetic forces generated in the coil to the structures that carry those forces. We note also that the thermal contraction of insulation must be properly matched to the rest of the coil structure so that large coil motions during magnet excitation are avoided. The maximum voltage exists between ground potential and the coil during a fast (τ = 45 sec) discharge. During such a discharge, the inductive voltage generated across the coil is 202 V [during a standard discharge (τ = 300 sec) this voltage would be only 30 V.] Since the coil is cryostable, it is unlikely that large resistive sections could develop. Nevertheless, we note that even if half of one turn of the magnet somehow became normal, the maximum turn to turn voltage, as calculated from the hot spot temperature, during the 45 s magnet discharge would be ~ 4V. Moreover, if many such half turns were normal, the magnet discharge time constant would be shortened so that the sum of the turn-to-turn inductive and resistive voltages would tend to be even lower.

The electrical insulation scheme* is shown in Fig. II(1). Covering the bore tube are sheets of epoxy fiberglass (e.g., G-10CR) which have stepped axial channels machined into their surface. Epoxy fiberglass spacers 0.049" (1.25 mm) thick are inserted into these channels as the conductor is being wound to provide the turn-to-turn insulation.

*The insulation scheme described here is one of several possible schemes considered. This particular one is described for the purposes of illustration but we note that cost or ease of fabrication may favor other schemes.

This geometry provides axial, radial and circumferential paths for He gas bubbles to escape from the coil package and exposes ~ 50% of the surface of the conductor to the He bath. The minimum coil to ground insulation is 2 mm of epoxy fiberglass. The spacers which provide the turn to turn insulation are Scotchply 1002 (Isotropic). With this material the differential thermal contraction of the spacers should be 0.00386 in/in from 300 K to 4 K which is smaller than the 0.004 in/in for aluminum. This prevents the coil from loosening up when it is cooled, and is discussed in the section on axial load analysis.

Conductor Joints

Lengths of conductor are joined by overlapping the ends by 80 cm then welding along the exposed 4 mm edges of the conductor [see Fig. II(3)]. This method of joining aluminum stabilized, EFT conductors was studied carefully by Hitachi Ltd. It was found to be superior to soldering and employed in a 1 m diameter test coil. Results from their measurements* of such joints are given in TableII (1). The resistance of the joints used in the test solenoid is given in TableII (2). We propose to use similar joints in the full sized magnet. Such a joint will generate a joule heating power $P = I^2R = (6600A)^2 (6.5 \times 10^{-10} \Omega) = 0.028$ W which is negligibly small. Epoxy fiberglass wedges will be used to smooth out local discontinuities in the coil structure caused by the joints.

*Hitachi, Ltd., Engineering Sheet ES 1123-0-48, (1981) (unpublished).

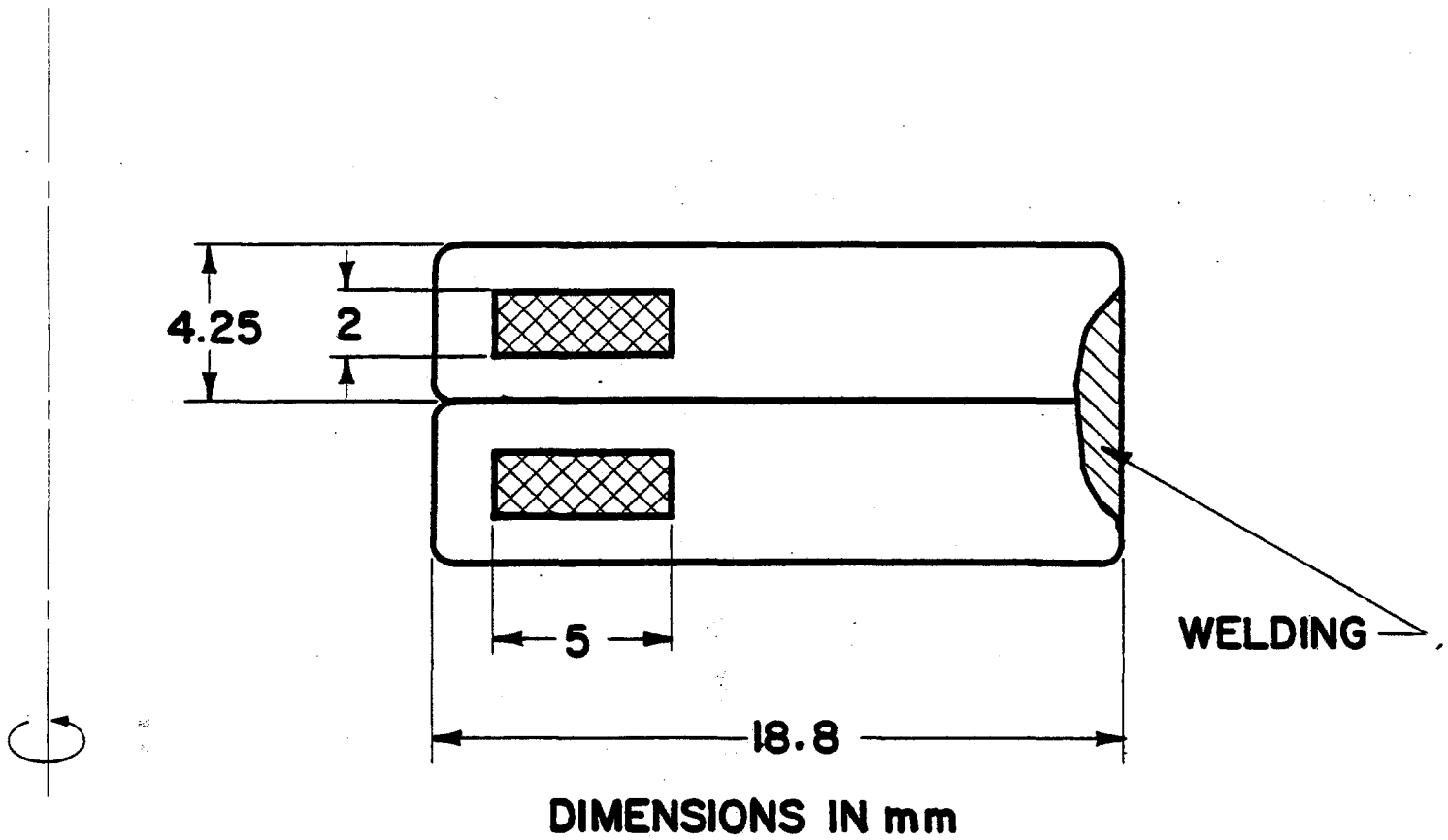

Fig. II(3). Joint in composite conductor

Table II(1). Conductor Joint Resistances

	Length	Aluminum Welding	Aluminum Soldering
Measured Resistance	50 mm	$9.3 \times 10^{-9}\Omega$	$2.4 \times 10^{-6}\ \Omega$
	100 mm	$5.0 \times 10^{-9}\Omega$	$1.6 \times 10^{-7}\ \Omega$
(at 1 T,4.2K,1 KA)	200 mm	$2.5 \times 10^{-9}\Omega$	$2.5 \times 10^{-8}\ \Omega$

Table II(2). Conductor Joints--Hitachi Test Coil

Joint method	Aluminum welding
Joint length	400 mm x 2
Resistance (4.2K)	$6.5 \times 10^{-10}\Omega$

Discharge Analysis of the CDF

The usual procedure for selecting the discharge time constant for a superconducting magnet that can quench is to choose a dump resistor that allows the stored energy of the magnet to be removed quickly enough to prevent excessive conductor temperatures, yet keeps the internal and external voltages manageable. For magnets with low stored energy this procedure is fairly easy. For larger magnets which can quench, these same procedures require large discharge voltages. In addition care must be exercised to avoid problems associated with eddy current generation in nearby structures. For large cryostable magnets which do not quench the discharge time is primarily determined by the maximum allowable coil voltage and safety in the unlikely event that a portion of the coil is some how not covered by liquid helium.

In the CDF case, eddy currents may present problems for the LN_2 shields, vacuum vessel, tracking chambers and calorimetry. Eddy current power generation in the aluminum helium vessel is an additional constraint on the speed of a superconducting discharge, since we do not wish to quench the coil upon discharge. If the coil should quench, however, the stored energy should be removed fast enough by the dump resistor to protect the coil against over temperature. We have not studied in detail the coupled quench/eddy current problem, but we have computer modeled what we consider to be the worst-case discharge scenario, the adiabatic behavior of a section of normal conductor during discharge. A computer program (described in Appendix C) was written, which enabled us to study the temperature/ discharge time relationship. Figure II(4) shows the results of the adiabatic calculations for τ = L/R time constants of 300, 60, 45, and 30 s. It is apparent that this ultra-conservative model indicates that $\tau \leq 45$ s is required. Because the eddy current power is excessively large with a τ = 45 s (The helium boil-off due to eddy currents corresponding to 176 L of liquid), we prefer not to discharge the magnet so rapidly during routine operation. Therefore,we have decided to use two dump resistors, as shown in Fig. II(5). The τ = 300 s resistors (4.6 mΩ) with switch S2 closed, will be used for routine discharging of the magnet in the superconducting state. (Total He boiloff of 26 L.) The switch S2 will be open to provide a resistance of 31 m (τ = 45 s) for a fast discharge in the very unlikely event that a large normal

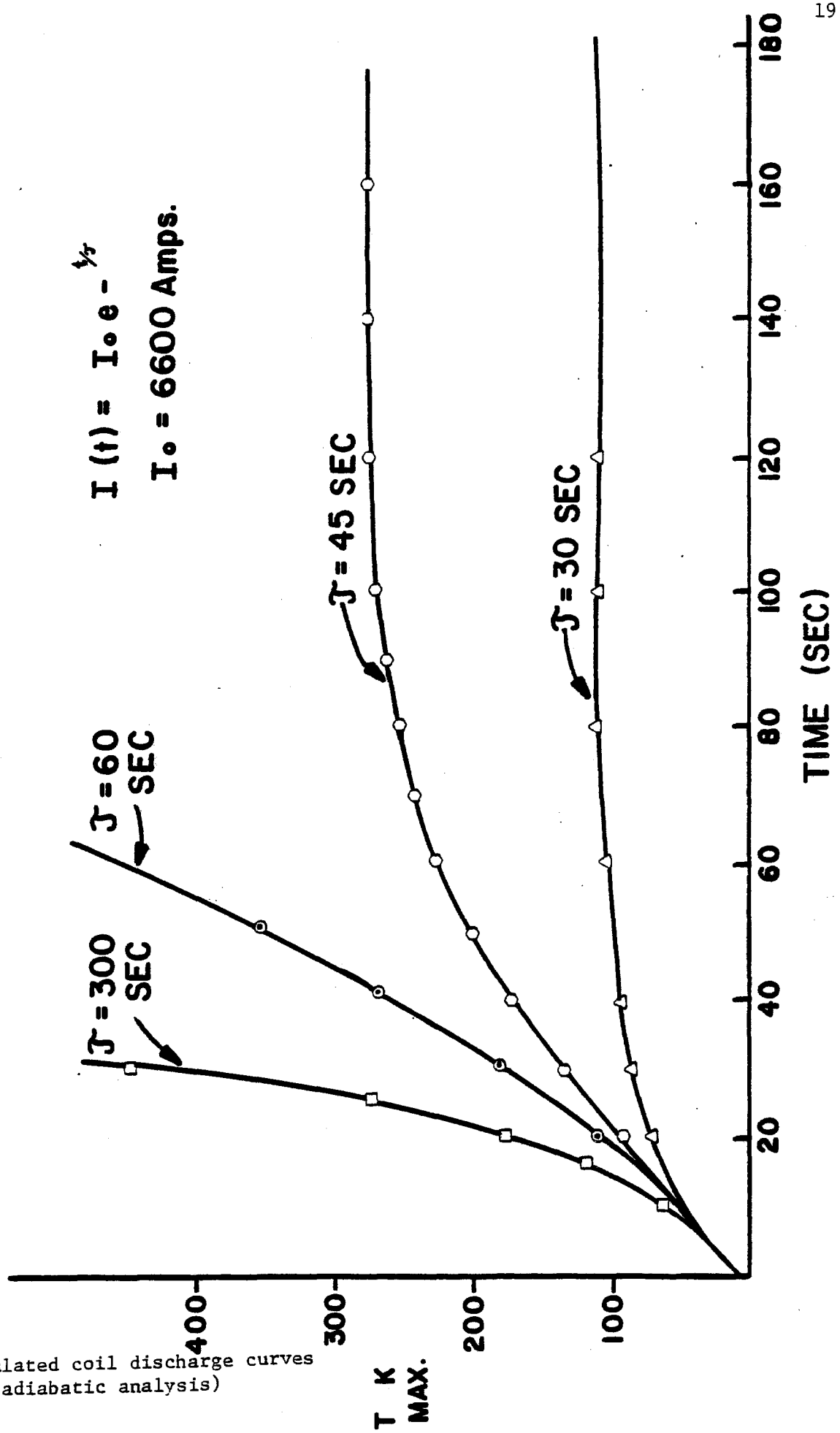

Fig. II(4). Calculated coil discharge curves (adiabatic analysis)

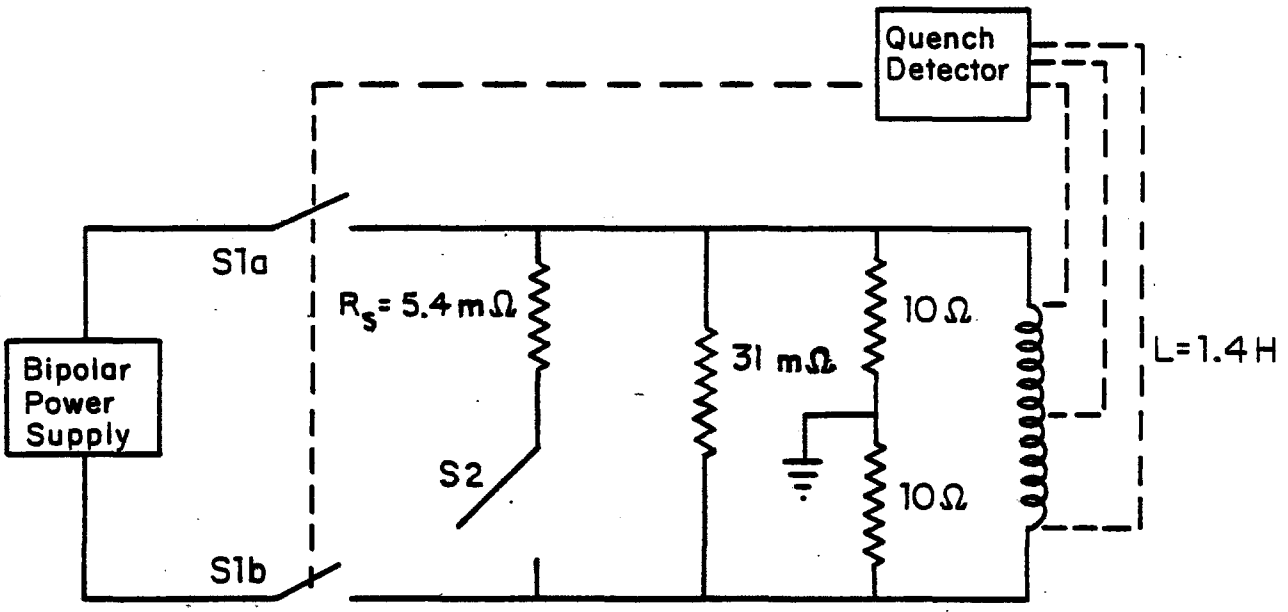

Fig. II(5). Schematic of electrical circuit

region is detected.

Eddy Current Losses in Coil Bobbin and Helium Vessel

Since the coil bobbin, which is also the helium vessel inner shell, is fabricated of aluminum, significant eddy current heating may occur in it during charge and discharge. This heating may compromise coil stability by generating large quantities of helium gas which must travel through the coil. In the extreme,this could cause the coil to quench. Calculations, found in Appendix D, show that for the proposed coil bobbin wall thicknesses of 0.625 in (15.9 mm): (1) the eddy current heating in the bobbin during a 10 minute charge is ~72 W, constant for a constant voltage charge, with a total energy loss of ~43 kJ, equivalent to ~ 17 L of LHe, and (2) the initial (maximum) eddy current power upon discharge is ~ 13.2 kW for τ = 45 s and ~300 W for τ =300 s.

The helium boil-off caused by eddy currents in both the bobbin and outer helium shell must also be considered in the design of the helium venting system to avoid over pressurizing the system. The maximum power dissipated in both bobbin and outer helium shell is ~20.0 kW and ~450 W for τ = 45 s and τ = 300 s, respectively.

As was discussed in the section on discharge analysis, a τ = 300 s discharge will be used during routine operation. It is felt that the eddy current power is sufficiently low for this value that coil stability will be unaffected and the coil will

remain superconducting during the discharge. For a τ = 45 s discharge the coil may or may not quench, but even if it does, the maximum temperature reached is acceptably small.

Transient Field Losses in Conductor

The Al/Cu/NbTi composite conductor is subject, during charge and discharge of the magnet, to a transient-field environment. The changing field causes losses in the composite conductor due to several mechanisms, the most significant of which are: (1) hysteresis losses caused by changing flux penetrating the surface of the superconducting component of the composite conductor, and (2) eddy current losses caused by eddy currents in the normal metal matrix surrounding the filaments and the normal metal outside the filament bundle. These loss mechanisms are well documented; we have used the treatment of Brechna* in our analysis. As shown in Appendix E, the hysteretic component of the losses is ~ 5 W during a 10 min charge and 44 W during a 45 s discharge. The eddy current component is 0.01 W (charge) and 1.8 W (discharge). We feel that with our bath cooled design these losses cannot have a significant impact on coil performance.

Coil Winding and Banding

Figure II(1)b is a cross section of the coil showing the bore tube, insulation, conductor and banding. The bore tube is

*H. Brechna, in "Superconducting Magnet Systems," Springer-Verlag, New York (1973), p. 250.

insulated with a 6 mm layer of fiberglass/epoxy laminate. This insulation has 4 mm deep axial grooves machined into its surface. Fiberglass epoxy laminate spacers coated with a B staged epoxy are inserted into these grooves as the conductor is wound on the insulated bore tube. With this arrangement 50% of the surface area of the conductor is exposed to the LHe bath. During this winding process the coil is compressed axially with a preload equal to the expected magnetic loading of 500 lbs/in. of circumference in a manner similar to that employed for the CELLO coil. After the conductor is wound, high strength aluminum banding is wound between the spacers on top of the conductor. The winding tension in the conductor and banding [123 lbs (550 N) and 1320 lb (5871 N) respectively] serve to keep the conductor/bore tube interface in compression even at full magnet excitation, thus preventing relative motions. Since the banding is in electrical contact with the conductor the only additional insulation required is at the banding terminations at the ends of the coil. A preliminary stress analysis of this coil geometry is presented in Appendix F.

Axial Load Analysis

In the axial direction, an electromagnetic pinch force amounting to 0.86 MN (94 short tons) in magnitude compresses the coil. To prevent bore tube/conductor relative motion, a minimum axial preload of 500 lbs/in of 4 K is required. This corresponds to a bearing stress at 1330 psi on the conductor at each spacer.

Because at the extremely low yield strength, ~ 2000 psi [see Fig. II(6)] of the very high purity aluminum in the conductor, one has to match carefully the total contraction from 300 K to 4.2 K, of the spacers to that of the aluminum so as to avoid the necessity of larger room temperature preloads or losing preload during cool down. Scotchply 1002 ($\Delta L/L$ = 0.00386) matches very well the thermal contraction of 5083 aluminum ($\Delta L/L$ = 0.0043). Thus, this is what we propose to use.

Spacing of the insulators is determined by the magnitude of the local electromagnetic force, the amount of bending stress and deflection that can be tolerated in the conductor. Calculations (Appendix G) show that a separation of 0.70" (17.8 mm) from edge to edge of the insulator/spacer would limit the maximum bending stress inside the conductor to 400 psi with a maximum deflection of $< 1 \times 10^{-5}$ inch. This appears to be a reasonable choice.

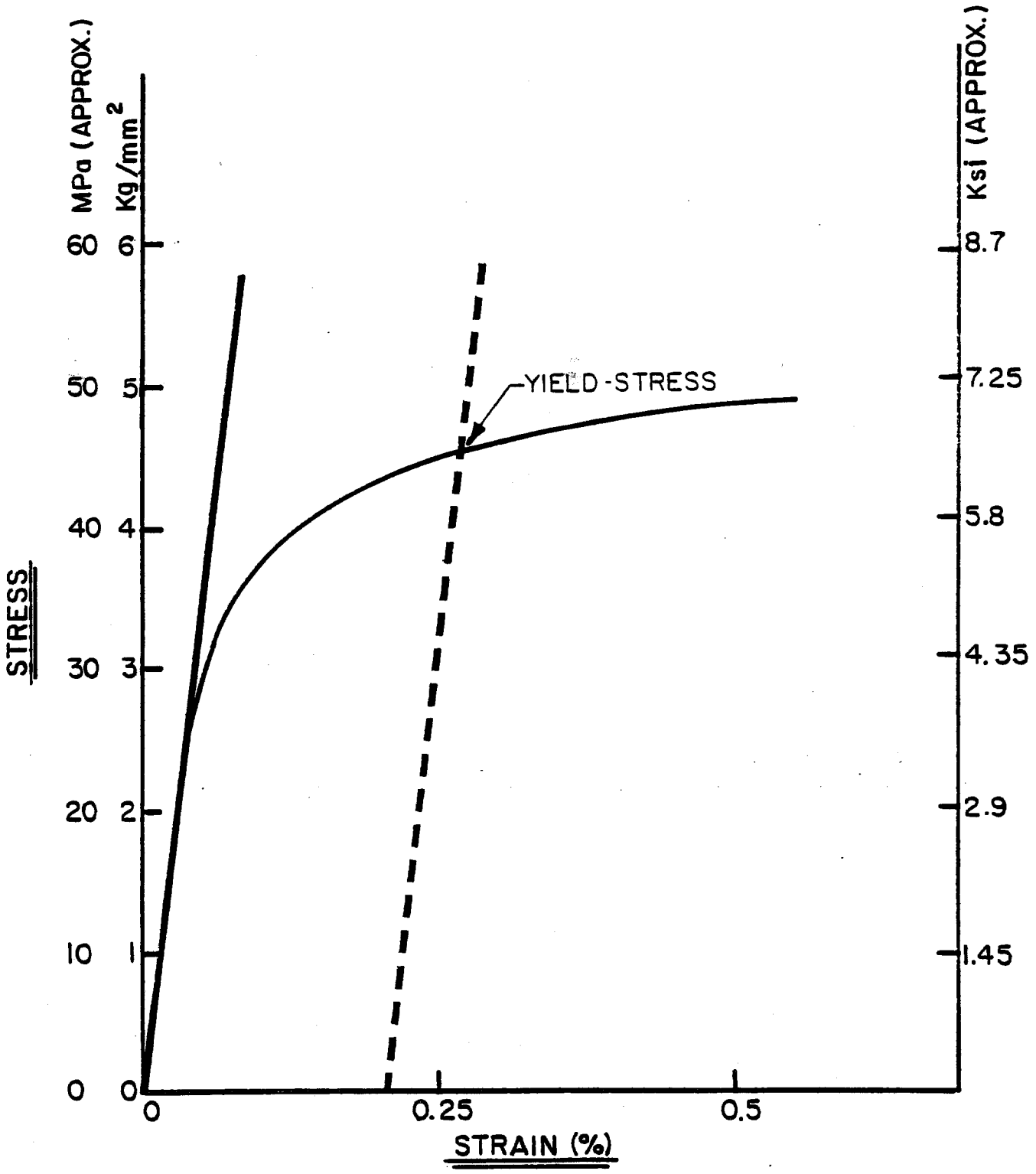

Fig. II(6). Stress-strain curve for aluminum (RRR = 1300) at 77 K

CHAPTER III. YOKE DESIGN

General Features

The function of the yoke is to provide a flux return path for the central solenoidal field. The magnet yoke also provides the structural support for most of the modules of the central detector. An isometric view of the bare yoke is shown in Fig. III(1). The basic structure is that of two end walls and four return legs. It is constructed of distressed (i. e. scrap low carbon steel plates approximately 8 in. thick, cut to size, machined on appropriate surfaces, and welded into pieces weighing approximately 50 tons each.

The two end walls are used as the structural support for the superconducting coil-cryostat package and for the calorimeter modules between 10° and 50° with respect to each beam. The edges are distressed steel plates. Extending in from the edges are 12 reinforcing ribs of 2 in. thick steel plate welded to a 2 in. thick stainless back plate that serves as support for the cryostat and for the conical end plug.

The four return legs are made of 8 in. distressed connecting the end walls. The two lower return legs act as the supporting structure for the four arches that carry the central calorimetry. The elevation of the upper surface of these lower return legs is set at 710 ft., the same as the predominate floor level in both the Collision Hall and Assembly Hall. This allows the arches to be rolled out onto the floor in the Assembly Hall or onto the transporter carts for servicing.

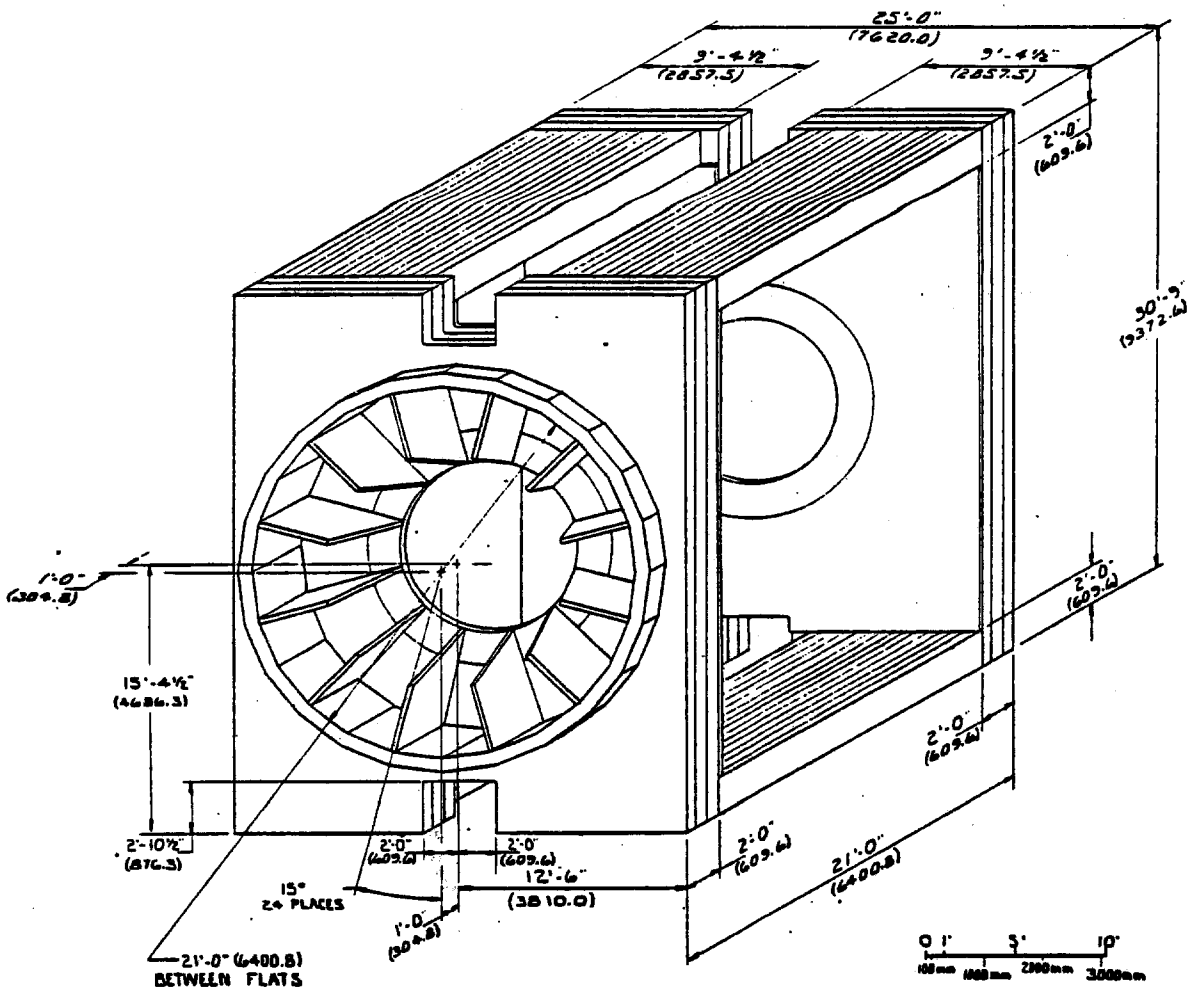

Fig. III(1). Iron yoke and flux return legs

The entire yoke will be assembled in the Assembly Hall with the help of the 50 ton crane. When the end wall and end plug calorimetry is in place, the yoke, coil, and cryostat can be tested and mapped without the central calorimetry.

The annular region between 30° and 50° is covered by end wall hadron calorimeter modules mounted between the 12 ribs of the end wall as shown in Fig. III(2). The annular region between 10° and 30° is covered by the end plug hadron calorimeter. These calorimeters are discussed in the next section. Both of these hadron, calorimeters are used in the flux return path for the central solenoidal field. Since the axial forces on these calorimeters are large (approximately 630 tons total on each end), the calorimeters are fabricated from 2 in. thick steel plates. The conical end plug rests on the 12 radial reinforcing ribs of the end wall. The axial compressive force will be carried through these ribs to the central calorimetry modules which will act as beams. When these central calorimetry modules are not in place (as in testing the coil), this function will be supplied by a set of separate beams.

Another function of the magnet yoke is to provide the support structure to roll the entire central detector between the assembly area and the collision hall. The actual rolling mechanism is provided by four 500 ton and four 300 ton Hillman rollers.

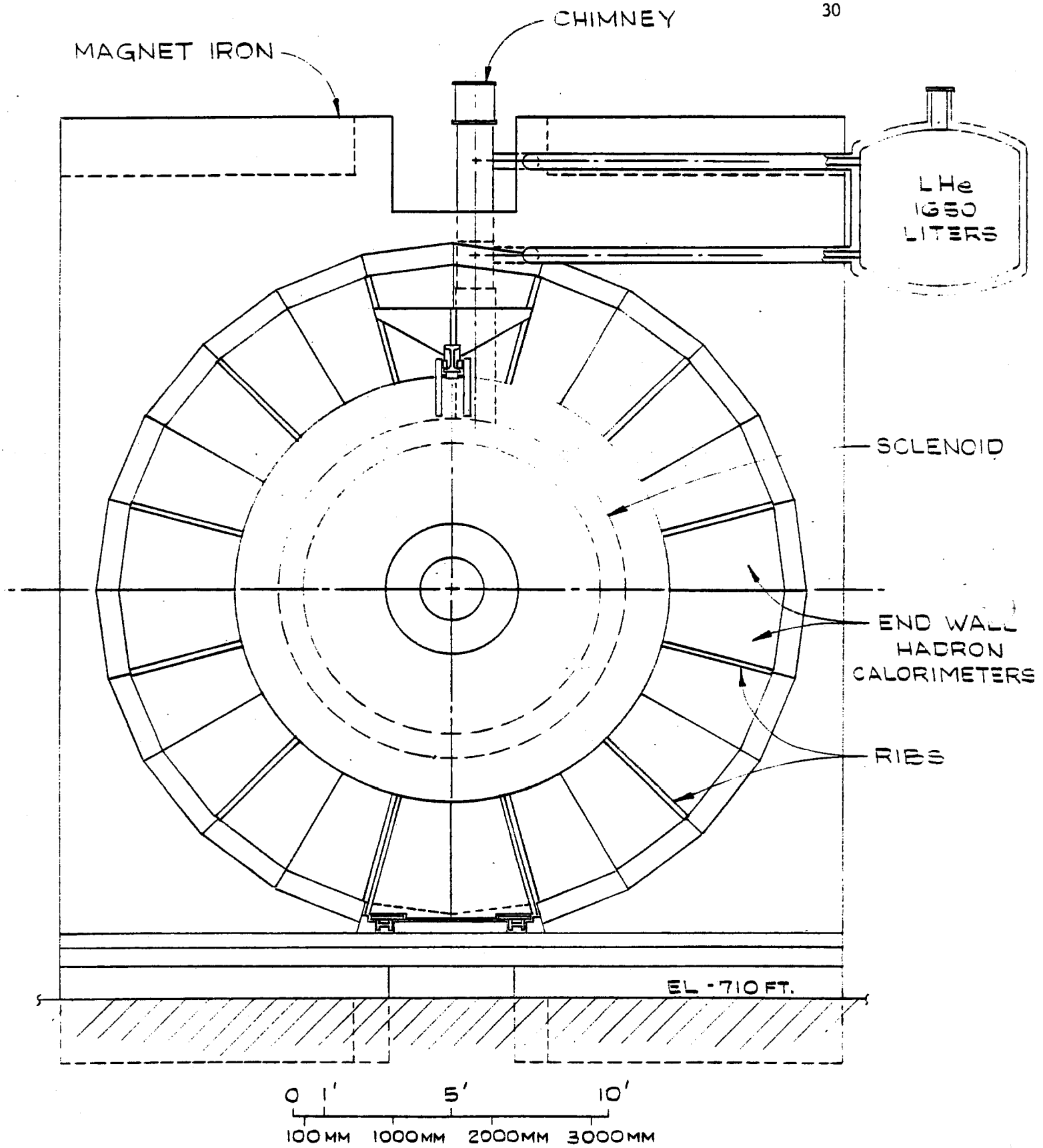

Fig. III(2). End view of yoke, end wall calorimetry, and solenoid

Access to all phototubes is from the outside of each of the central and end wall calorimetry modules. The end plug calorimetry electronics is mounted on the end wall of the end plug itself. The only parts of the central detector that must move for service access are the central arches to service the central EM position chambers and the end plugs to provide access to service the central and intermediate tracking chambers. Figure III(3) shows the end plug extended for access.

End Cap Hadron Calorimeter A side view of the detector is shown in Fig. III(3) with the end plug extended. The detector consists of a stationary hadron calorimeter and a movable end plug hadron calorimeter. Both parts are made up of a series of 2" (508 mm) steel plates separated by 3/4" (19.0 mm) air gaps. The stationary portion consists of 24 modules. The bottom two of which are mounted to the end plug and will serve as part of the structural support used in moving it to permit access to the central tracking chamber. The outer portion of the end plug is cone shaped with the outside having an included angle of 60° with its vertex at the center of the detector. The bore of the end plug also is conical in shape, uses the same vertex, and has an included angle of 20°. The four innermost plates of the end plug hadron calorimeter form a cylinder with a diameter slightly smaller than the I.D. of the bore of the coil. The end plug electromagnetic shower counter will be mounted to the innermost plate of the end plug hadron calorimeter.

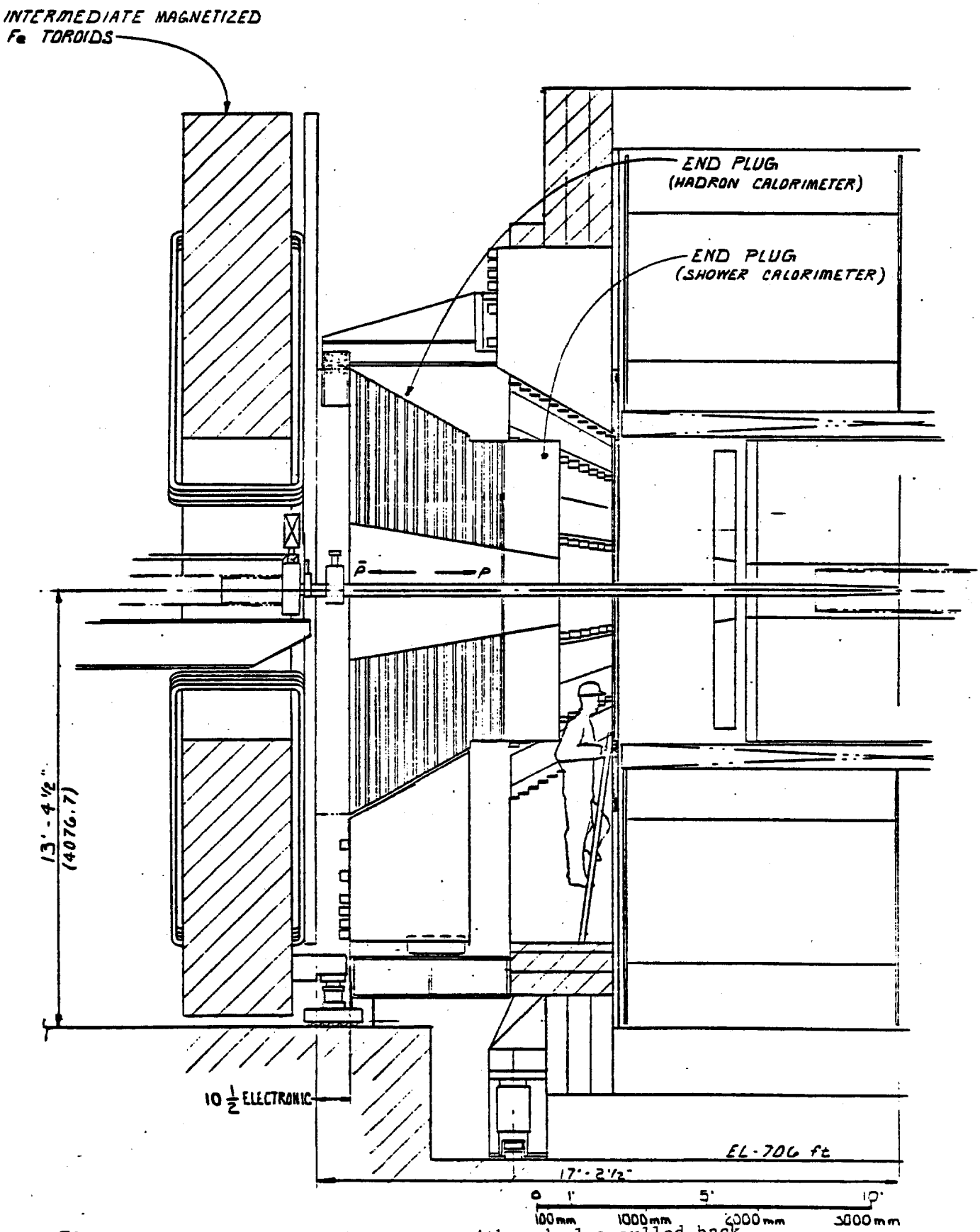

Fig. III(3). Side view of detector with end plug pulled back

Magnetic Field Calculations

Two-Dimensional Magnetic Field Calculation. A two dimensional magnetostatic program called TRIM* was use to calculate the magnetic field distribution of the CDF magnet. Its accompanying subroutine FORGY** was applied to estimate forces on the calorimetry, the yoke and the coil. These programs are useful for axisymmetrical cases, but do not actually calculate in three dimensions.

The geometry used for a preliminary calculation (Run "A12 CDF") is shown in Fig. III(4) (only a quadrant is shown). The CDF detector is not completely axisymmetric, but the main parts of the magnetic structure including the central calorimeter, end plugs, end wall, and the superconducting solenoid coil are axisymmetric. The return legs of the yoke which are far away from the central solenoid are nonaxisymmetric. For the calculation we have assumed perfect axisymmetry and have taken into account the non-symmetric yoke by using an effective width for the yoke of 10.7 inches (272 mm). As a result the calculated field around the yoke should be regarded as an average value with more accurate values to be determined in the future using three-dimensional programs.

* R.J. Lari and J.K. Wilhelm, Computer Program TRIM for Magnet Design, Argonne Internal Repot, unpublished (May 22, 1972).

**T.K. Khoe and R.J. Lari, "FORGY" A Comparison Computer Program of "TRIM" to Calculate Forces and Energy in Electromagnets, an Argonne Internal Report, unpublished (Jan. 4, 1972).

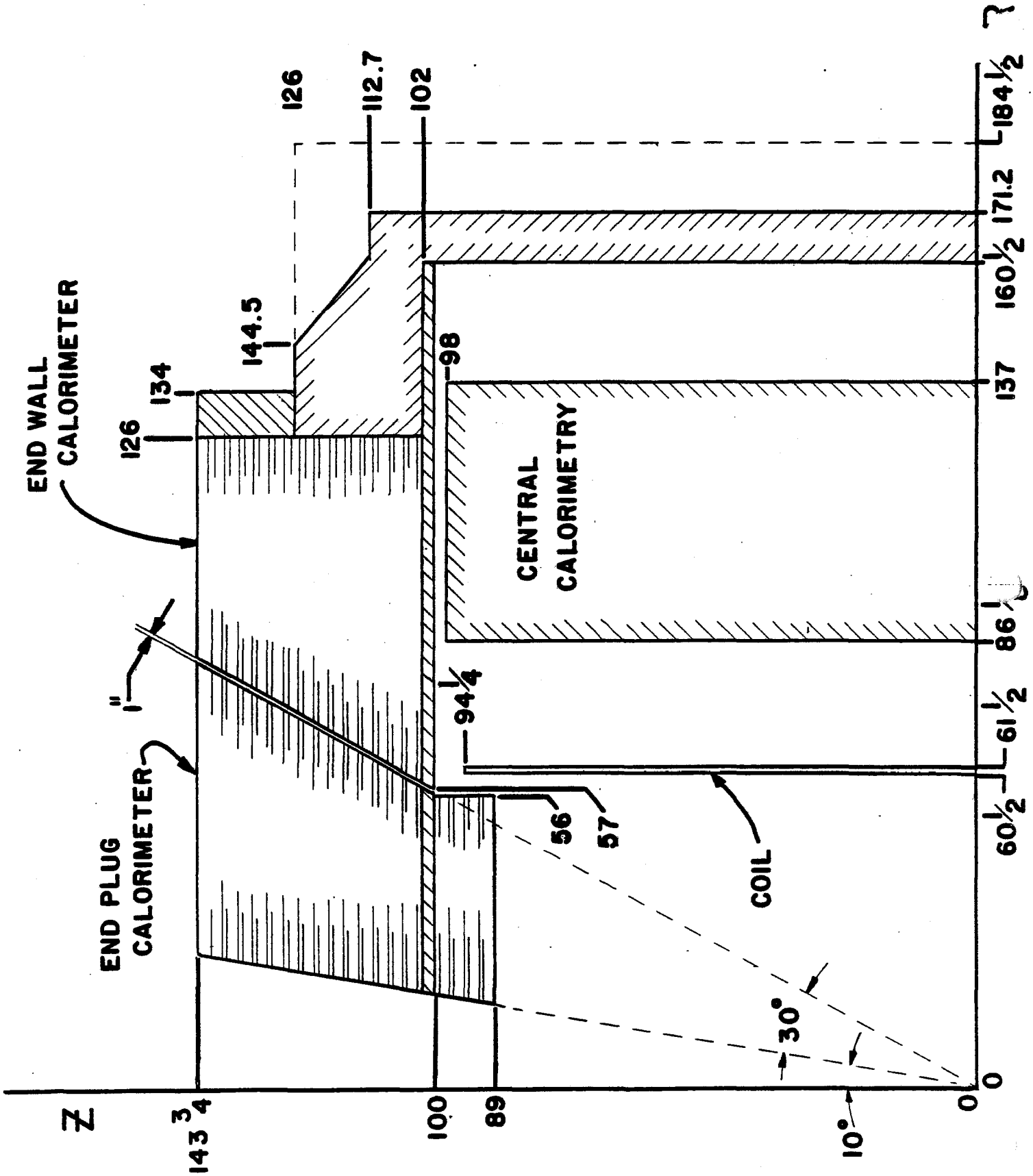

Fig. III(4). Iron and coil geometry for TRIM run "A12" and, with iron block at upper right, run "A12"

The field shape around the end of the superconducting coil depends strongly on several factors as will be discussed. To achieve the most uniform axial field distribution, it is preferable to put the end of the conductor layer as close to the yoke surface as possible. However, with a superconducting coil, we need some gap between coil and yoke for insulation and structure. To improve the axial field uniformity, several steel plates (which act also as part of the end plug hadron calorimeter) extend into the bore of the coil.

To optimize the magnetic field and reduce the resulting magnetic forces on the coil, the following major parameters can be adjusted. The numbers for the run "A12 CDF" are added in parenthesis.

1. Number of the re-entrant iron plates in the coil bore (4 plates).
2. Axial gap between the end of the superconducting conductor and the surface of the yoke (5.75 inches/146 mm).
3. Radial gap between the re-entrant iron plates and the superconducting conductor (4.5 inches/114 mm).
4. B-H curves of iron plates.

The dependence of magnetic forces on these parameters as well as their values for the proposed "best" geometry are presented in Appendix H. The flux distribution in the iron for "A12 CDF" is shown in Fig. III(5). The axial component of the magnetic field is uniform to $\leq$ 2%. The flux density at the center of the coil and in the yoke are about 1.49 T and 1.36 T,

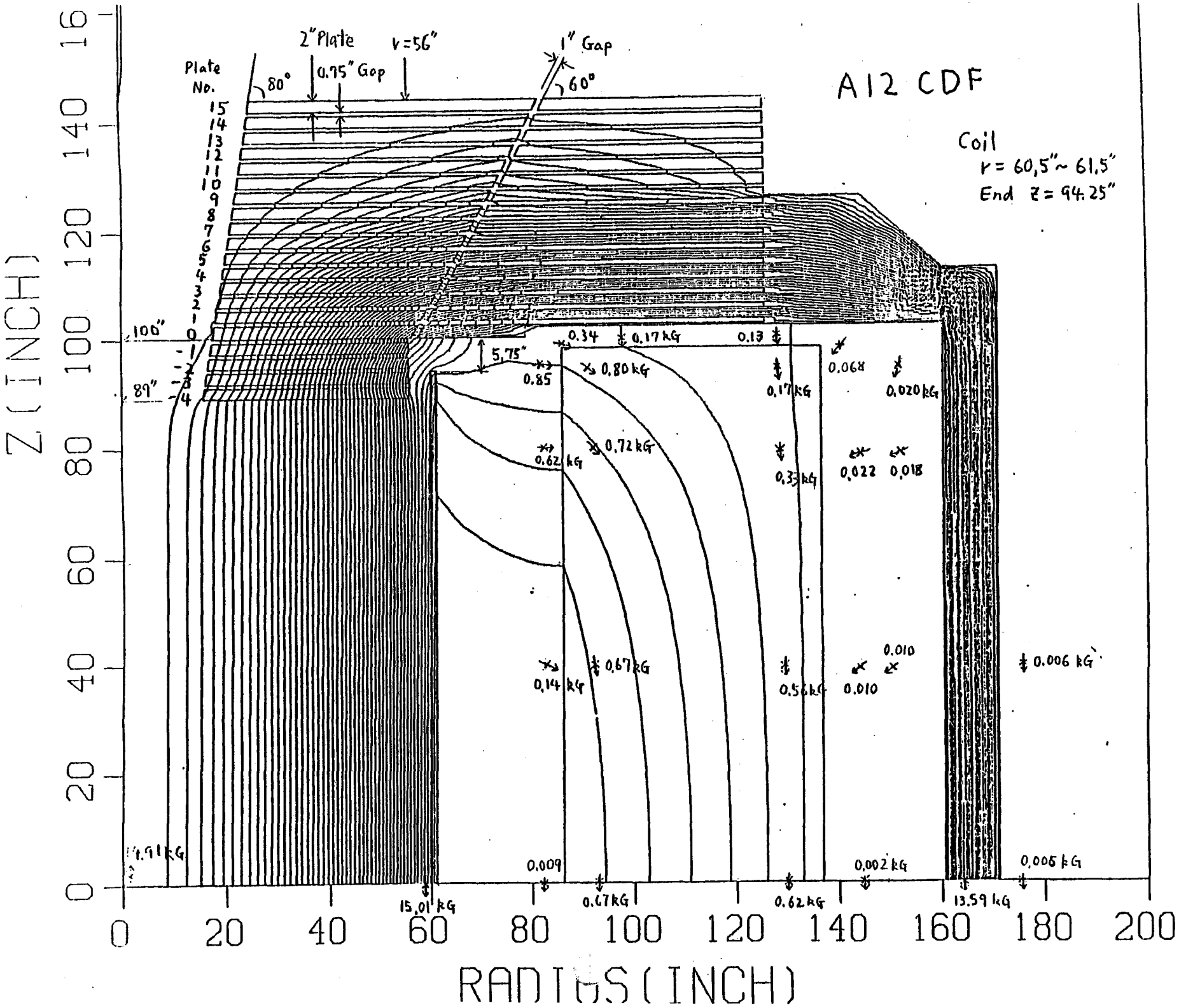

Fig III(5). Flux plot for TRIM run "A12"

respectively. The central hadron calorimeter was modeled as a solid iron block instead of a multiple-plate structure due to a shortage of regions in TRIM program. The flux density inside this block is estimated to be 0.07 T. In reality the front few plates of the multiple plate calorimeter may be driven to high flux density, outside the calorimeter should not be changed too much. The general area where the photomultipliers will be placed will be in a field of ~ (20 Gauss (2 mT) or less).

The detailed flux density in the iron around the end of the coil and in the re-entrant plates is shown for "A12 CDF" in Fig. III(6). The maximum flux density reaches 2.5 T in a limited corner area. Eventually we will measure the B-H curve of the iron to be used around the end plug, and recalculate the magnetic field using those numbers.

Electromagnetic Forces on Detector Components

There are five major components of the CDF detector which are affected by the magnetic forces. They are the superconducting solenoid coil itself, the end plug calorimeters, the end wall calorimeters, the yoke, and the central calorimeters. The forces on these components were calculated by using run "A12 CDF" and are given in Table III(1).

Some components, especially the thick iron yoke, and the aluminum disks and cylinders of the central tracking chamber and the coil cryostat, are subject to magnetic forces due to eddy currents in them when the magnet is discharged rapidly. There are also gravitational forces on each component and a force due to

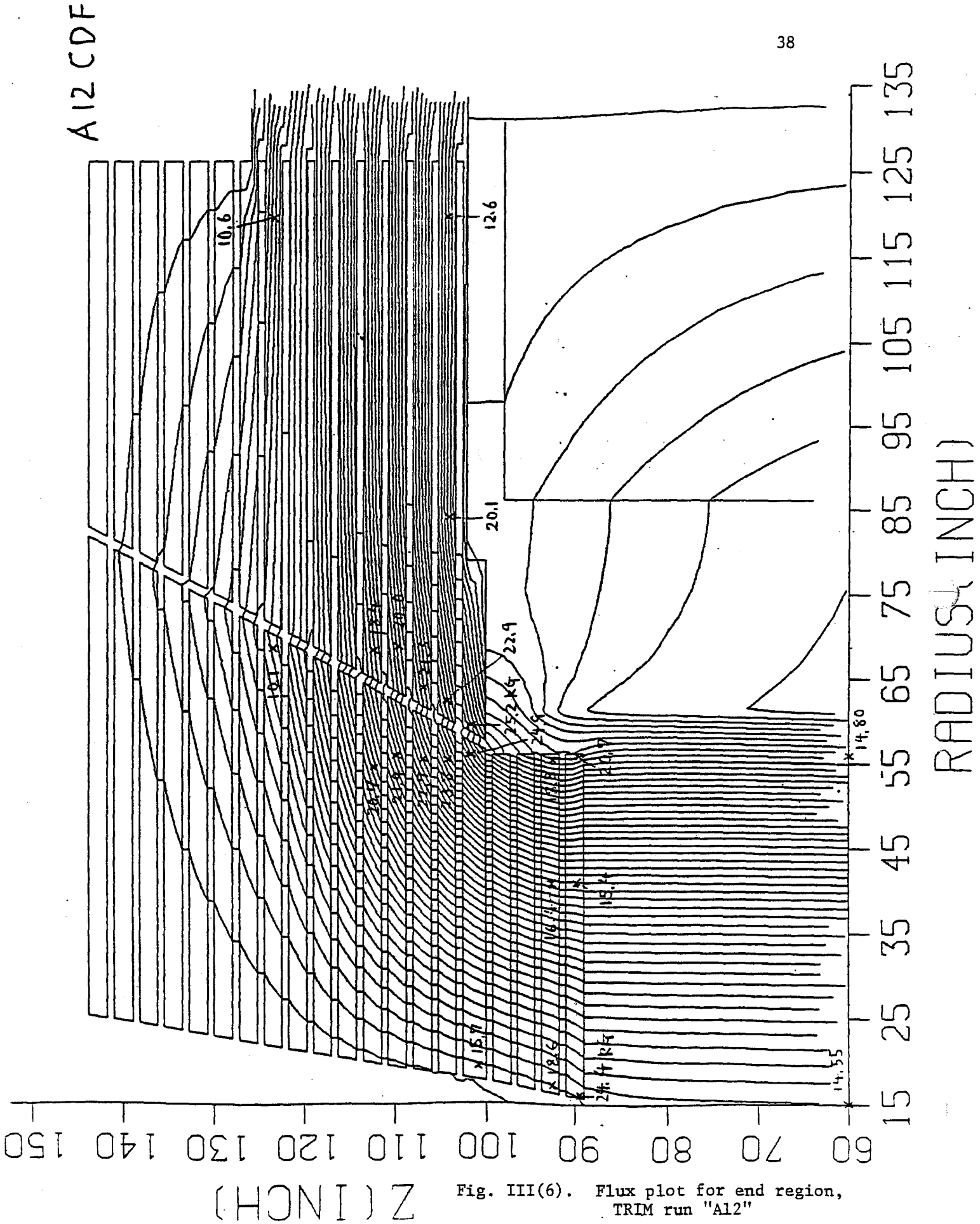

Fig. III(6). Flux plot for end region, TRIM run "A12"

Table III(1). The distribution of axial forces among the components of solenoid magnet. The major parameters are 3 m ϕ, 5 m long, 1.5 Tesla. All forces A_z are given in metric tons.

Run No.	Major Characteristics	B_o (Tesla)	R (in.)	A_z on Coil	A_z on End Plug	A_z on End Wall	A_z on Calorimeter	A_z on Back Leg	Total A_z
A12	10° opening	1,491	60.5	-123.2	-481.5	- 26.3	+ 0.5	$\sim$ + 0.2	- 630.3
A200	Air core	$\sim$1.3	60.0	-537.5					
(A200)		(normalized to 1.49)		(-706.1)					(-706.1)
CSL0126	Ideal Case No Hole	1.51	60.0	- 4.2	-678.7	$\sim$0			-678.7.

atmospheric pressure on components which are under vacuum. The superconducting coil is subject to $\vec{I} \times \vec{H}$ forces while ferromagnetic components experience the $(\vec{m}\cdot\vec{\nabla})\vec{H}$ force.

Force on Coil. The force on the coil during magnetic excitation has been studied in detail and reported elsewhere.* There are two force components. One is the radial component which corresponds to a magnetic pressure of about 130 psi (0.9 MPa, 9 kg/cm^2), and the other is an axial force component caused by the radial component of the fringing field at the end of the conductor. This axial force can be minimized by choosing the optimum iron/coil geometry. The A12 CDF case calculated has an axial force of 1.2 MN (135 short tons) toward the coil midplane. The present best design has four re-entrant plates, axial gap of 4.75 inches and radial gap of 3.5 inches. This results in an axial force of 0.86 MN (94 short tons) toward the coil midplane. The forces from both ends of the coil compress the coil but do not result in a net force on the coil if the coil is axially centered in the iron yoke.

Force on End Plug. The end plug hadron calorimeter is made of a stack of 2 inch (50.8 mm) thick washer-shaped iron plates. The end plug is pulled as a unit into the center of the coil during magnet excitation. The total inward force calculated for "A12 CDF" is 4.72 MN (530 short tons) for each end plug. The distribution of the total force on individual plates is shown in Table III(2) for "A12 CDF" case. Interestingly the innermost

*R. Yamada, Can We Test Large Solenoid Coils Safely Without Yoke, Jan. 26, 1981, Fermilab Internal Report, CDF-86, unpublished.

re-entrant plates are not being pulled inwards strongly, because they are in a more or less uniform field. The radial force on these plates are also shown in the table.

Force on End Wall. The forces on the end wall calorimeter, which is also made of two inch (50.8 mm) thick iron plates, are also listed in Table III(2). Only the first three plates are being pulled inwards, the remaining plates are rather moderately being pushed outward. The total inward force is 0.26 MN (29.1 short tons), for the total structure of the end wall calorimeter. There are structural iron side plates perpendicular to the two inch plates for the end wall calorimeter, which were not taken into account in the field calculation, and which will cause some change in the force on the end wall calorimeter.

The radial force on the end wall is also listed in the Table III(2). As is expected, its total radial force of 35.2 MN (392 short tons), matches that of the end plug.

Force on Central Calorimeter. The forces on the central calorimeter are also listed in Table III(2). The total radial inward force is 0.022 MN (2.4 short tons) corresponding to roughly 980 N (220 lbs)/15° unit. The axial force is 5 kN (1100 lbf) toward the end wall calorimeter for the 2.5 m long circular assembly. Thus, the forces on the central calorimeter can be easily handled.

Total Axial Force. The total axial force on these four components is 6.2 MN for 1.5 T. This force is the same as that for the ideal case with no hole in the end plug. Therefore, if

Table III(2). FORCES ON END PLATES OF A12 CDF

Parameters

4 re-entrant iron plates, r = 56"

2" iron plates and 3/4" gap, 10° opening

Coil r = 60.5" ∿ 61.5" Gap between coil & re-entrant plates = 4.5"

End at Z = 94.25" Gap between coil & 100" plate = 5.75"

Forces on End Plates

	End Plug		End Wall	
	FZ	FR	FZ	FR
Plate No.	Total Axial Force per Plate (N)	Total Radial Force per Plate (N)	Total Axial Force per Plate (N)	Total Radial Force per Plate (N)
Re-entrant				
-4	$+17.7 \times 10^{4}$	$+3.5 \times 10^{4}$		
-3	-13.7	+ 2.6		
-2	-28.6	+13.4		
-1	-36.9	+19.5		
Regular				
0	-86.0	+49.3	-12.2×10^{4}	-60.9×10^{4}
1	-60.6	+35.5	-27.1	-50.2
2	-47.2	+44.0	-10.7	-49.9
3	-48.1	+41.4	- 3.1	-45.2
4	-44.7	+38.1	+ 3.2	-39.5
5	-42.7	+30.9	+ 6.2	-33.7
6	-32.2	+25.4	+ 5.3	-25.4
7	-21.3	+16.5	+ 5.1	-18.0
8	-11.4	+11.4	+ 3.5	-11.4
9	- 7.1	+ 6.8	+ 3.0	- 7.3
10	- 4.0	+ 4.3	+ 0.2	- 4.1
11	- 2.3	+ 2.5	+ 0.3	- 2.6

Plate No.	End Plug FZ Total Axial Force per Plate (N)	End Plug FR Total Radial Force per Plate (N)	End Wall FZ Total Axial Force per Plate (N)	End Wall FR Total Radial Force per Plate (N)
Regular (Contd)				
12	-1.4×10^{4}	$+1.6\times10^{4}$	$+0.1\times10^{4}$	-1.5×10^{4}
13	- 0.8	+ 1.1	+ 0.2	- 1.1
14	- 0.5	+ 0.8	+ 0.2	- 0.8
15	- 0.3	+ 0.8	0.0	- 0.6
	-472.1×10^{4}	$+349.1\times10^{4}$	-25.8×10^{4}	-352.2×10^{4}

<u>Force on central calorimeter</u>

Radial Total	-2.2×10^{4}	pulling inwards
Axial Total	$+0.52\times10^{4}$	pulling out in Z

the coil has a big internal axial force, then the axial force on the end plug is correspondingly smaller, as is explained in the Appendix H.

Decentering Forces on Coil

There are two decentering forces of the solenoid, one axial and the other radial. These forces are generated when the coil is not placed perfectly symmetrical relative to the iron yoke, or when the coil is not perfectly cylindrical.

Axial Decentering Force. The axial decentering force was estimated from two computer runs with TRIM and FORGY. In one case the coil is made one inch longer toward the end wall, and in the other one inch shorter. The axial spring constant for the proposed design was calculated from these two runs. It is 15.2 MN/m (8.7×10^4 lbf/inch). The magnitude of this spring constant is almost independent of small changes in the configuration of the magnet. It is not affected by the number of the re-entrant plates, nor by the length of the coil.

Radial Decentering Force. The radial decentering force was also estimated from two computer runs. In this case the diameter of the coil was made one inch bigger for one case and one inch smaller for the other. Then the case with one inch displacement with correct radius was assumed to be composed of a half of the small coil and the matching half of the big coil.

The radial spring constant was taken as the difference between the forces acting on each half coil. The value obtained in this way for the proposed design is 12.3 MN/m (7.0×10^4

lbf/inch) toward the bigger coil (i.e., decentering). This may be an over-estimation for the following reasons: If we take into account the contribution from two two-inch segments connecting these two half coils, assuming the average field over these segments in half the central field B_o. Then the total force will cancel to zero. Therefore, the actual spring constant must be somewhere from 0 to 12.3 MN/m. We used 12.3 MN/m for design purposes, but a more correct number will eventually be determined from a three-dimensional calculations.

Testing of Coil Without Yoke

We would like to test the finished coil without the iron yoke. The force distribution in this case is quite different from that with yoke, and its detailed study is reported.* This fact must be considered both in designing the solenoid coil and when we test it without the yoke.

When the solenoid coil is excited to the design current of 6600A without the yoke, the radial field component at the ends of the coil is larger and the total compressive force on the coil becomes correspondingly stronger. The differential compressive force on each conductor diminishes toward the center of the coil as usual, but the accumulated force on the coil increases toward the midplane, where it is 5.5 MN (486 short tons) for the same current, but with a smaller central field. If we raise the current up to the point where the central field of the coil is 1.5 T, then the total axial compression is 7.2 MN

*R. Yamada, op cit.

(635 short tons). Roughly speaking the accumulated axial compression on the coil without the yoke at half the designed current still exceeds that with the yoke at full current.

If we are going to test the coil without the yoke, the coil should be designed to withstand the axial compressive force at the test current.

Interaction of Yoke and Coil Upon Fast Coil Discharge

In a previous report the possibility of a tensile force on the coil during fast coil discharge is described.* It is reasoned that in the event of a quench the field from the coil might die out faster than eddy currents would permit the field from the iron to die out, thus the coil would experience a net axial tension sometime during the decay. We must also take into account the eddy current effects in the aluminum bobbin and cryostat components. This problem should be worked out in detail.

*D. Cline, et al., "Conceptual Design of a Large, Thin Coil Superconducting Solenoid Magnet for Colliding Beam Experiments at Fermilab,"Technical Memo TM-826, Fermilab, Batavia, IL (October 25, 1978).

CHAPTER IV. CRYOSTAT DESIGN

General Features

The cryostat consists of five major components: (1) the 4.2K coil vessel, (2) the support system, (3) the radiation shields and thermal intercepts, (4) the vacuum vessel, and (5) the external helium system and power chimney. The helium vessel, radiation shields and vacuum vessel are all made of aluminum. This chapter summarizes the basic design features of the five components. The detailed design, including fabrication methods and procedures, will be done at a later time.

Helium Vessel

Requirements. The helium vessel must provide an enclosure for the superconducting coil and an annular volume for LHe. The annulus has been minimized to reduce the LHe inventory in the coil vessel to 800L. The vessel must also have the rigidity and strength to resist the electromagnetic decentering forces associated with normal operation. These forces are 8.7×10^4 lbs/in (15.2 MN/m) in the axial direction and $\lesssim 7.0 \times 10^4$ lbs/ (12.3 MN/m) in the radial direction. (See Chapter III for a discussion of these forces.) Finally, it must be designed to maintain its structural integrity under the internal pressure generated by a fault condition. The differential pressure rating was chosen to be 70 psi (0.48 MPa) as will be explained later.

Construction. The helium vessel viewed normal to a diametral plane is shown in Fig. IV(1). It consists of:

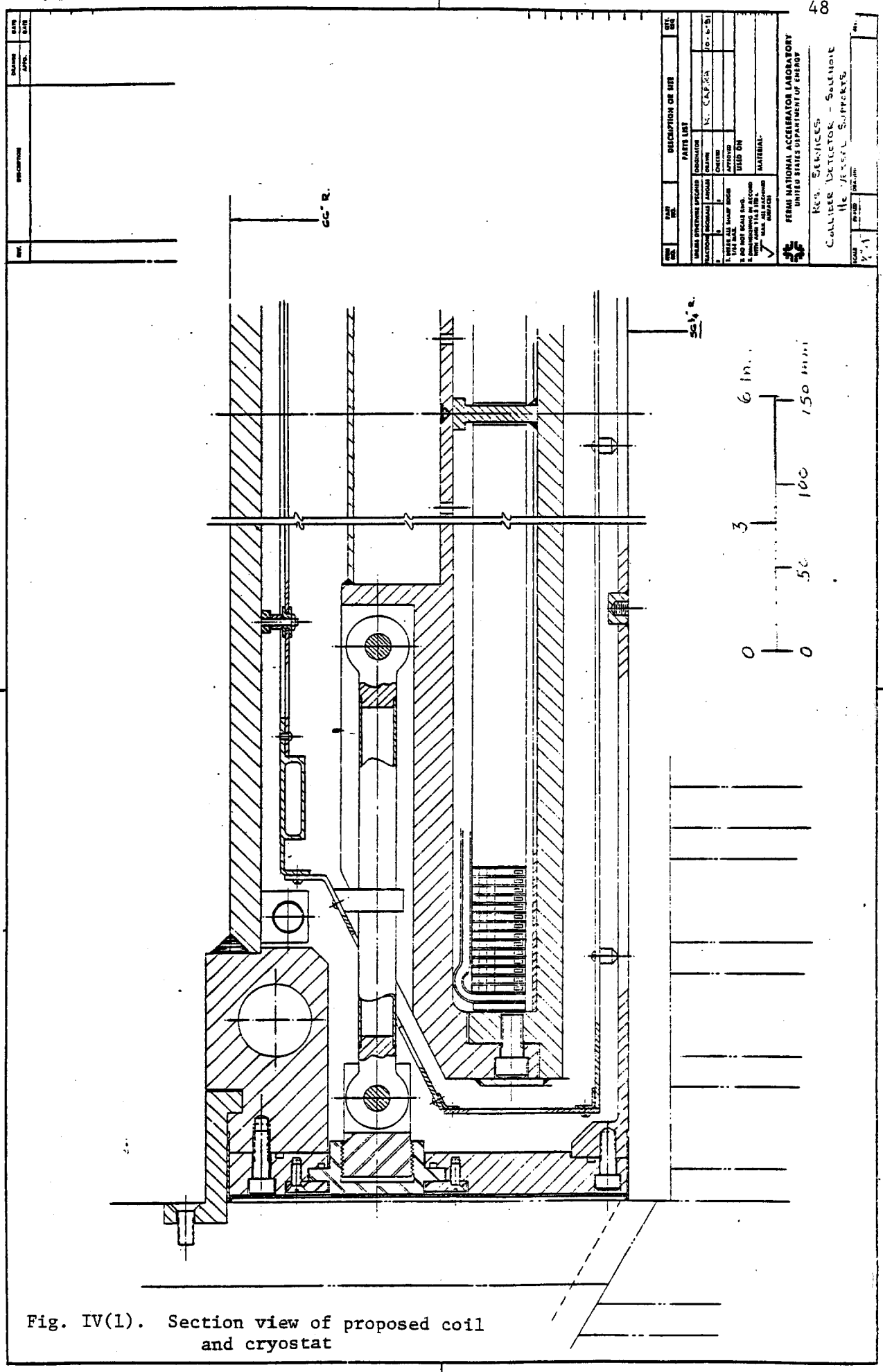

Fig. IV(1). Section view of proposed coil and cryostat

1. An inner cylindrical shell of 5083-0 Al, 0.625" thick (15.88 mm), with a mean radius of 58.313" (1481 mm). This shell serves as the bobbin upon which the superconductor is wound, and is sized to withstand the external pressures generated by winding the conductor and banding, ~130 psi (0.09 MPa), calculated in Appendix F, as well as external pressure due to pressure differential between the annular LHe space and the vacuum annulus. To reduce the shell thickness, a circumferential stiffening ring is located at the longitudinal center of the shell.

2. An outer cylindrical shell of 5083-0 Al, 0.313" (7.94 mm) thick, with a mean radius of 60.84" (1545 mm). To provide a longitudinal manifold for boil-off gas, an additional 17 L reservoir is welded to the top of this shell [Fig. IV(2)]. This manifold subtends an arc of approximately 3.8°, and communicates with the annular vessel through holes drilled in its outer shell.

3. A two-piece 5083-0 Al end ring at each end. These rings serve to seal the annular volume, and provide rigid attachment points for the external supports which suspend the helium vessel in the vacuum jacket.

<u>Structural Assembly.</u> The ANSYS large scale finite element program was used to analyze the vessel under electromagnetic and pressure loading. The results indicate that the vessel end ring stresses using the Von Mises effective stress criterion do not

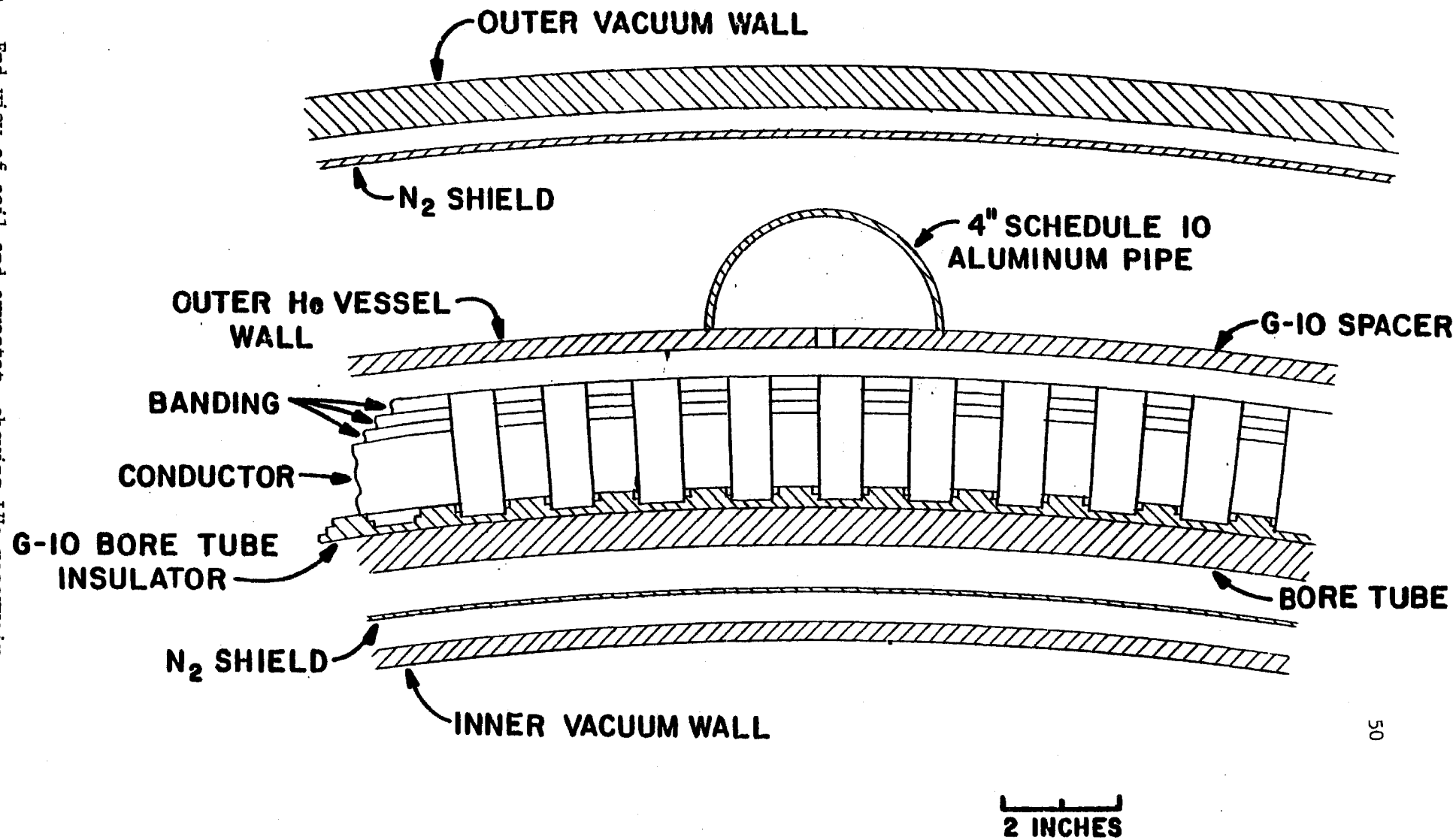

Fig. IV(2). End view of coil and cryostat, showing LHe reservoir

exceed 3000 psi (20.7 MPa) under electromagnetic loading if the magnet is located within 1" of the magnetic center of the yoke. Maximum vessel stresses for an internal pressure differential of 70 psi do not exceed 11,000 psi (75.9 MPa) in the vessel shells or 10,000 psi in the end rings. We use a maximum allowable stress of 14,100 psi in the 5083 aluminum at 4 K. This is consistent with the safety factors recommended by the ASME Boiler and Pressure Vessel Code. The analysis included a structure that simulated the bolted end flanges. We conclude that with proper bolt preloads, the entire bolted surfaces remain in contact even at 70 psi pressure differential and that there exists sufficient bolting area to provide these preloads. Elastic buckling of the bore tube limits the pressure rating of the vessel to 70 psia. Details of these calculations are in Appendix I.

Assembly. The outer shell is fabricated in two half length cylindrical sections. End rings are welded to one end of each section and matching rings are welded to both ends of the inner shell. When the coil has been wound on the inner shell, the outer shell sections are slipped over from each end. The end rings are then joined by 72, 1/2" (13 mm) silicon bronze bolts evently spaced on a 58.563" (148.7 cm) radius. A preload of 25 ksi (172 MPa) on these bolts appears adequate to maintain flange closure under electromagnetic and pressure loading. To provide a seal, a thin, aluminum cover is welded over the bolt circle. The center is joined by welding the outer shell to the stiffening ring of the inner shell. The manifold and power chimney are then

attached.

Additional internal or external stiffening rings will be used to stabilize the thin outer shell when the vessel is evacuated for leak testing.

Support System

The purpose of the coil support system is to transmit both gravitational and electromagnetic loads from the 4.2K coil package to the magnet yoke which is at 300K. The gravitational loads are due to the weight of the coil bobbin, conductor, insulation, LHe cryostat,and LHe inventory. The sum of these weights is expected to be about 7600 kg (16,500 lbs). The magnetic forces are much larger than the gravitational forces and thus dominate the design of the coil support structure.

The magnetic field produced by the coil/yoke combination has been calculated using TRIM as described previously. The expected magnetic field distribution is such that if the geometric center of the coil were located at the magnetic center of the yoke, the coil would be in unstable equilibrium with no net electromagnetic body forces acting upon it. However, if the coil were displaced from its equilibrium position, forces would act upon the coil in such a way as to increase the displacement. The magnitude of these forces has been estimated using TRIM (see Chapter III) and for displacements of interest was found to be linear with displacement with spring rates $k_z \sim 15.2$ MN/m (8.7×10^4 lbf/inch) of axial displacement and $k_r \sim 12.3$ MN/m (7.0×10^4 lbf/inch) of radial displacement. Clearly, if the support system

is to be stable and deflections kept small the support system must be much stiffer than these magnetic spring rates. In addition to this stiffness requirement, the support system must have sufficient strength so that if the coil is not positioned at the magnetic center, it can safely handle the resultant body forces on the coil. For the purposes of designing the support system, we have assumed that the coil may be located as much as 1" (25.4 mm) from the yoke magnetic center in either direction. This choice is somewhat arbitrary but is based on the following considerations: (1) the coil can only be located to $\pm$ 1/4" of the geometric center of the yoke due to tolerances in the yoke itself, (2) the geometric center of the yoke may not coincide with the magnetic center. The steel to be used for the yoke (namely reject, low carbon steel) is such that considerable variation in magnetic properties may exist from one portion of the yoke to the next. These variations in magnetic properties may cause the position of the magnetic center to vary somewhat as the magnet is excited. (3) The return paths contain several air gaps whose dimensions could change, especially the air gaps between the movable calorimeterized end plugs and the yoke or coil. (4) The space available to attach the coil to the yoke and the limited access to this space makes attractive a design that does not require careful adjustment of the coil position to place it on magnetic center.

The support system consists of 12 axial and 24 radial metallic supports. This system is shown schematically in Fig. IV(3). All 12 axial supports are located at the power chimney end of the coil, and are designed to work either in tension or compression. There are 12 radial supports at each end of the coil which are connected approximately tangentially between the coil package and the vacuum vessel and which are preloaded so that they are always in tension. The axial supports determine the axial position of the coil. The coil position with respect to the vacuum chamber is fixed by these supports but the entire package can be shimmed by about $\pm$ 1/2" (13 mm) axially if necessary. Similiarly the radial position of the coil is adjustable by $\pm$ 1/4" (6.4 mm) during installation, but is then fixed. Differential thermal contraction of the coil in the radial direction is taken care of by allowing both the radial and axial supports to rotate about spherical bearing on the end of each support. The spherical bearings insure that stresses due to bending in the supports are small. The axial supports rotate through an angle of 1.2° during cooldown while the radial supports rotate through angles of 1.3° on the chimney end and 4.1° on the non-chimney end of the coil. The preload on the radial supports will be adjusted while the magnet is cold during its first cryogenic test. Thereafter, Belleville washers located on the radial support adjustment bolts would compensate for elongation of the radial supports when the magnet is warmed up. All 36 supports will contain strain gauges so that the forces on

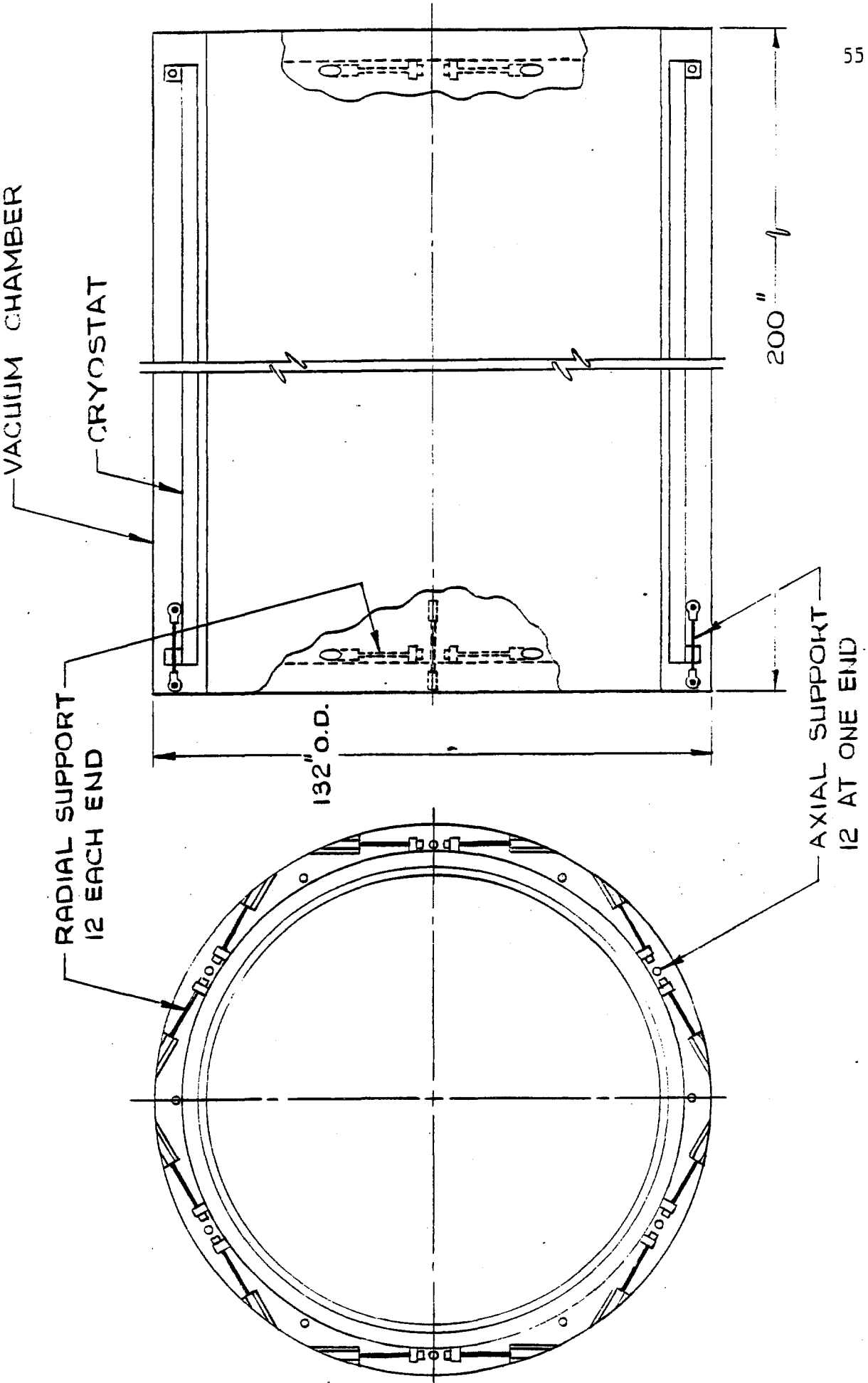

Fig. IV(3). Axial and radial supports

the support elements can be monitored during magnet excitation. The supports themselves would be fabricated from an alloy that exhibits a high strength to thermal conductivity ratio such as Inconel 718. The properties of this material are given in Appendix B. Stress, deflection, and elastic buckling calculations and a thermal analysis for the supports are presented in Appendix J. The calculated heat load for these supports is 10.8 watts at 4.2K and 94 watts at 80K.

Radiation Shields and Thermal Intercepts

General Considerations. In order to reduce the thermal radiation load on the 4.2K helium vessel, a radiation shield cooled by force flow LN_2 is provided. It consists of two aluminum cylinders connected by thermal links at each end and fastened to an aluminum extrusion through which LN_2 flows. The shield nitrogen supply is used at both ends for the support intercepts. The shield nitrogen supply is used at both ends for the support intercepts.

Inner Shield Design. The inner shield is designed to be supported from the inner vacuum shell by G-10 epoxy-fiberglass standoffs, and is cooled by conduction from the outer shield. The shield is made of a semi-cylindrical 1/8" (3.2 mm) thick 1100-F aluminum panels. The support standoffs are fastened to the aluminum shield, and only rest on the inner vacuum shell with approximately point contacts. The shield is securely fastened to the vacuum shell at one location only. This fixed point is located at the top of the shield near the axial supports. The

shield is split at the top and bottom. A G-10 piece is used to fasten the halves together at the top. At the bottom, the halves are connected with stainless steel tension springs, which keep the diameter of the shield constant during cooldown and hence maintain the relative position of the shield and shell. The inner shield is cooled with conduction links at both ends. The links are connected to the coolant circuits on the outer shield.

Outer Shield Design. The outer shield also consists of two 1/8" (3.2 mm) thick 1100-F aluminum semi-cylindrical panels which are edge cooled with liquid nitrogen. Each panel is cooled along its perimeter by a special 6063 aluminum extrusion which is mechanically fastened and welded to the edge. The extrusion provides a curved frame to maintain the shield curvature. Thermal conduction is sufficient to maintain the shield at an effective temperature. Fins on the extrusion facilitate attachment of the aluminum panels. The shields are fastened to the outer vacuum shell with G-10 bolts, through holes in the panel which are slotted to allow contraction towards a fixed point near the chimney.

Support Cooling. The axial and radial supports are intercepted with conduction straps attached to fins on the LN_2 manifold extrusion at the perimeter of the outer shield. For the expected heat loads and strap geometry, we calculate the intercept temperature to be 80K.

Flow Pattern. A schematic of the flow pattern is shown in Fig. IV(4). The liquid nitrogen is supplied from a source outside the Collision Hall. The nitrogen is force flowed through the two nitrogen circuits, which correspond to the two halves of the outer shield. Each circuit has a modulating valve on the exit line which is controlled by the temperature of the exhaust gas. The valve dynamically regulates the LN_2 flow to keep the shields at some preset temperature.

The liquid is supplied with a 120' vacuum insulated transfer line which will supply LHe and LN_2 at the same time. The line has a central tube for liquid helium. A G-10 spacer separates the LHe tube from a pair of tubes which form the channel for liquid nitrogen. Figure IV(5) shows the transfer line. The outer tube of nitrogen keeps the LHe line cool at all times, and thereby enhances LHe transfer efficiency. The transfer line terminates on both ends in bayonet boxes. U tubes connect these boxes to the magnet and to the sources of the cryogens. A phase separator in the bayonnet box improves the quality of the LN_2 entering the shields.

Performance. The shields have conduction heat loads from their supports in addition to the radiation load. The outer shield has an additional heat load from the coil support system. The outer shield is cooled by LN_2 and the inner shield from the outer shield through conduction links. A simple one-dimensional analysis, including the conduction links, was performed. This analysis indicates that the maximum temperature in the inner

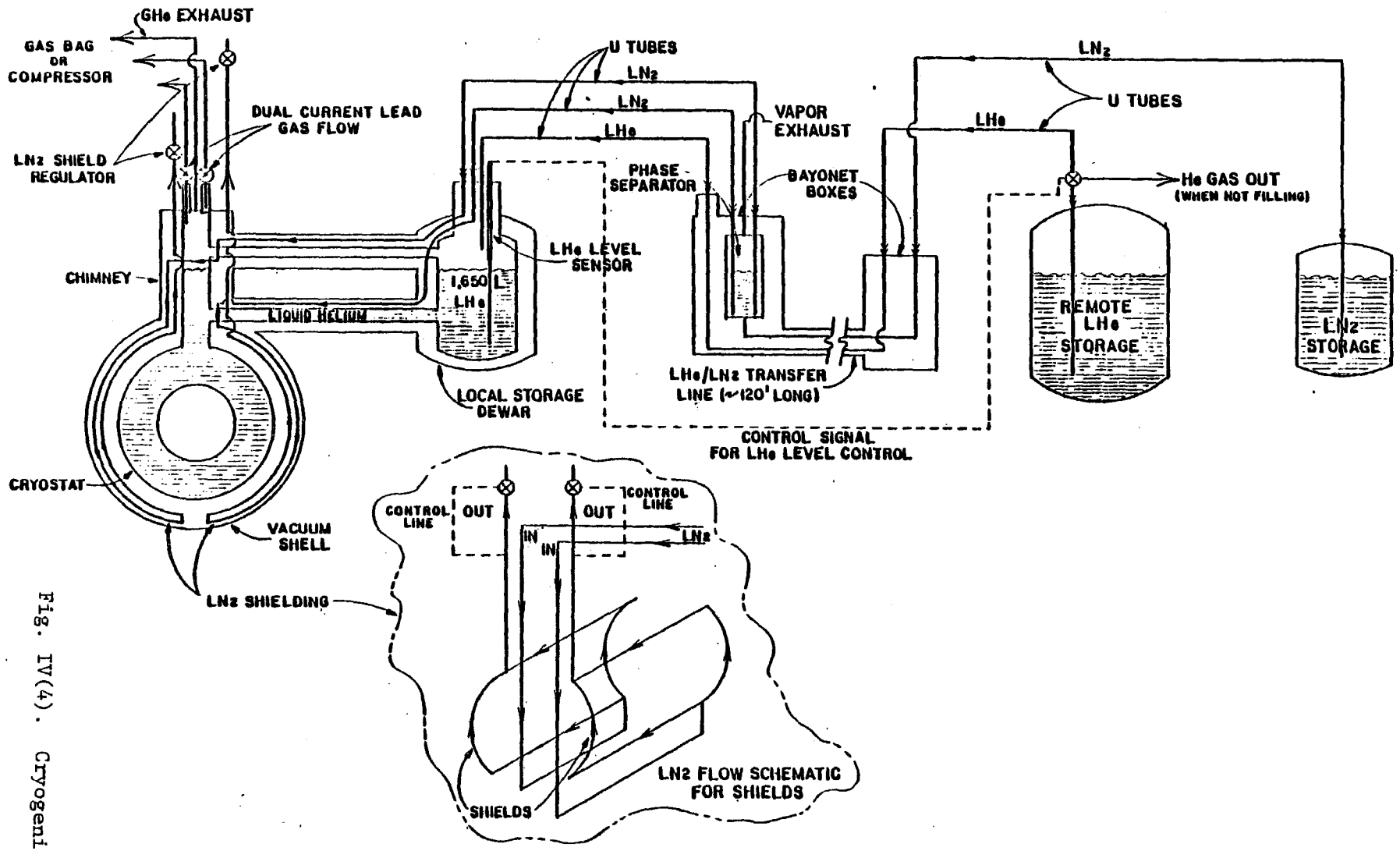

Fig. IV(4). Cryogenic system

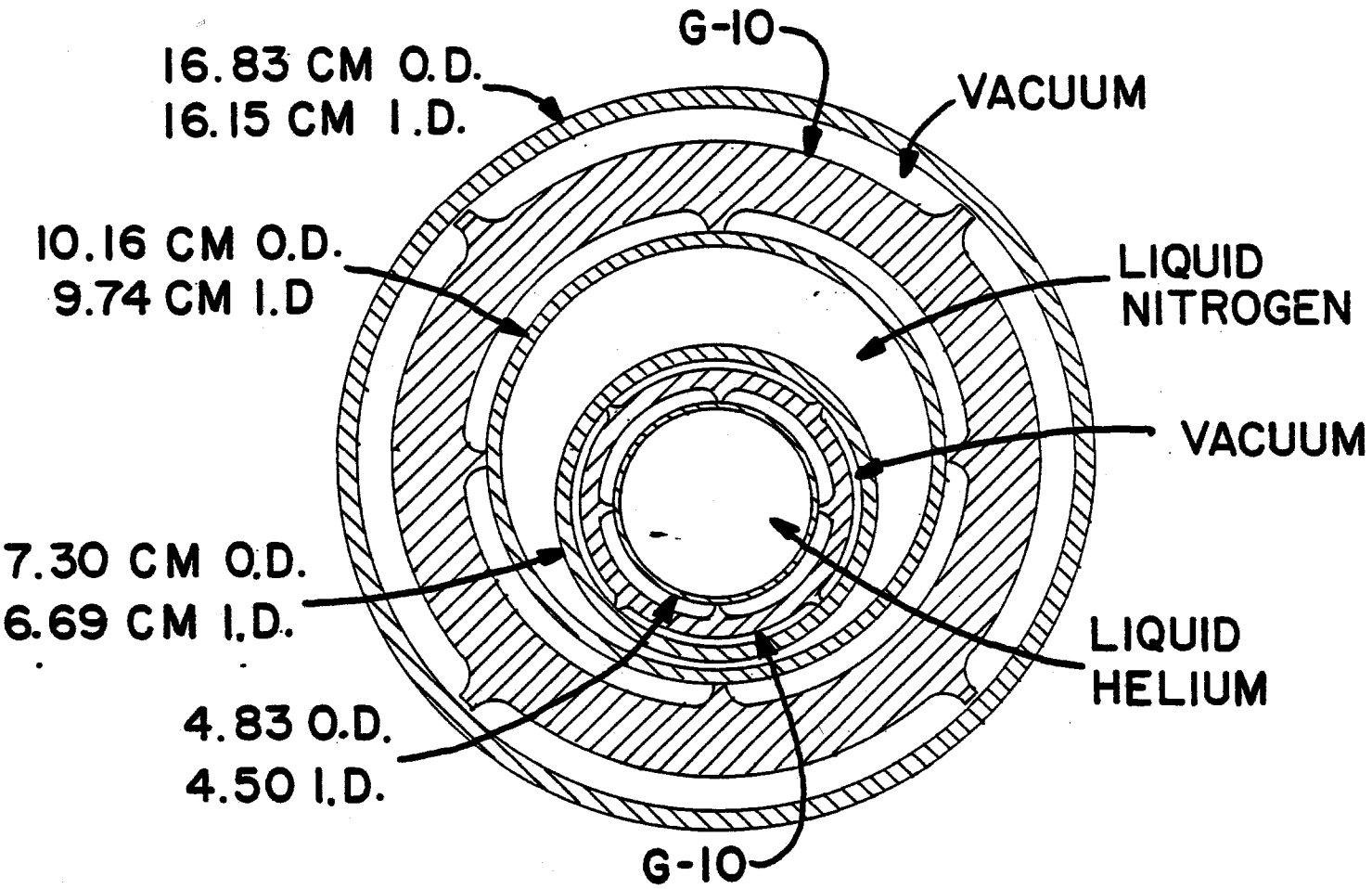

Fig. IV(5). LHe/LN_2 transfer line

shield is 89K and in the outer shield is 91K (see Appendix K).

Vacuum Vessel

General Design Philosophy. Fermilab Engineering Standards (SD-24 and SD-37) require that all room temperature pressure vessels in use at Fermilab be designed and constructed in accordance with the ASME Boiler and Pressure Vessel Code, Sec. VIII, Div. 1 (the "Code"). We have investigated the penalty paid with respect to radiation transparency by following these standards. We found* that for the outer shell the difference in $\lambda_r(\lambda_a)$ between a non-code design (safety factor = 1.2) and a Code design (safety factor ~ 3) is 0.052 λ_r, (0.013 λ_a). Because of the uncertainties inherent in aluminum tank construction, we designed the vacuum vessel in accordance with the Code. This design is shown in Fig. IV(1).

Inner Shell. The inner shell is fabricated of 6061-T6 aluminum alloy, rolled and welded to form a cylinder. The shell is held circular by a 0.75" x 1.375" (19 mm x 35 mm) flanges at the ends, but does not have additional stiffening rings.

The inner shell dimensions are given in the table:

Inner Shell Dimensions

Inner diameter	112.5 inch	(2857 mm)
Outer diameter	113.0 inch	(2870 mm)
Wall thickness	0.25 inch	(6.4 mm)
Nominal length of shell	197.5 inch	(5016 mm)

*R.W. Fast, R.D. Kephart, CDF Coil Engineering Design Note #8, Fermilab, unpublished (1981).

We note that with these dimensions the maximum allowable positive pressure in the vacuum annulus is 1.17 psig (8.09 kPa-gauge) and the vessel must be protected accordingly. Detailed calculations are found in Appendix L.

Outer Shell. The outer shell is also fabricated of 6061-T6, 0.75 in (19.0 mm) thick. The outer shell dimensions are given in the table. It has end flanges 3.00" x 5.0" (76 mm x 127 mm) on both end to which the radial supports are attached.

Outer Shell Dimensions

Inner diameter	130.50 inch (3315 mm)
Outer diameter	132.00 inch (3353 mm)
Wall thickness	0.75 inch (19 mm)
Nominal Length of Shell	197.50 inch (5015 mm)

Shell Tolerances. The Code specifies (see Appendix L) the permissible out-of- roundness of the inner and outer shells. The inner diameter of the shell must be constant to within ± 0.625 in. (15.9 mm) and the shell must not deviate from circular by more than 0.375 in (9.5 mm) over an chord length of 30 inches.

Penetrations into Outer Shell. The vacuum vessel of the chimney is attached to the top of the outer vacuum shell. This penetration of the shell is reinforced in accordance with the Code. This reinforcement is described in the section of this report dealing with the chimney (Appendix M).

Annular End Flanges. The annular end flanges serves as a closure for the vacuum space and as the attachment for the axial supports. They are essentially flat, i.e., non-dished, annular plates bolted to the end flanges of the two shells.

The flange thickness is 1" (25.4 mm) which is in excess of the Code requirement (see Appendix L).

Welded Fabrication

The detailed design of all weld joints in the vacuum vessel will be in accordance with the Code, Part UW (Welded Vessels). The intention is to follow the fabrication and inspection provisions of Part UW also.

Power Chimney

The power chimney is the penetration that contains all cryogenic and electrical connections to the coil. It serves as a relief port in the event that a large quantity of LHe in the coil is somehow rapidly vaporized, and provides the 4K to 300K temperature transition for the magnet power leads while minimizing the 4K heat load. Since the chimney requires a "hole" in the central calorimetry of the detector, it is important to make the chimney as small as possible consistent with safety and structural integrity. All plumbing, bus bars and cables from the power chimney must come out of the detector through an opening in the magnet iron yoke on the downstream (relative to the p beam) side of magnet which is 3 x 5 ft^2 (0.91 x 1.5 m^2). A design intended to meet these requirements is shown in Fig. IV(6). The chimney contains LHe and LN_2 supply lines, a He cooldown line, instrumentation connections and a pair of gas cooled power leads. (8000 A rating).

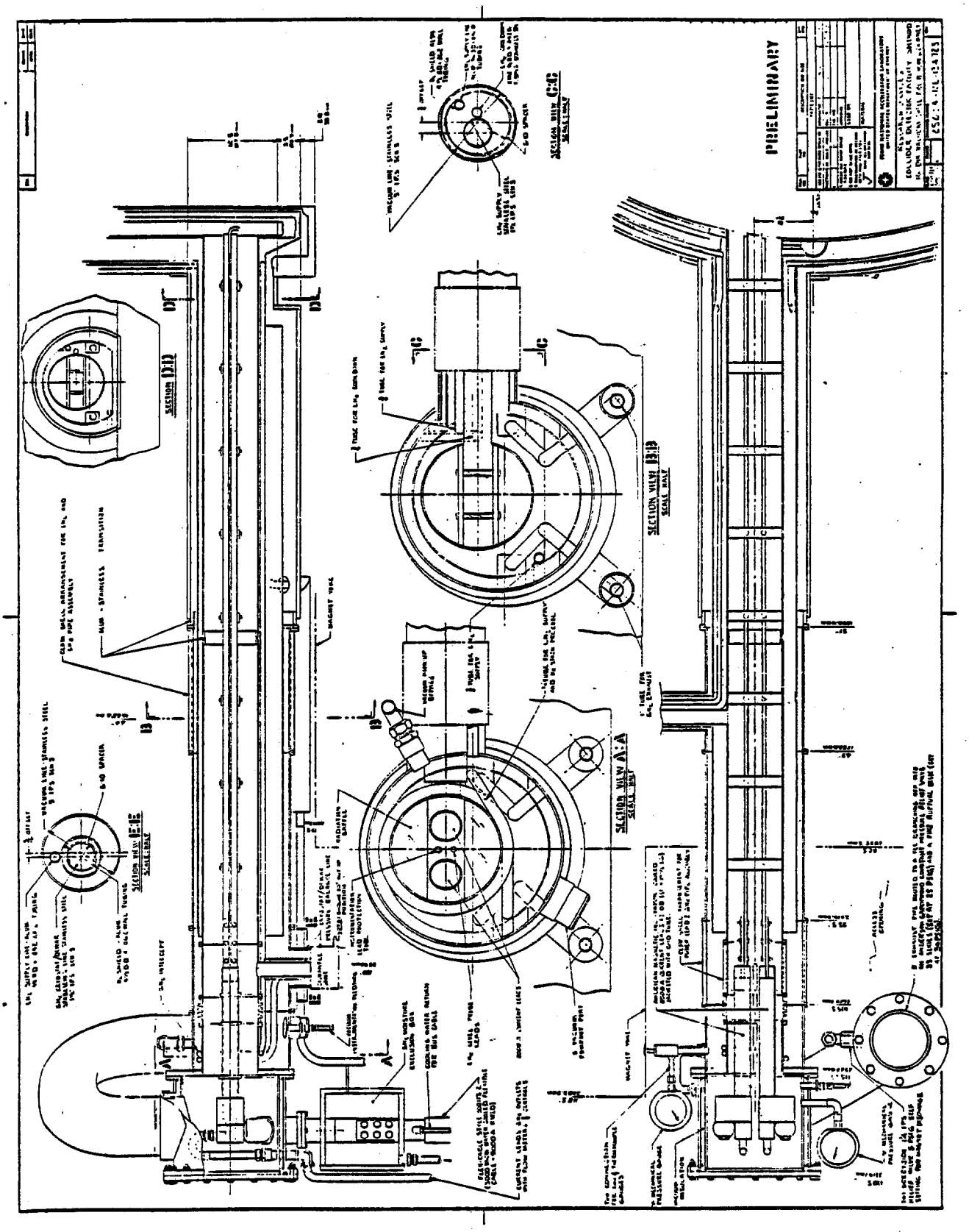

Fig. IV(6). Cryostat power chimney

An 8" pipe contains the current leads and connects the LHe volume in the coil to the outside. Protection against over-pressure is provided both by relief valves and an 8" dia. (203 mm) burst disk. We have calculated that the combination of this burst disk and the one on the LHe dewar should comfortably handle "worst case" cryogenic failures such as complete loss of insulating vacuum (600 kW continuous heat flux) etc, with small pressure rises in the He system (see Appendix Q). The pressure rise from an electrical failure within the magnet is more difficult to estimate and depend on the details of the failure. Preliminary calculations, however, do not indicate serious difficulties.

The cryostat is constructed of aluminum. We therefore employ an aluminum/stainless steel transition joint in the chimney so that the large temperature gradient is across a thin stainless steel bellows. The bellows provides a high thermal impedance and permits differential thermal contraction in the chimney. The LN_2 and LHe cooldown lines have similar transitions and provisions for thermal contraction.

Liquid Helium System

Liquid helium is gravity fed to the coil from a dewar with a useful volume of 1650 L mounted on the magnet yoke [see Fig. III(2)]. The dewar is connected to the magnet power chimney via two LN_2 shielded ~ 2" lines which insure that the LHe level in the power chimney is the same as that in the dewar. Both the vacuum jacket and inner vessel of the dewar will be fabricated

from 304SS. The pressure rating of the dewar is 75 psig, and calculations of the shell thicknesses required are in Appendix N. It is protected from over-pressure both by relief valves and a 4" diameter (102 mm) burst disk. Its 4" OD (102 mm) neck is LN_2 intercepted. The dewar employs a radiation shield cooled by LN_2. The dewar has provisions for LHe fill and cooldown lines, as well as the magnet's LN_2 supply lines. U-tubes connect the dewar to a bayonet box at the end of the LHe/LN_2 transfer line. The coil will be serviced by two different transfer lines ~120' long for operation in either the Collision Hall or Assembly Hall. The magnet is intended to move while it is cold and full of LHe. Connecting and reconnecting the cryogenic system is a matter of removing and inserting U-tubes and thus should be both simple and expedient.

Support Of The Central Tracking Chamber

The central tracking chamber fits inside the inner vacuum shell. The outside diameter will be about a half inch smaller than the inner diameter of the inner vacuum shell. Its total weight is estimated about 2.5 metric tons. It has an outside cylindrical wall of drift tubes made from aluminum extrusions. It has two end plates, which are made of concave aluminum plates. Between these two plates, 10000 sense wires (30000 field wires) will be strung at the tension of 120 gram (500 gram) for each wire , resulting in about 16 metric tons of wire tension force.

The total length of the chamber is about 340 cm. The chamber is mounted to the inside of the inner vacuum shell via mounts at each end of the coil. These mounts form a horizontal plane. The chamber is bolted rigidly to the mounts at one end. The holder on this end is a ring which is either bolted or welded to the inside diameter of the solenoid. At the other end of the chamber the mounting is arranged to allow extension or contraction of the chamber due to temperature and pressure changes. These mounts must be removable and therefore will be bolted to the vacuum shell I.D. We feel that bolting can be accomplished by a limited number of blind tapped short round rods welded into radial holes in the inner vacuum wall of the coil [see Fig. IV(1)].

CHAPTER V: COOLING CONSIDERATIONS

System Description

The cooling of the CDF magnet system is done by two separate systems. The LHe system consists of: (1) the helium vessel and chimney, (2) a 1650 L local storage dewar, (3) a 120 ft (~36 m) transfer line (4) a remote storage dewar (supplied LHe from an as yet undetermined source). and (5) automatic He fill system. The forced-flow LN_2 system consists of: (1) the radiation shields and thermal intercepts in the cryostat and local LHe dewar, (2) a 120 ft transfer line with phase separator and (3) flow controls. The source of LN_2 is as yet undetermined. The system is shown schematically in IV(4).

Summary of Heat Load

Calculations of the heat fluxes (see Appendix O) show that the total heat load to be used for system design are 500 W into the LN_2 system and 40 W into the LHe system. These correspond to a boil-off rate of 11 L/h for LN_2 and 56 L/h for LHe.

With an estimated LHe boil-off of 56 L/h, the local storage dewar must be filled at least once every 30 h. We presently plan to transfer LHe automatically from the remote storage dewar to the local dewar mounted on the detector.

Cooldown and Warm-Up

The cold mass of the magnet is calculated (see Appendix P) to be approximately 15,800 lbs of aluminum and 2600 lbs of G-10. When cooling down, 1.25 GJ of thermal energy must be removed from 300K to 80K and a further 79.2 MJ from 80K to 4.2K. The method of

cooling down the system has not been finalized, but there seems to be two alternatives, described below.

Cooldown Using Cold Helium Gas One method to extract the 300K-80K enthalpy from the system is to circulate helium gas which has been heat exchanged with LN_2. The great advantage of this method is that, following an initial clean up, the helium system is never contaminated with air or nitrogen. Large superconducting magnet systems with dedicated refrigerator/liquefiers are almost universally cooled down with this method. We have not calculated the cooldown of the CDF magnet using this method, but estimate the time to reach 4.2K as 8 days.

Cooldown Putting LN_2 Into Helium System In this method LN_2 is added to the helium until the helium vessel is full of LN_2. It is routinely used for cooling down the large superconducting analysis magnets at Fermilab. Using the latent heat of LN_2 and 50% of the enthalpy of nitrogen gas from 77K to 300K ~ 5000 L of LN_2 and ~ 3000 L of LHe is required. Subcooling the coil by reducing the nitrogen partial pressure (pressurizing the vessel with LHe at low pressure) will probably save at least 50% of the LHe cooldown requirement. To avoid excessive thermal stresses, it is recommended that the coil be cooled down to 77K in 6 days, with two additional days required to reach 4.2K and fill the helium vessel and dewar.

Warm-Up

If we have plenty of time for warm-up, we can allow liquid cryogens to boil away and then spoil the vacuum and let the magnet warm up slowly. If under a tight schedule, we can blow out the liquid helium with gaseous helium, then warm up the cryostat by passing warm gaseous helium through the system continuously.

CHAPTER VI. POWER SUPPLY AND INSTRUMENTATION

Magnet Power Supply

The power supply for the CDF magnet provides 6600 A of D.C. current into a 1.4 H inductive load. It is rated for 22.5 V and 148.5 kW and is bipolar. Regulation at full current is ± 0.1%. The supply uses both voltage and current regulation, a shunt for current monitoring. The supply can be turned off by a signal from the interlock system. Such a supply is commercially available and would be approximately 72" (1.8 m) high x 48" (1.2 m) wide x 48" (1.2 m) deep and weigh ~ 4,000 lbs (1818 kg).

Interlock System

The magnet has an extensive protection system. Various sensors and interlocks monitor important system parameters and initiate a discharge if an unacceptable value is detected. The magnet will discharge if any of the following conditions occur:

1. Excessive ground current
2. Excessive operating current
3. Center tap voltage imbalance too large.
4. A significant increase or decrease in LHe boil-off.
5. Either of two LHe probes reads low
6. Power supply begins to overheat
7. Insulating vacuum failure
8. Excessive voltage across current leads, or for power bus.
9. Excessive magnet pressure

Other interlocks will be chosen as the design is developed.

Instrumention

A system of instrumentation that can be remotely monitored is planned for the coil package. Strain gages will be mounted on the supports and bore tube to monitor stresses during magnet operation. Thermocouples on the nitrogen shield and support intercepts will measure these temperatures. Gas flow through the exhaust lines of the current leads and chimney gas outlet will be measured. Information on the magnet pressure and LHe levels will be provided to the magnet operator. During cooldown and warm-up the resistance of the coil itself will act as a thermometer.

Bus Circuit

We propose to use water cooled aluminum bus conductor to connect the power supply to the magnet. The one-way distance from the power supply to the magnet location in the Collision Hall is 104 ft (31.7 m). An aluminum conductor developed for a large analysis magnet at Fermilab* will be used. The conductor is extruded of 6101-T63 into a square cross section 2.42" x 2.42" (61.5 mm x 61.5 mm) with a 0.55" (14.0 mm) diameter cooling water hole. The extrusion die for this conductor is the property of Fermilab and is stored at Arizona Aluminum, Inc., Phoenix, Arizona.

*R.W. Fast, et al., 14.4 m Large Aperture Analysis Magnet with Aluminum Coils, IEEE Trans. on Magnetics, MAG-17 (5):1903, (1981).

In order to reduce the power dissipated in the bus, we propose to use four conductor bars in parallel. The results of the power calculation is given in the table:

Table Power Loss in Bus Conductor

Number of bars	1	2	4
Over-all size of each bus, with insulation	2.5"sq. (63.5mm)	2.5 x 5.0" (63.5mmx127mm)	5.0" sq. (127mm)
Total resistance (mΩ) at 125°F (51.7°C)	0.578	0.289	0.144
Total voltage (V)	3.82	1.91	0.95
Total power (kW)	25.0	12.5	6.25
(BTU/hr)	86,000	43,000	21,500
Total water flow (gal/h) required, with	228	114	57.0
ΔT=50F (28C) (L/min)	14.4	7.2	3.60

CHAPTER VII. CONCLUSION

On the basis of the calculations we have completed so far, we conclude that the CDF solenoid could be built as a cryostable pool boiling magnet using high purity aluminum as a stabilizer. The inherent ease of operation and stability of such magnets is well documented and seems attractive. Moreover, the thickness penalty in both radiation length and physical space for this type of coil versus a contact cooled, adiabatically stabilized, coil like CELLO or CLEO seems minimal for a magnet of this size.

We, therefore, recommend that a coil of this type be seriously considered for the Fermilab Collider Detector Facility magnet.

ACKNOWLEDGMENTS

We wish to thank A. V. Tollestrup, R. F. Schwitters, and the members of the Collider Detector Department for the stimulating discussions which helped us to clarify the solenoid design. We want to acknowledge the contributions of Lee Mapalo and John Rauch to the mechanical design. Ray Carra and Phil Calahan are thanked for their drafting assistance. We thank Shirley Jones for word processing this document and making the innumerable revisions.

APPENDIX A. SYSTEM PARAMETERS

General

Overall inner diameter:	2857 mm (112.5")
Overall outer diameter:	3353 mm (132")
Overall length (nominal):	5067 mm (199.5")
Central field:	1.5T
Approximate weight of cryostat:	12000 kg (26500 lb)

Coil

Inner diameter:	2990 mm (117.7")
Circumference:	9394 mm (369.8")
Winding length:	4788 mm (188.5")
Linear current density:	1200 A/mm for 1.5 T
Operating current:	6600 A
Winding scheme:	Single layer helix
Number of turns:	870
Inductance:	1.38 H
Stored energy:	31×10^6 J at 1.5T
Charge time:	10 min

Coil discharge	Slow	Fast
Time constant	300 s	45 s
Dump resistor	4.6 mΩ	31 mΩ
Max. discharge voltage	30 V	202 V

Conductor

General:	Cu/NbTi coextruded with high purity aluminum stabilizer
Overall dimensions:	4.25mm x 18.8 mm (0.167 in x 0.740 in)
Al:Cu:Nb-Ti area ratios:	14:1:1
Peak field at conductor:	1.5 T
Bare conductor current density:	8260 A/cm^2
Total weight:	2250 kg (4940 lbs)
Total length:	8.2 km (27000 ft)

Cu/NbTi Composite

Alloy:	Nb 46.5 a/o Ti
Matrix:	copper ASTM B170-1; CDA 101
Bare width:	5.0 mm
Bare thickness:	2.0 mm
Short sample current:	13.2 kA at 2.0T, 4.2K
NbTi short sample current density	2.64 x 10^9 A/m^2 at 2T and 4.2K
Filament diameter:	50 μm
No. filaments:	2400

Twist pitch:	10 mm
Aluminum Stabilizer	
Alloy:	99.995 + %
Residual resistivity ratio:	$\geq$ 1200
EFT boundary	
Thickness:	$< \sim 2\ \mu m$
Resistance:	$24 \times 10^{-11}\ \Omega$-m
Shear strength:	> 10 MPa
Electrical Insulation	
On-coil bobbin	epoxy-fiberglass with channels
Turn-to-turn:	0.050" (1.25 mm) epoxy fiberglass
Fraction of conductor surface exposed to LHe	~ 50%
Forces Acting On Coil	
Total compressive axial force at midplane:	0.86 MN (1.9×10^5 lbf)
Axial decentering force:	15.2 MN/in (8.7×10^4 lbf/in)
Max. Radial decentering force	12.3 Mn/m (7.0×10^4 lbf/in)
Vacuum Vessel	
Inner vacuum shell material/ OD/thickness	6061-T6 Al 2870 mm (113.0")/ 6.4 mm (0.25")
Outer vacuum shell material/ OD/thickness:	6061-T6 Al 3353 mm (132")/ 19.0 mm (0.75")

Radiation Shields

Inner radiation shield material/thickness:	1100-F Al 2 mm (0.078")
Outer radiation shield material/thickness:	1100-F Al 2 mm (0.078")

Helium Vessel

Inner helium shell (winding bobbin) material/OD/thickness:	5083-0 Al/2987 mm (117.25")/ 15.9 mm (0.625")
Outer helium vessel material/ OD/thickness	5083-0 Al/ 3099 mm (122") 7.9 mm (0.3125")

Thermal Insulation Vacuum Plus Multilayer Insulation

Between 4.2 and 77K:	Aluminum tape 3M#425 ~ 12 layers NRC-2 (500 Å)
Between 77 and 300K:	~ 40 layers NRC-2 (300 Å)

Liquid Nitrogen Cryogenics

Cooling mode:	Forced flow
Liquid reservoir (if req'd):	2 m^3 500 gal minimum
Steady state heat load:	425 W (est.)

Liquid Helium Cryogenics/Refrigeration

Coil cooling mode:	pool boiling LHe at 0.113MPa (abs.) (2psig)
Liquid temperature:	4.3 K
Liquid capacity of cryostat:	~800 L
Reservoir capacity (of dewar and chimney)	1750 L
Cold mass (magnet):	7200 kg (15800 lb)
Cooldown time:	300K to 80K $\leq$ ~ 6 days 80K to 4.2K $\leq$ 2 days

Steady-state heat load:	~ 40 W, 56 L/h
Discharge heat load:	176 L at τ = 45 s, 26L at τ = 300 s

<u>Power Supply</u>

Rated voltage:	225 V
Rated current:	6600 A
Rated power:	148.5 kW

<u>Iron Yoke</u>

Total weight; including end plugs	909000 kg (1000 short tons)
Moving weight of each end plug	100,000 kg (110 short ton)

THICKNESSES

(average at $\theta = 90°$)

Item	Material	inches	cm	Radiation Length	Absorption Lengths
Inner vacuum shell	Aluminum	0.250	0.64	0.071	0.0170
Inner shield	Aluminum	0.080	0.20	0.022	0.0053
Inner helium shell (coil bobbin)	Aluminum	0.625	1.59	0.178	0.0426
Inner shell insulation	Epoxy/fiberglass	0.236	0.60	0.022	0.009
Conductor	Aluminum Copper NbTi	0.67	1.7	0.232	0.0400
Coil insulation	Epoxy/fiberglass	1.26	3.2	0.024	0.010
Banding	Aluminum	0.591	1.5	0.169	0.0404
Outer helium shell	Aluminum	0.313	0.79	0.089	0.0213
Outer shield	Aluminum	0.080	0.20	0.022	0.0053
Outer Vacuum shell	Aluminum	0.750	1.90	0.214	0.0512
TOTALS				1.04	0.242

(λ_R = 8.9 cm) (λ_a = 37.2) for Aluminum

(λ_R = 1.6 cm) (λ_a = 15.cm) for Cu/NbTi

(λ_R = 18 cm) ($\lambda_a \sim 45$) for G-10

MATERIAL	Specific Gravity	Young's Modulus of Elasticity E at 4.2 K 10^6 psi	E at 77 K 10^6 psi	E at 300 K 10^6 psi	Yield Strength at 4.2 K ksi	at 77 K ksi	at 300 K ksi	Code Allowable Stress ksi
Pure aluminum	2.65	—	—	—	—	6.5 (RRR = 1200)		—
Al 6061-T6	2.65	11.3	11.2	10.2	51.8	47.8	39.2	6.0 (welded)
Al 5083-0	2.65	11.7	11.6	10.4	25.0	23.0	21.0	10.0
Al 7075-T6	2.65	12.0	11.2	10.6	99.6	89.5	73.0	—
SS 304	8.9	30.5	31.1	28.9	70.0	60.0	35.0	18.8
Inconel 718	8.5	32.0	31.5	31.0	199.0	186.0	157.0	—
Ti(6Al4V)	4.5	19.1	17.2	15.7	278.0	229.0	138.0	—
Epoxy-Fiberglass Nema G-10	1.8	3.9 ∥ "CR"	3.7 ∥ "CR"	3.2 ∥ "CR"	—	—	—	—
Cu (OFHC)	8.9	21.5	20.0	17.2	13.1	12.8	10.9	6.7

MATERIAL	Radiation Length cm	$\frac{\Delta L}{L}\Big\vert_{4.2\,K}^{300\,K}$	Electrical Resistivity at 4.2 K $\mu\Omega$-m	at 77 K $\mu\Omega$-m	at 300 K $\mu\Omega$-m	Intagrated Thermal Conductivity $\int_{77}^{300K} k(T)dT$ W/cm	$\int_{4.2}^{77K} k(T)dT$ W/cm	$\int k(T)dT$ W/cm	Enthalpy $\Delta H_{4.2\,K}^{300\,K}$ J/g
Pure Aluminum	90.0	0.0043	0.000018	0.0020	0.025	—	—	—	170.4
Al 6061-T6	90.0	0.0042	0.014	0.017	0.039	—	—	—	170.4
Al 5083-0	90.0	0.0043	0.030	0.033	0.057	169.0	25.5	—	170.4
Al 7075-T6	90.0	0.0042	0.028	0.030	0.053	—	—	—	170.4
SS 304	17.3	0.00304	0.496	0.514	0.704	27.5	31.8	—	76.6
Inconel 718	—	0.0024	1.18	1.19	1.25	22.0	3.5	—	
Ti(6Al4V)	37.2	0.00154	1.47 at 20K	1.50	1.675	13.5	1.8	—	101.4
Nema G-10	180.0	0.0071 ⊥ 0.0025 ∥	Insulator	Insulator	Insulator	0.96 ⊥ 1.41 ∥	0.139 ⊥ 0.20 ∥	—	91.1
Cu (OFHC)	14.5	0.00325	0.00016	0.002	0.0156	934.0	586.0	—	79.6
Nb-Ti	16.0	—	—	—	—	—	—	—	80.3

REFERENCES:

1. Mech. Prop. of Structural Materials at Low Temperatures, R. Michael McClintock and Hugh P. Gibbons, NBS Monograph 13, June 1, 1960.
2. Handbook on Materials for Superconducting Machinery, James E. Campbell, Metals and Ceramics Information Center, Battelle-Columbus Laboratories, November 1974.
3. A Compedium of the Properties of Materials at Low Temperature (Phase I) Part II. Properties of Solids, Victor Johnson, General Editor, NBS, October 1960.
4. LNG Materials and Fluids, Douglas Mann, Owain Diller, Hassell Ledbetter, Cryogenics Division, Inst. for Basic Standards, NBS, First Edit. 1977.
5. Standard Handbook for Mechanical Engineers, Baumeister and Marks, Seventh Ed., McGraw Hill.
6. Lawrence Berkeley Lab., Engineering Note, Michael Green. Minimag Experiment, Large Superconducting Solenoid Magnet, Code AB0103, Serial M4835, March 21, 1975.
7. ASME Boiler and Pressure Vessel Code, Section VIII, Division 1

APPENDIX C: COIL DISCHARGE ANALYSIS

The adiabatic coil discharge was modeled by assuming that a section of conductor is normal and insulated perfectly from its surroundings. An initial temperature of 10K is assumed. The conductor is supplied with an exponentially decaying current with time constant τ and an initial value of 6600 A. The input to the program is quite limited, consisting of material properties, mass per unit length of conductor, discharge time constant, operating current, magnetic field and the cross sectional area of the stabilizer. The program was run to determine the effect of various discharge time constants, τ , on the temperature-time profile of the conductor. Results from several such calculations are in Fig. II(4). The program was verified by comparing the calculated results to the measured data from the Hitachi test coil.* The agreement between the calculations and the test data is good.

When using the program for the proposed coil, the decaying current was allowed to flow only in the aluminum stabilizer while the enthalpy of both the banding and the composite was included.

* M. T. Mruzek, Computer Model of Hitachi Coil During a Quench Using the Program NZONE, Fermilab CDF Coil Engineering Design Note #5A (1981), unpublished.

APPENDIX D: EDDY CURRENT LOSSES IN HELIUM VESSEL

Objective:

To derive an equation for the eddy current power generated in the vessel walls as a function of time during a charge or discharge.

Assumptions:

The vessel fabricated of 5083-0 aluminum, with

ρ = 3.3×10^{-8} Ω - m

r = mean radius of bobbin = 58.3125" (1481 mm)

r' = mean radius of outer helium shell = 60.844" (1545 mm)

Δr = thickness of bobbin = 0.625" (15.9 mm)

$\Delta r'$ = thickness of outer helium shell = 0.3125" (7.9 mm)

E_o = stored magnetic energy at 1.5 T = 31 MJ

I_o = operating current = 6600 A

B = magnetic field

B_o = max magnetic field = 1.5 T

E = energy deposited in bobbin

E' = energy deposited in outer helium shell

Calculations

In a Linear Charge:

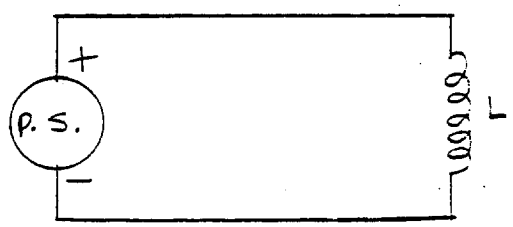

With the approximation that

$$B(t) = C\ I(t)$$

it can be shown that

$P_{(t)}$ = power in bobbin

$$P_{(t)} = \frac{\mu_o\ E_o\ r\ \Delta r}{t^2_{chg}\ \rho} \text{ (watts)}$$

where t_{chg} = charge time = 10 minutes and

$$E = \frac{\mu_o\ E_o\ r\ \Delta r}{t_{chg}\ \rho}$$

Substituting values for the parameters:

$$p = \frac{(4\pi \times 10^{-7})(31 \times 10^{6})(1.481)(15.9 \times 10^{-3})}{(600)^{2}(3.3 \times 10^{-8})}$$

$$= 77.2 \text{ W}$$

$E = 46.3$ kJ ~ 18 liquid liters of LHe

<u>For an Exponential Discharge:</u>

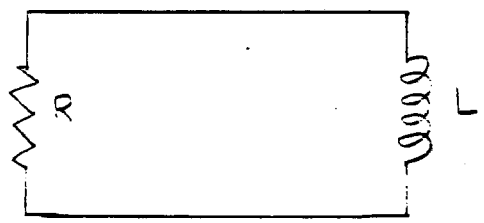

since $I(t) = I_o \exp[-(Rt)/L] = I_o \exp[-(t)/\tau]$

$$P(t) = \frac{\mu_o E_o r \Delta r}{\tau^2 \rho} \exp[-(2t)/\tau]$$

and

$$E = \int_{t=0}^{t=\infty} P(t)\, dt$$

$$E = \frac{\frac{1}{2} \mu_o E_o r \Delta r}{\rho} \frac{1}{\tau}$$

$$p_{max} = p(0) = \frac{{}_{o} E_{o}\, r\Delta r}{\tau^{2}\, \rho}$$

Results

	Charge	Slow Discharge	Fast Discharge
Time Constant	600s	300s	45s
Outer Helium Shell			
Max Power	38.5 W	154 W	6840 W
Inner Helium Shell (coil Bobbin)			
Max power	72.2 W	297 W	13200 W
Both helium shells			
Max power	110.7 W	451.0 W	20000 W
Energy	67.5 kJ	67.6 kJ	450 kJ
Total LHe loss	26.0 L	26.0 L	176 L
Max LHe boil-off	157.0 L/h	638.0 L/h	28300 L/h
Max gas flow rate	~67.0 scfm	~273.0 scfm	~12000 scfm
(at STP)	~1.8 m^3/s	~ 7.4 m^3/s	~ 330 m^3/s

Bobbin - Coil Coupling

Following the analysis of Green*, it can be shown that coupling between the coil and bore tube has a negligible effect in the above results.

*M.A. Green, The development of large high current density superconducting solenoid magnets for use in high energy physics experiments, Lawrence Berkeley Lab Report. LBL - 5350 (1977).

APPENDIX E: TRANSIENT FIELD LOSSES IN CONDUCTOR

OBJECT

To determine charging and discharging losses in the composite conductor due to hysteresis and eddy currents.

REFERENCE

H. Brechna, Superconducting Magnet Systems, L. Springer-Verlag, New York (1973) p. 250 ff.

ASSUMPTIONS

Treat the proposed conductor as cylindrical with the same cross sectional area. (All dimensions in mm.)

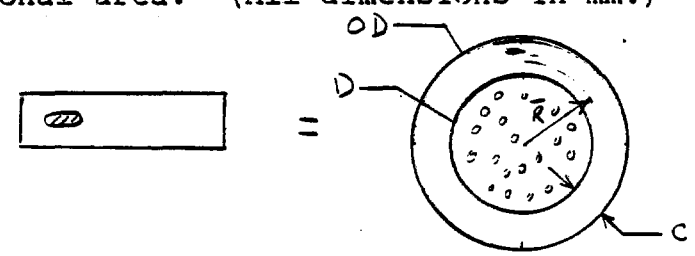

1. Hysteresis losses are caused by changing flux penetrating the surface of the superconducting material.

2. Eddy current losses are caused by eddy currents in the normal metal matrix surrounding the filaments and the normal metal outside the filament bundle.

CALCULATIONS

Equivalent Conductor

For each 6600A conductor

Cu/Nb-Ti area = 0.10 cm^2 and

D = diameter of filament bundle

$$\sim \left[\frac{4(0.10)}{\pi}\right]^{1/2} = 0.356 \text{ cm}$$

Pure aluminum area = (1.88 x 0.425) - 0.10 cm^2

= 0.699 cm^2

and

OD = 1.009 cm

C = 1/2 (OD-D) = 0.326 cm

$\bar{R}$ = 1/2 (OD+D) = 0.682 cm

Hysteresis Losses

From Brechna, Eq. 4.1.42 (pg. 247)

$$\frac{P_h}{V} = \frac{8}{3\pi} \mu_o J_c(H) \frac{d}{4} \dot{H}_{ext} \quad (W/m^3)$$

where

μ_o = $4\pi \times 10^{-7}$

d = filament diameter = 50 μm

H_{ext} = external field

$J_c(H)$ = critical current density at H

V = volume of superconductor

Since

$$V = N\left(\frac{1}{4}\ \pi\ d^2\right)L$$

N = number of s.c. filaments = 2400

L = length of each filaments = length of conductor

$$\frac{P_h}{L} = \frac{1}{6}\ N\ \mu_o\ d^3\ J_c(H)\dot{H}_{ext} = \frac{1}{6}\ N\ d^3\ J_c(B)\dot{B}_{ext}$$

<u>Hysteresis Power During 10 min. Charge: with</u>

$$\dot{B}_{ext} = \frac{1.5\ T}{10\ min} = 0.0025\ T/s = \text{constant}$$

The maximum power occurs at $\vec{B} = 0$, since J_c is a minimum.

For the Japanese conductor used in the 1 meter model

$$J_c(0) = 4.93 \times 10^9\ A/m^2$$

Using this value of $J_c(0)$ then,

$$\frac{P_h}{L} = \frac{1}{6}\ (2400)(50\times10^{-6})^3\ (4.73\times10^9)(0.0025)\ \frac{W}{m}$$

$$= 5.9 \times 10^{-4}\ W/m$$

since

$$L \sim 8200\ m, \quad (P_h)_{max} \sim 4.8\ W$$

Hysteresis Power During τ = 45 s Discharge. The maximum power occurs at the maximum value of $[J_c(B)\dot{B}]$. This is at t = 0 (the start of the discharge).

$$\dot{B}_{max} = \frac{1.5T}{6600}\dot{I}_{max} = \frac{1.5T}{6600}\frac{I_o}{L/R} = \frac{1.5T}{L/R} = 0.033 \text{ T/s}$$

$$J_c(1.5T) = 3.27 \times 10^9 \text{ A/m}^2$$

$$\frac{P_h}{L}_{max} = \frac{1}{6}(2400)(50\times10^{-6})^3 (3.27\times10^9)(0.033) \text{ W/m}$$

$$= 5.45\times10^{-3} \text{ W/m}$$

$$(P_h)_{max} \sim 44\text{W}$$

Hysteresis Power During τ = 300 s Discharge

$$\dot{B}_{max} = 0.005 \text{ T/s and } (P_h)_{max} \sim 6.5 \text{ W}$$

Eddy Current Losses

From Brechna, Eq. 4.1.53 (pg 252)

$$\frac{P_e}{L} = \frac{\pi}{4} D^2 \frac{\dot{B}\, l_p}{2\pi} \frac{w-d}{w} + \frac{C}{R} \frac{1}{\rho_{matrix}}$$

where

D = diameter of filament bundle

l_p = twist length

w = distance between adjacent filaments

d = filament diameter

C = thickness of matrix outside bundle

$\bar{R}$ = average radius of outside bundle

ρ_{matrix} = matrix resistivity

For the proposed conductor

$d = 50\ \mu m$

w = (is not known so assumed to be 75 μm)

l_p = assumed = 1 cm

$C = 0.326$ cm

$\bar{R} = 0.682$ cm

$D = 0.356$ cm

$\rho_{matrix} = 0.006 \times 10^{-8}\ \Omega\text{-m}$ at 4.2K

So,

$$\frac{P_e}{L} = \frac{\pi}{4}\left[\frac{(0.00356)(0.01)}{2}\right]^2\left[\frac{75-50}{75} \times 10^{-6} + \frac{0.00326}{0.00682}\right]\frac{B^2}{0.006 \times 10^{-8}}$$

$$= 2.52\text{x}10^{-11}\ (0.33\text{x}10^{-6} + 0.48)\ \frac{\dot{B}^2}{0.006 \times 10^{-8}}$$

$$= 0.201\ \dot{B}^2$$

During Linear 10 min Charge

$\dot{B} = 0.0025$ T/s, $\frac{P_e}{L} = 1.25 \times 10^{-6}$ W/m, and for L ~ 8200 m

P_e ~ 10 mW

During $\tau = 45$ s Discharge

$\dot{B} = 0.033$ T/s and P_e ~ 1.8 W

CONCLUSIONS

Transient field losses in the superconductor are negligible for a bath-cooled coil.

APPENDIX F: CDF WINDING AND BANDING

Object

Calculate the winding tension required in the conductor and banding for a pool boiling CDF solenoid.

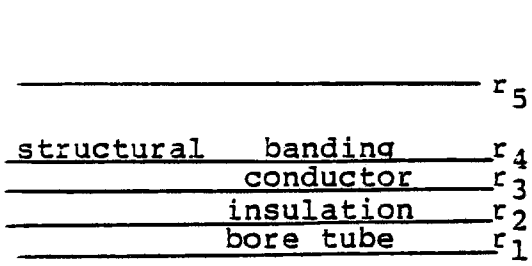

ASSUMPTION

$r_1 \sim r_2 \sim r_3 \ldots r_5$

(A) neglect hoop strength of insulatic

(B) neglect superconductor

c = circumference = $2\pi R$

t_B = thickness of bore tube

t_c = thickness of conductor

w = width of conductor

w' = width of conductor plus insulation

t_{ec} = effective thickness of conductor =

$$= t_c \frac{w}{w'}$$

CALCULATION

Conductor Winding

When the conductor is wound on the bore tube + insulation, the hoop stress σ_c in the conductor is given by

(1) $\sigma_c = \dfrac{P_w R}{t_{ec}}$ $\qquad \mathcal{T}_c = \dfrac{T_c}{w t_c}$, where

T_c = winding tension in the conductor

P_w = average radial pressure on the bore tube due to conductor winding.

Thus

$$p_w = \frac{t_{ec}}{R} \frac{T_c}{wt_c} = \frac{t_c \ (w/w') \ T_c}{R \ wt_c}$$

$$(2) \qquad P_w = \frac{T_c}{w'R}$$

NOTE: This pressure should not exceed the critical pressure for elastic collapse of the bore tube.

With this winding tension the bore tube is in compression and deflects by a distance ΔR_1.

$$\frac{\Delta R_1}{R} = \frac{\Delta_c}{c} = \frac{\sigma}{E} = \frac{P_w R}{E \ t_B}$$

$$\Delta R_1 = \frac{P_w R^2}{Et_B} = \frac{[T_c/w'R] \ R^2}{Et_B}$$

$$\Delta R_1 = \frac{T_c R}{w' t_B E}$$

Banding

Let t_s = thickness of the banding

t_{es} = effective thickness of the banding = $t_s \left(\frac{w}{w'}\right)$

P_s = radial pressure at outside of conductor due to banding

T_s = tension in banding

from (2)

$$P_s = \frac{T_s}{w'R}$$

This causes both the conductor and bore tube to change radius by an amount

$$\Delta R_2 = \frac{T_s R}{w'(t_B + t_{ec})\ E}$$

Thus the total change in the bore tube radius after winding and banding is

$$\Delta R_1 + \Delta R_2 = \frac{T_c R}{w' t_B E} + \frac{T_s R}{w'(t_B + t_{ec}) E}$$

The total stress in thee bore tube after winding and banding is

$$(2) \quad \sigma_B = E\left(\frac{\Delta R_1 + \Delta R_2}{R}\right)$$

Insulation Effects

Under a radial pressure P the insulation changes radial thickness by an amount

$$\Delta R = t_I \left(\frac{P}{E_I}\right)$$

for

P = 150 psi (1.03 MPa)

$E_I \sim 1.5 \times 10^6$ psi (10.3 GPa) [half that of G-10]

t_I = insulation thickness = 0.24" (6.0mm)

$$\Delta R = (0.24)\left[\frac{150}{1.5 \times 10^6}\right] = 2.4 \times 10^{-5} \text{ inches } (0.6 \times 10^{-6} \text{ m})$$

This change in radius due to the compressive load on the insulation is negligible.

Differential thermal contraction of the insulation relative to aluminum 300 K - 4 K

$\Delta R_3 \sim 0.003$ (t) $\Delta L/L = 0.0071$ for G-10 fiberglass epoxy laminates $\perp$ to fiber direction

$\Delta R_3 \sim 0.003(0.25")$ $\Delta L/L = 0.004$ for 5083 aluminum

$\Delta R_3 \sim 0.001$ (negligible)

<u>Magnet on Effects</u>

When the magnet is energized, a pressure of p_m = 130 psi (0.896 MPa) appears at the conductor. Assume this acts at the inner radius of the conductor. If the conductor stays in contact with the bore tube, then the entire coil moves out radially by ΔR_4.

$$\Delta R_4 = \frac{p_m R^2}{E(t_{ec} + t_{es} + t_B + t_o)}$$

where t_o = the thickness of the outside wall of the He vessel. Since the outside wall of the He vessel is attached after the coil and banding is applied, then the maximum change in radius of the bore tube occurs if the winding preload is completely relaxed

(i.e., when the magnet is excited and the conductor just starts to pull away from the bore tube). When this occurs, the following is true:

$$\frac{\Delta R_B'}{R} = \frac{\Delta R_o'}{R}$$ (no relative motion of outer He wall with respect to bore tube), and

$$\frac{(\sigma_B - \sigma_B')}{E} = \frac{\sigma_o'}{E}$$

or

(3) $\sigma_B - \sigma_B' = \sigma_o'$

where σ_B = initial stress in bore tube after winding and banding

σ_B' = stress in bore tube just as conductor and banding pulls away from bore tube when magnet is excited.

σ_o' = stress in outer He shell just as conductor and banding pull away from bore tube

(4) $\sigma_B' \, t_B = \sigma_o' \, t_o$ (equilibrium condition for forces)

Combining Eq. (3) and (4)

$$\sigma_B - \sigma_B' = \sigma_B' \, (t_B/t_o)$$

$$\sigma_B' = \sigma_B \left(\frac{t_o}{t_B + t_o} \right)$$

then

$$\frac{\Delta R_B'}{R} = \frac{\sigma_B - \sigma_B[t_o/(t_B + t_o)]}{E_o} = \frac{\sigma_B}{E} = \left(\frac{t_B}{t_B + t_o}\right)$$

or

$$\Delta R_B' = \frac{\sigma_B}{E} R \left(\frac{t_B}{t_B + t_o}\right)$$

Then the condition that the conductor does not break free of the bore tube is

$$\Delta R_B' \geq \Delta R_4$$

or

$$\frac{\sigma_B R}{E}\left(\frac{t_B}{t_B+t_o}\right) \geq \frac{P_m R^2}{E(t_{ec} + t_{es} + t_B + t_o)}$$

$$\sigma_B \geq \frac{P_m R}{(t_{ec}+t_{es}+t_B+t_o)}\left(\frac{t_B + t_o}{t_B}\right)$$

or substituting from Eq. (2)

$$\frac{E(\Delta R_1 + \Delta R_2)}{R} \geq \frac{P_m R}{(t_{ec} + t_{ees} + t_B + t_o)} \frac{(t_B + t_o)}{t_B}$$

or substituting from Eq. (1)

$$\frac{T_c}{w' t_B} + \frac{T_s}{w'(t_B+t_{ec})} \geq \frac{P_m R}{(t_{ec}+t_{es}+t_B+t_o)}\left(\frac{t_B + t_o}{t_B}\right)$$

solving for the banding tension gives

$$(6) \quad T_s \geq \left[\frac{P_m R}{(t_{ec}+t_{es}+t_B+t_o)} \left(\frac{t_B + t_o}{t_B} \right) - \frac{T_c}{w' t_B} \right] w'(t_B + t_{ec})$$

for

p_m = 130 psi (0.896 MPa)

R = 59.5" (1511 mm)

w = 0.167" (4.25 mm)

w' = 0.217" (5.5 mm)

t_B = 5/8" = 0.625" (15.9 mm)

t_o = 0.313" (7.9 mm)

t_c = 0.740" (18.8 mm)

t_s = 0.555" (14.1 mm)

t_{ec} = 0.572" (14.5 mm)

t_{es} = 0.429" (10.9 mm)

Then using

$T_c = \sigma_a A = \sigma_a wtc$ with

σ_a = 1000 psi (6.7 MPa) for the allowable stress in the high purity aluminum stabilizer the required winding tension of the conductor is:

T_c = (1000)(0.167)(0.740) = 123 lbs tension (550 N)

and the required banding tension is:

$$T_s \geq \left\{ \left[\frac{(130)(59.5)}{(.572+.429+.625+.313} \right] \left(\frac{0.625+0.313}{.625} \right) - \frac{123}{.217 x .625} \right\} (0.217)(.625+.572)$$

$$T_s \geq 1320 \text{ lbs}$$

This corresponds to a stress of 14200 psi in the banding which is comfortably low. The stress-strain behavior of the EFT conductor is shown in Fig. E(1).

Conclusion

With a winding tension of 123 lbs (550 N) in the conductor and 1320 lbs (5871 N) in the banding, then the conductor should remain in contact with the bore tube at full magnet excitation of 1.5 T. Note, however, that due to the high tension required in the banding, it is probably desirable to use several layers rather than just one layer of banding.

APPENDIX G: AXIAL LOAD ANALYSIS

Required Spacing for Insulator

Moment of inertia for the chosen pure aluminum stabilized conductor

$$= \frac{1}{12} bh^3$$

$$= \frac{1}{12} (0.74)(0.167)^3$$

$$= 2.89 \times 10^{-4} \text{ in}^4$$

the local electromagnetic force acting on per unit length of the conductor is

$$\vec{F} = \vec{I} \times \vec{B}$$

I = operating current of magnet = 6600 A

B = max. radial field in coil (near the end) = 0.9 T

$$F = 6600 \times 0.9 \ \frac{N}{m}$$

$$= 6600 \times 0.9 \times 0.06852 \times \frac{1}{12} \text{ lb/in}$$

$$= 33.9 \text{ lb/in}$$

Using simple beam analysis, (case 2d on p. 100 of Roarke & Young 5th ed.), uniform loading and fixed at both ends.

Max. bending moment $M = \frac{w\ell^2}{12}$

Max. bending stress $_{max} = \frac{Mc}{I} = \frac{w\ell^2 c}{12I} = 811\ \ell^2$

Let $\sigma_{max} = 400$ psi

$$\ell^2 = \frac{400}{811} \qquad \text{and}$$

$$\ell = 0.70"$$

For this spacing the deflection $y = -\frac{w\ell^4}{384\ E\ I} = 7.3 \times 10^{-6}$

APPENDIX H: MAGNETIC FORCES ON DETECTOR COMPONENTS

Magnetic Force in Ideal Case

If the iron surface of the end plug and the end wall were completely flat and uniform, with infinite permeability iron, and if the end of the coil conductor were up to the iron surface, the magnetic field inside the coil would be in the axial direction and uniform. There would be no axial forces acting on the coil. There would, however, be a radial force on the conductors that would produce a hoop load in the coil, but there would be no net radial force on the coil. In this case the total inward force on the end plug will be given by

$$\frac{B_o^{\,2}}{2\mu_o} \times \pi R^2$$

which is about 645 metric tons, for a central field of $B_o = 1.5$ T and end plug radius of $R = 1.5$ m.

Magnetic Force in Real Cases

In reality the iron has finite permeability, there are holes in the end plug plates, and a gap between the iron surface and the end of the coil conductor as shown in Fig. H(1). This introduces a radial field component B_r near the end of the coil, which will cause an axial force on the coil. In order to make more uniform field at the end, and reduce the fringing field and its resulting axial force, several iron plates are introduced into bore of the coil.

However, if the coil is not coaxial with these plates, or if the coils is not made axially symmetric, then there will be a net radial decentering force on the coil. For the proposed 4 plates the axial force F_z is directed toward the longitudinal center [downward in Fig. H(1)] of the coil. This compressive force could be made zero or tensile by increasing the number of plates.

If the coil is displaced axially from the center position, then there is unbalance between two forces at the ends, and that will cause an axial decentering force. In our case, the force between the iron and the end of the coil, where a radial magnetic field component exists, is repulsive in the axial direction. The more the coil moves away from the one end, the stronger the repulsive force becomes. Therefore, if the coil is displaced axially, the coil will not be pulled to the pole piece where the gap is decreasing but rather the coil will be pushed from the other end of the coil, where the gap is increasing. This action may introduce a rotational instability.

We note that this situation is different than for example the cyclotron magnet shown in Fig. H(2). The radial field component in this case at the coil is inward. The resultant force is toward the steel and the coil is pulled toward the iron yoke.

The Total Axial Force on the Magnet System

Assume a cylindrically symmetric magnet system with fairly uniform field B_o on the median plane inside the coil radius R, as shown in Fig. H(3).. If we do the surface integration of Maxwell stress on the median plane of this figure and on the surface of a hemisphere with infinite radius

then

$$\frac{B^2}{2\mu}\,ds = \int_{\text{coil}} \frac{B_o{}^2}{2\mu_o}\,ds + \int_{\text{yoke}} \frac{B^2}{2\mu_o{}^2\mu'}\,ds + \int_{\text{between}} \frac{B^2}{2\mu}\,ds - \int_{\text{bore}} \frac{B_o{}^2}{2\mu_o}\,ds = 0$$

or

$$\frac{B_o{}^2}{2\mu_o}\,dS = \frac{\pi R^2}{2\mu_o}\,B^2{}_o = \Sigma \text{ (axial forces on components of magnets)}$$

bore

The major components for the summation includes the axial forces on the coil, the end plug and the end wall. There is also some small forces on the surfaces of the yoke and the central calorimeter.

Even if the shape of the end plug and/or the geometry at the end of the coil is changed, the total axial force of the components is the same, as long as the magnetic field B_o is kept the same by adjusting the magnet current. The total axial force is the same as in the ideal cas ine.

In the ideal case with no holes in the end plug, the axial force on the end plug is 645 metric tons as explained earlier. The axial force distribution for several other cases was

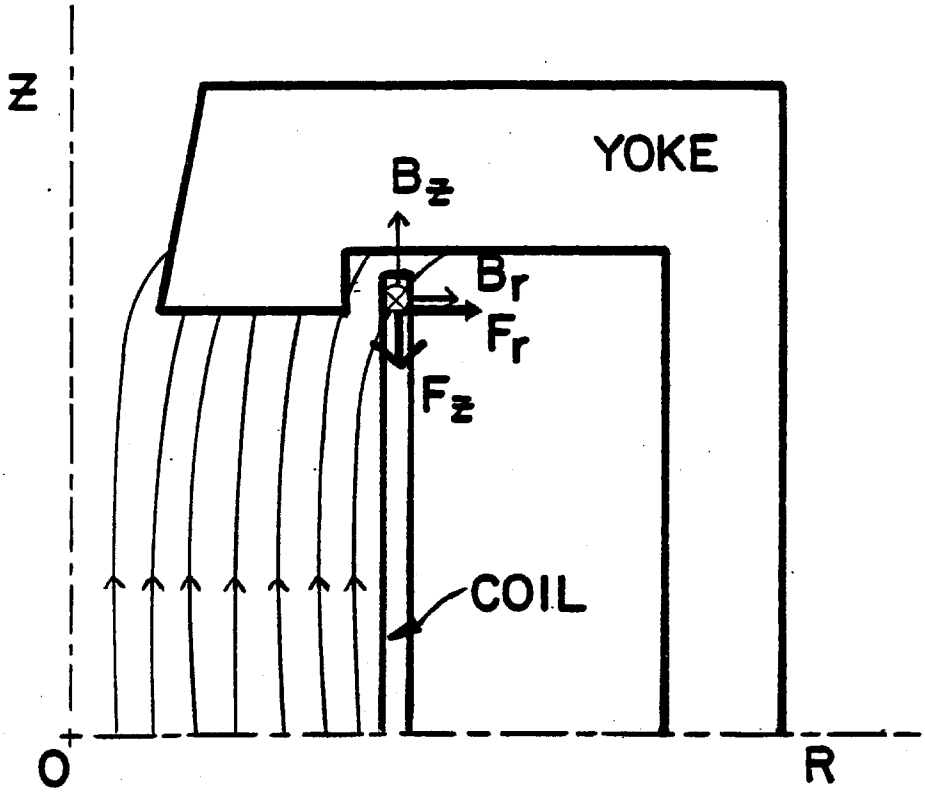

Fig. H(1). Iron-coil geometry (one quadrant) for CDF solenoid

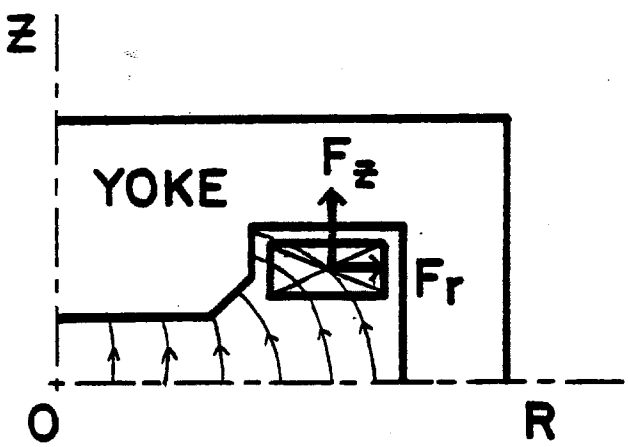

Fig. H(2). Iron-coil geometry for cyclotron magnet

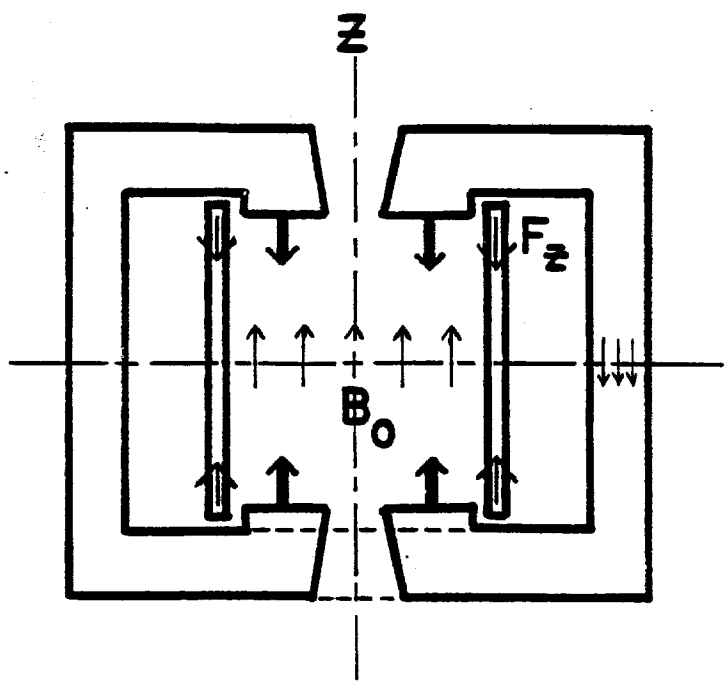

Fig. H(3). Iron-coil geometry (four quadrants) for CDF solenoid

calculated with FORGY and is summarized in Table H(1). The ideal case with finite permeability is listed as "CSL0126" with a total force of 679 metric tons. In the design, "A12 CDF" the summation of the axial forces of the coil, the end plug, and the end wall is about 630 metric tons. The coil has an axial force of 123 metric tons, and the end plug has an axial force of about 480 metric tons. In the extreme when there is no yoke, the axial forces on the coil is about 700 metric tons for B_o = 1.5T as is shown as normalized "A200". In this case it is bigger than 645 metric tons because the return flux is not contained in the yoke.

Axial Force on Coil

The axial force on the coil for different iron/coil geometries was calculated using TRIM, and the results are summarized in Table H(2).* The proposed design "J13" has the axial gap of 4.75" and the radial gap of 3.5" with the resulting axial force of 88 metric tons.

Number of Plates in Magnet Bore

These effects were studied in detail with the "505 CBD" series of TRIM runs. In this old series, the thickness of the

*R. Yamada, CDF Coil Engineering Design Report 16, Fermilab Internal Report (unpublished) (1981).

TABLE H(1). The distribution of axial forces among the components of solenoid magnet. The major parameters are 3 m ϕ, 5 m long, 1.5 Tesla. All forces A_z are given in metric tons. All runs are calculated with finite permeability.

Run No.	Major Characteristics	B_o (Tesla)	R (in.)	A_z on Coil	A_z on End Plug	A_z on End Wall	A_z on Calorimeter	A_z on Back Leg	TOTAL A_z
A12	10° opening	1,491	60.5	-123.2	-481.5	-26.3	+ 0.5	∿ + 0.2	- 630.3
	∿ 15° opening	1.495	60.0	- 77.5	-591.9		+ 0.5	(∿ + 0.2)	- 668.7
A200	Air core	∿ 1.3	60.0	-537.5					
(Normalized A200)		(normalized to 1.49)		(-706.1)					(- 706.1)
CSL0126	Ideal Case No Hole	1.51	60.0	- 4.2	-678.7	∿ 0			- 678.7

TABLE H(2). RUN SUMMARY OF AXIAL FORCES OF COIL

RUN	NO. OF RE-ENTRANT PLATES	GAP AROUND END PLUG	AXIAL GAP	RADIAL GAP	RE-ENTRANT PLATE GAP	AXIAL FORCE OF COIL (N)	COMMENTS
A12	4	1"	5.75"	4.5"	0.75"	-120.8×10^4	Standard, same as A12 with iron block added at end of end wall.
A13	4	1"	5.75"	4.5"	0.75"	-124.4×10^4	
D13	5	1"	5.75"	4.5"	0.75"	-76.5×10^4	Added one more re-entrant plate
E13	4	1"	4.75"	4.5"	0.75"	-95.9×10^4	1" longer coil at one side
F13	4	1"	5.75"	3.5"	0.75"	-105.7×10^4	1" smaller radius coil
G13	4	1"	5.75"	4.5"	0.5"	-119.7×10^4	0.5" re-entrant plate gap
J13	4	1"	4.75"	3.5"	0.75"	-86.4×10^4	Proposed design

re-entrant iron plates is 2 inches with a half inch spacing between them. The width of the coil conductor is one inch and the radial gap is 4 inches. There is no air gap between the end plug and the end wall as in the present design.

For cases with three, four, five and seven plates, the axial gap D is changed and the resultant axial forces on the coil are shown in Fig. H(4). Except for the seven plate case all the axial forces are negative, indicating a compressive force on the coil. In the case of seven plates, the integrated total force becomes positive, meaning a tensile force on the coil. As can be seen in Fig. H(4), there exists cases with zero total axial force on the coil, if we can afford to install as many re-entrant plates as needed. In this case the integrated axial force will be zero, but locally there are regions in compression and regions in tensional within the coil.

In this series the axial spring constant is about 50 metric tons/inch for all of the cases independent of the number of re-entrant plates.

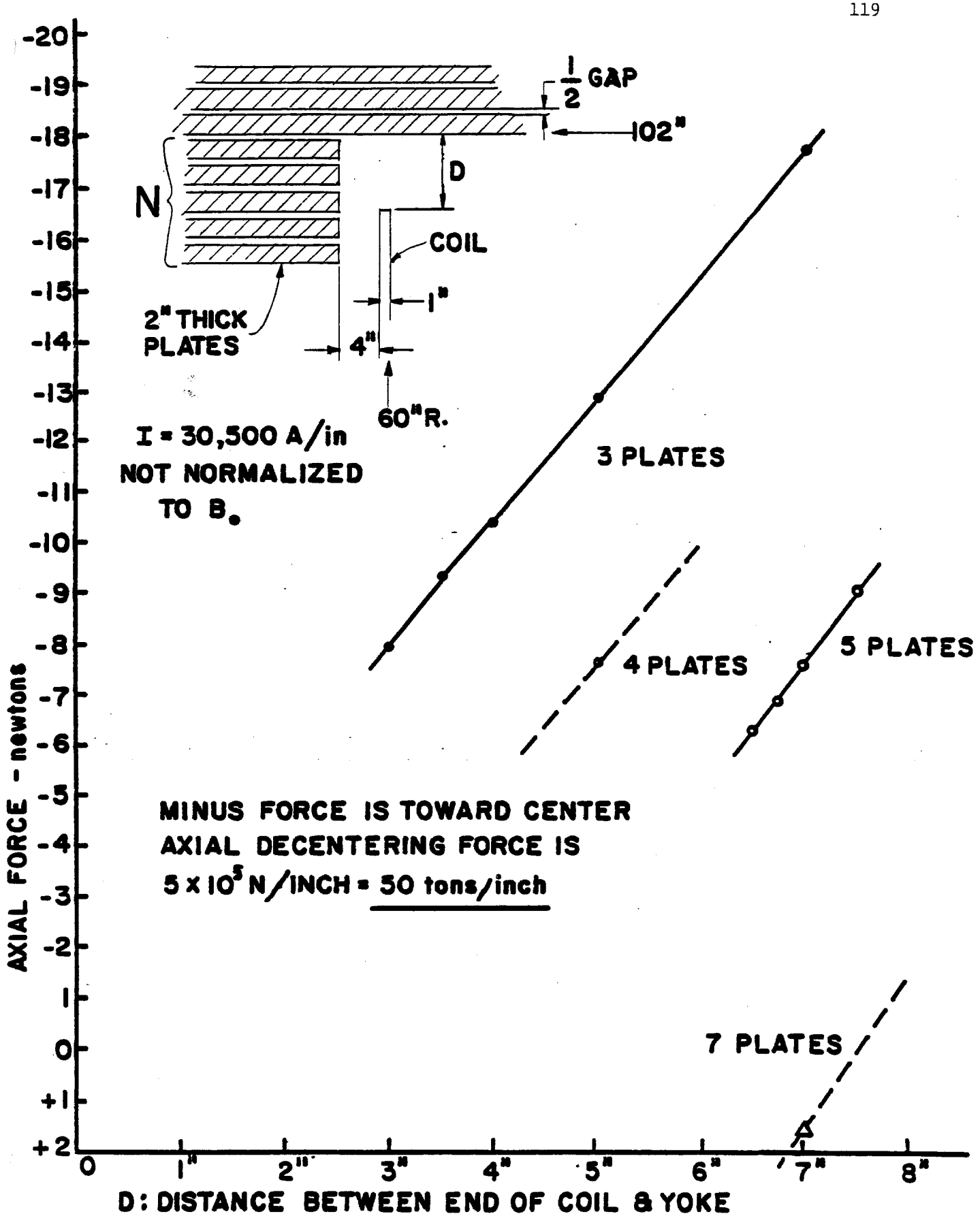

Fig. H(4). Axial force on CDF solenoid as a function of axial coil-iron separation and number of plates

APPENDIX I: STRESS ANALYSIS OF HELIUM VESSEL

Introduction

The helium vessel is the annular container which houses the superconducting coil and its helium bath. It provides the means by which the electromagnetic decentering forces are transmitted to the rest of the structure, and must withstand the internal pressure which could result from a rapid coil discharge. In addition it must perform these functions in a minimal amount of physical space with maximum radiation transparency.

In the design of this vessel, analytic calculations*, ASME Boiler and Pressure Vessel Code**, as well as the finite element numerical method were used. In the components whose design did not require consideration of elastic stability, stresses were not allowed to exceed those consistent with the Code. The finite element calculations were done with the ANSYS large-scale finite element program as installed at Fermilab.

The proposed helium vessel geometry is shown in Fig. I(1). This vessel consists of:

* Boresi, A.P. , Sidebottom, O.M., Seely, F.B., Smith, J.O., "Advanced Mechanics of Materials," Third Edition, Wiley, 1978.

**ASME Boiler & Pressure Vessel Code, Sect. VIII, Div. 1.

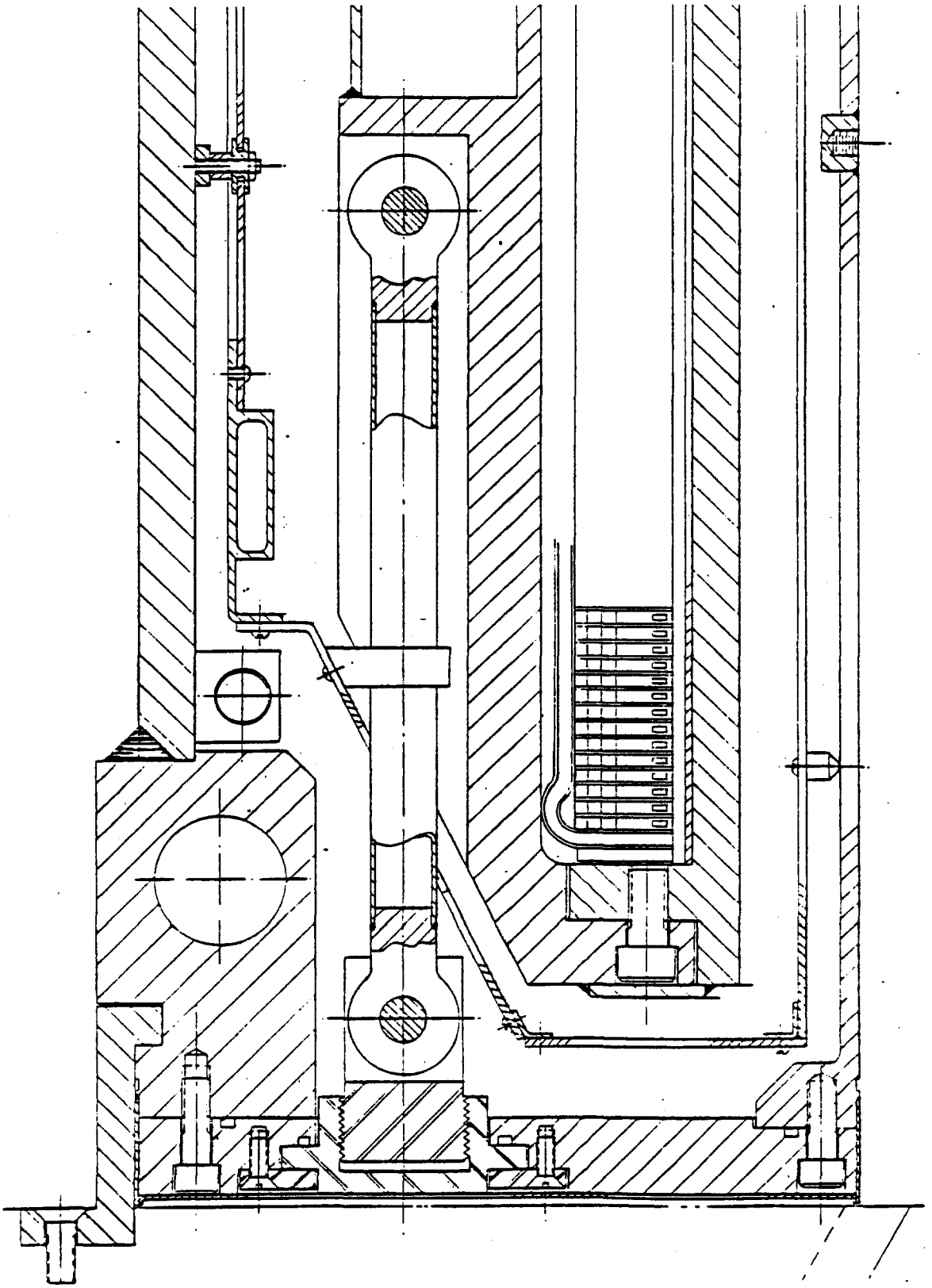

Fig. I(1). Proposed helium vessel end ring geometry

1. An outer cylindrical shell of 5/16" (7.9 mm) 5083-0 aluminum, with a mean radius of 60.84" (154.5 mm).

2. An inner cylindrical shell of 5/8" (16 mm) 5083-0 aluminum, with a mean radius of 58.312" (1481 mm).

3. Two two-piece 5083-0 aluminum end rings.

The vessel shells are sized to withstand the pressure which could be generated by a rapid coil discharge. The inner shell (coil bobbin) must also support the pressure produced by winding the coil and banding. The two-piece end rings provide a means of assembling the vessel shells, and function as the stiffening rings to which the metallic coil supports are attached. Additional stability of the inner shell is achieved by connecting the shells in the center with a stiffening ring. The outer shell has welded to its exterior a 4" semi-circular reservoir of 0.12" (3 mm) thick aluminum, which subtends an angular region of 3.8°.

The analysis was intended to verify the feasibility of the basic helium vessel design through the use of pressure vessel calculations and idealized finite element models employing axisymmetric and beam characteristics. No attempt was made to accurately model in three dimensions areas of highly localized stress, such at the bolt hole/flange region in the end rings, however, these stresses can be estimated fairly accurately from the axisymmetric model we used.

The finite element calculations were performed with the following basic models and loadings:

1. Two-dimensional outer shell reservoir model;Pressure loading.
2. Axisymmetric model of shells and end rings, without reservoir; Pressure loading, axial electromagnetic loading.
3. Three-dimensional beam model; Radial and axial electromagnetic loading.

The axisymmetric model was based on an earlier vessel design, which differs slightly from the vessel as currently proposed. A later section of this appendix will deal with the effects of these small differences on the calculated stresses.

It is important to note that the vessel cross section of Fig. I(1) represents the smallest end ring cross section in the structure, which occurs only near the axial support locations. The same is true of the earlier geometry. Thus the following analysis is conservative in this respect.

Allowable Stress and Failure Modes

The requirement of maximum radiation transparency has led to the choice of 5083 aluminum alloy for the helium vessel material. This alloy is non-heat treatable and thus has a very high weld efficiency.

Material properties at 4.2K for this alloy are available in Appendix B. The Code does not specify maximum allowable stresses for materials at 4.2K. However, by observing the safety factor which the Code applies to room temperature properties, a maximum

allowable stress for 5083 aluminum at 4.2K can be estimated consistent with the Code philosophy.

If

$$K = \frac{\sigma_T}{S} \tag{1}$$

where K = ASME Code safety factor

σ = Yield strength of 5083-0 Al at 300K = 18 ksi

S = Maximum allowable stress at room temperature as given in ASME Code = 10 ksi

then,

$$K = \frac{18}{10}\frac{\text{ksi}}{\text{ksi}}$$

$$K = 1.8$$

Applying this safety factor to the yield strength at 4.2K as given in Appendix B,

$$S_{4.2} = \frac{\sigma_{4.2}}{K} \tag{2}$$

where $S_{4.2}$ = maximum allowable stress at 4.2K

$\sigma_{4.2}$ = yield strength at 4.2k = 25 ksi

then,

$$S_{4.2} = \frac{25 \text{ ksi}}{1.8}$$

$$S_{4.2} = 14 \text{ ksi}$$

Stresses in the helium vessel should not exceed 14 ksi (96.5 MPa) to maintain consistency with the Code.

The evaluation of the finite element results was based on the von Mises effective stress criterion*, a failure criterion shown to be in good agreement with experimental results for ductile materials. The maximum allowable von Mises effective stress was taken to be the 14 ksi (96.5 MPa).

The failure mode for the outer vessel shells and end rings is assumed to be material yield. The inner shell, however, must withstand considerable external pressure and elastic instability is the most probable failure mode.

Loading. The helium vessel is subject to electromagnetic forces during normal operation resulting from the interaction of the current sheet and the magnetic field. The force-displacement relationship produces a positive spring constant effect. That is, an offset of the coil from magnetic center produces a force in the direction of the offset which tends to move the current sheet/helium vessel even further from center. For the coil/iron design proposed, these spring constants are 8.7×10^4 lb/in (1.5×10^7 N/m) in the axial direction and 7.0×10^4 lb/in (1.2×10^7 N/m) in the radial direction. For the purpose of analysis,

*C.S. Desai and J.F. Abel, "Introduction to the Finite Element Method," Van Nostrand, NY (1972), p. 45.

it was assumed that the coil, when installed, could be 1 in. (2.54 cm) off of magnetic center in the axial and radial direction.

The helium vessel must also be prevented from failing catastrophically under high internal pressure, such as might be produced by a fast coil discharge or loss of insulating vacuum. Because of the uncertainty of transient effects the helium vessel was designed to withstand a pressure differential of 70 psi (0.5 MPa).

Stress Analysis of Outer Vessel Shell and Reservoir-Pressure Loading. The outer shell must withstand an internal pressure differential of 70 psi (0.5MPa). The ASME Code was used to calculate the minimum shell thickness:

$$t = \frac{pR}{SE - 0.6P} \qquad (3)$$

where t = shell minimum thickness

p = pressure differential

R = inside radius of outer shell

E = joint efficiency

S = maximum allowable stress

Substituting the appropriate values, based on the geometry of Fig. I(1)

$$t = \frac{70(63)}{(14000)(0.95) - 0.6(70)}$$

$$t = 0.33'' \simeq 5/16$$

The above calculation assumes ASME Code specifications will be followed in the preparation and welding of all seams in the vessel shell.

The stresses resulting from the presence of the helium reservoir were determined by constructing a plane strain two-dimensional finite elment model of a cross section based on the geometry of Fig. I(1). A crude half-model was first analyzed, and reactions from this model were applied to a refined grid in the region of interest around the reservoir. As a check of model accuracy, the hoop stress in the outer shell was computed by the formula

$$\sigma = \frac{PR}{t} \qquad (4)$$

where σ = hoop stress

P = pressure differential

R = mean radius of shell

t = shell thickness

This figure was compared to the finite element results far from the reservoir. For the geometry of Fig. I(1), the value of hoop stress from Eq. (4) is 13,629 psi (94.0MPa). The finite element results give the hoop stress as 13,565 psi (93.5 MPa). These figures agree within 0.5%.

The finite element refined model is shown in Fig. I(2). Figure I(3) shows the von Mises effective stress contours at the junction of the reservoir and shell. The maximum stresses do not exceed 13000 psi (90.6 MPa).

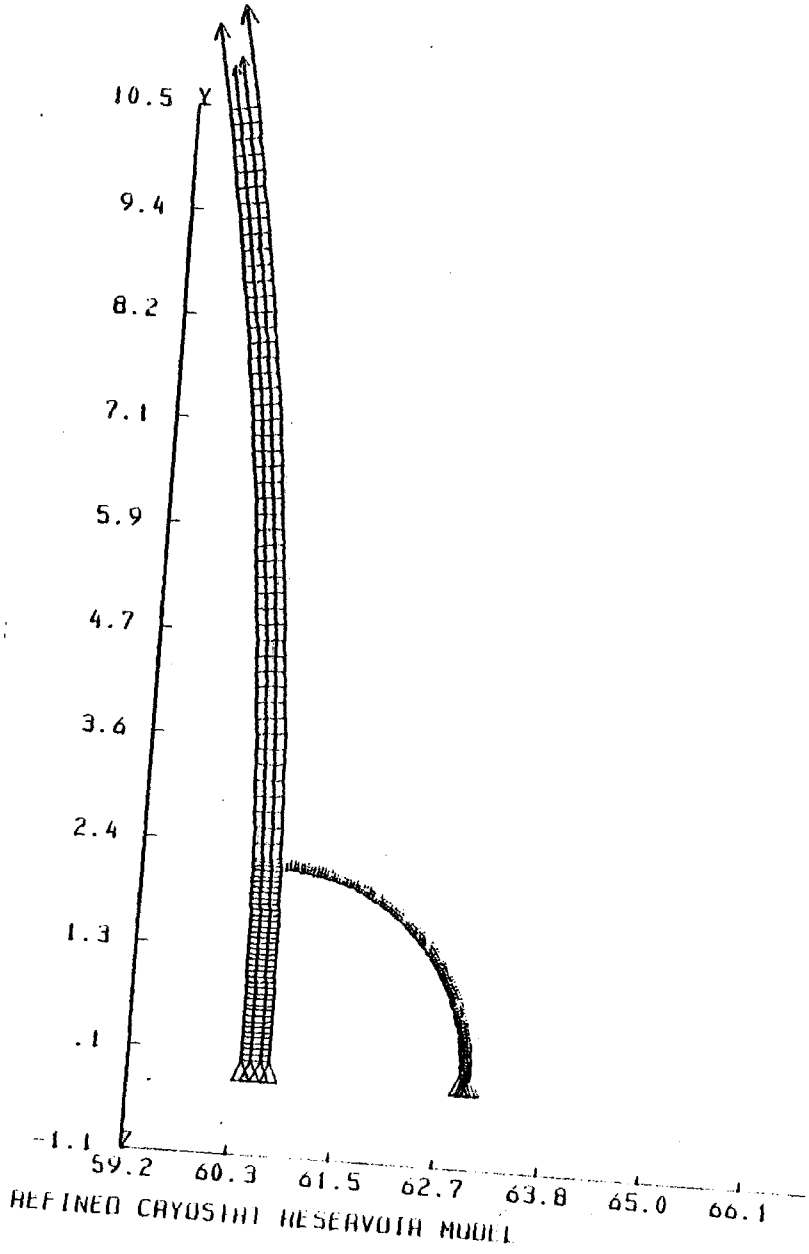

Fig. I(2). Refined reservoir model

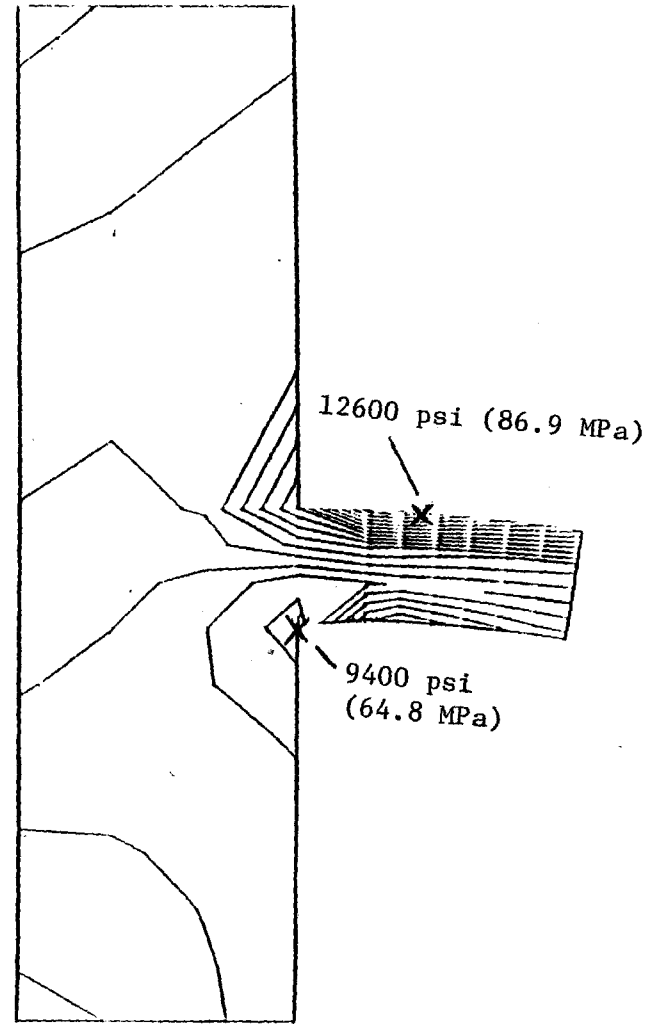

Fig. I(3). Von Meses effective stress at reservoir-shell jenction

Helium Vessel Shells and End Rings--Pressure and Axial Loading

Quasi-axisymmetric finite element closure analysis techniques* were applied to the vessel end ring and shells based on an earlier vessel geometry. Area reduction calculations were used to modify the material properties of the bolt and flange area account for the presence of holes. The nominal bolt preload of 25 ksi (172.0 MPa) was produced by applying a negative thermal gradient to the bolt elements. Interface elements, which can model surface separation, were used to judge the effectiveness of closure at the flange. In addition to axial symmetry, advantage was also taken of the vessel symmetry about the mid-plane. The presence of the outer shell reservoir was neglected.

Figure I(4) illustrates the axisymmetric grid at the end ring. Pressure loading was applied as face pressure on the internal shell and end ring elements. As a model check, the outer and inner shell hoop stresses as predicted by Eq. (4) were compared to the finite element results at a distance of 60 in from the end ring. The figures agreed within 0.3% and 0.2% respectively.

*Perlman, R.M. and Dietrich, D.E. "Comparative Closure Analysis, AIAA/ASME/SAE 16th Structures, Structural Dynamics and Material Conference, Denver, Colorado, May 1975; and also Raju, P.P. "Simplified Analysis of Closure Flanges under Mechanical and Thermal Loads", ASME Paper No. 80-C2/Ne-16, March 1980.

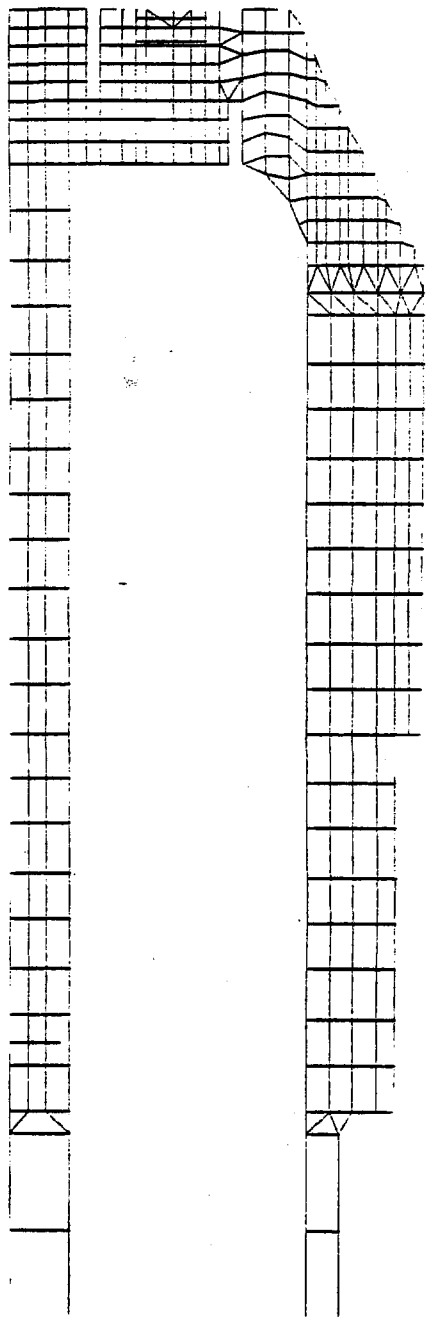

Fig. I(4). Axisymmetric end ring grid

Due to the introduction of fictitious material properties necessary to model bolts and flanges, the finite element stress results within a bolt radius of the bolt circle cannot be considered accurate. The interface elements should give a good indication of closure effectiveness, however.

Figure I(5) show the von Mises stress contours in the inner and outer end ring halves for the 70 psi (0.5) pressure load. A concentration of stress is observed near the curved boundary of the outer ring half. The peak value of 9800 psi (67.6 MPa) is within the design constraints. Interface element results indicate that the flange surfaces remain in contact.

The axial electromagnetic loading was simulated using the same model and adding material with reduced properties to represent the twelve discreet axial support brackets. The loading was applied as face pressures on end ring elements at a radius corresponding to the current sheet location. The dominant stress was the hoop stress, Fig. I(6). The maximum hoop stress was 3500 psi (24.1 MPa). The maximum von Mises effective stress did not exceed 4000 psi (27.6 MPa).

<u>Helium Vessel End Ring--Radial and Axial Loading,Beam Model</u>

A finite element model based on the geometry of Fig. I(1) was constructed using 180 beam elements along a 180° arc at a radius corresponding to the centroid of the end ring section. Shear deformation was considered negligible and the vessel shells were ignored. Rigid elements were used to connect the supports to the ring centroid nodes. These elements allowed the offset of the

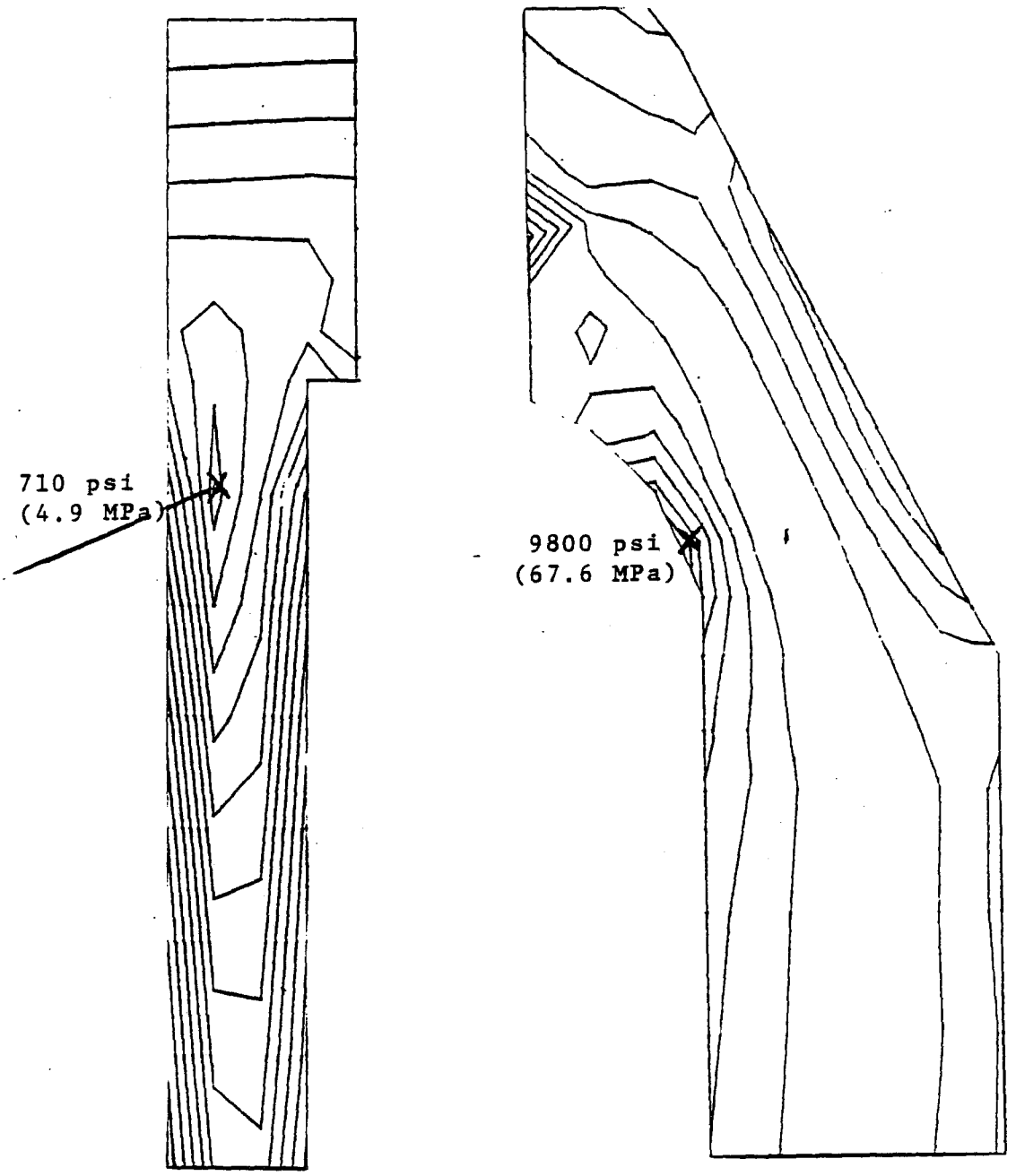

Fig. I(5). Von Mises effective stress in helium vessel end ring for internal pressure of 70 psi (0.49 MPa)

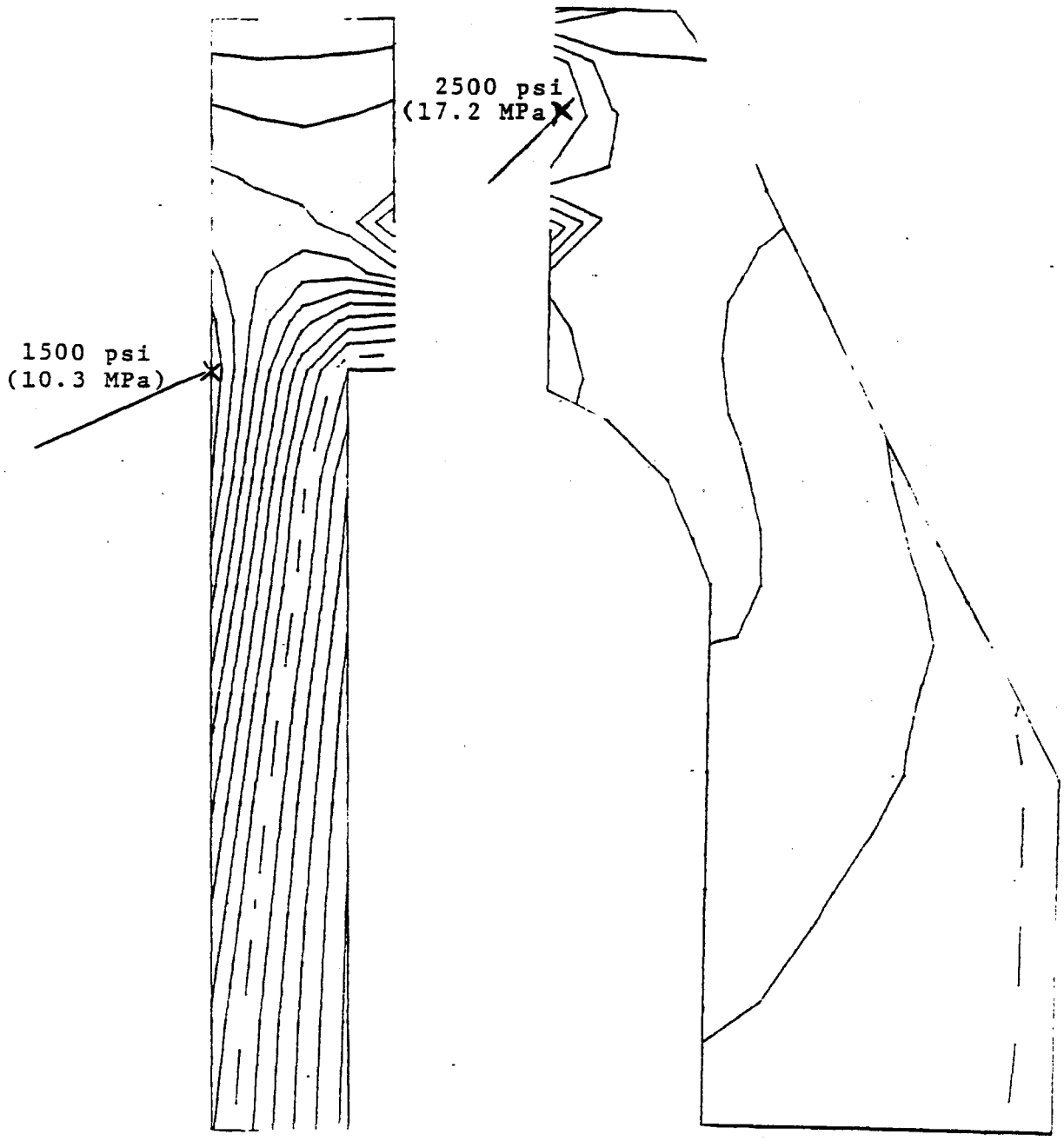

Fig. I(6). Hoop stress in helium vessel end ring for axial loading

support points from the ring centroid to be taken into account. Supports were modeled as spar elements, which allow no bending moments, as is the case with the ball-ended rods of the actual supports. Symmetry constraints were applied at the symmetry plane, and the tangential supports were placed in the position judged to be the least stiff relative to the direction of the radial load. (see Appendix J). Figure I(7) shows the end ring beam model and loading directions. Radial and axial electromagnetic loading were applied as concentrated forces on the beam centroid nodes.

The resulting deformation under the electromagnetic loading is shown in Fig. I(8). Examination of the displacement results shows the ring to be very stiff, with most of the deflection being due to support deformation. The maximum fiber stress was 2440 psi (16.82 MPa). This beam model cannot, by its nature, model regions of localized stress. It is, however, a good indication that the end ring section possesses the stiffness and strength to perform well under the electromagnetic loading.

Extrapolation of Results to Proposed Geometry

There are three differences between the geometry analyzed in the axisymmetric finite element model and the vessel geometry as currently proposed:

1. A decrease in outer shell radius of 0.625" (1.59cm)
2. A decrease in the radius of the curved inner surface of the end ring from ~ 2 cm to ~ 1 cm
3. An expansion of the flange area for the end ring halves

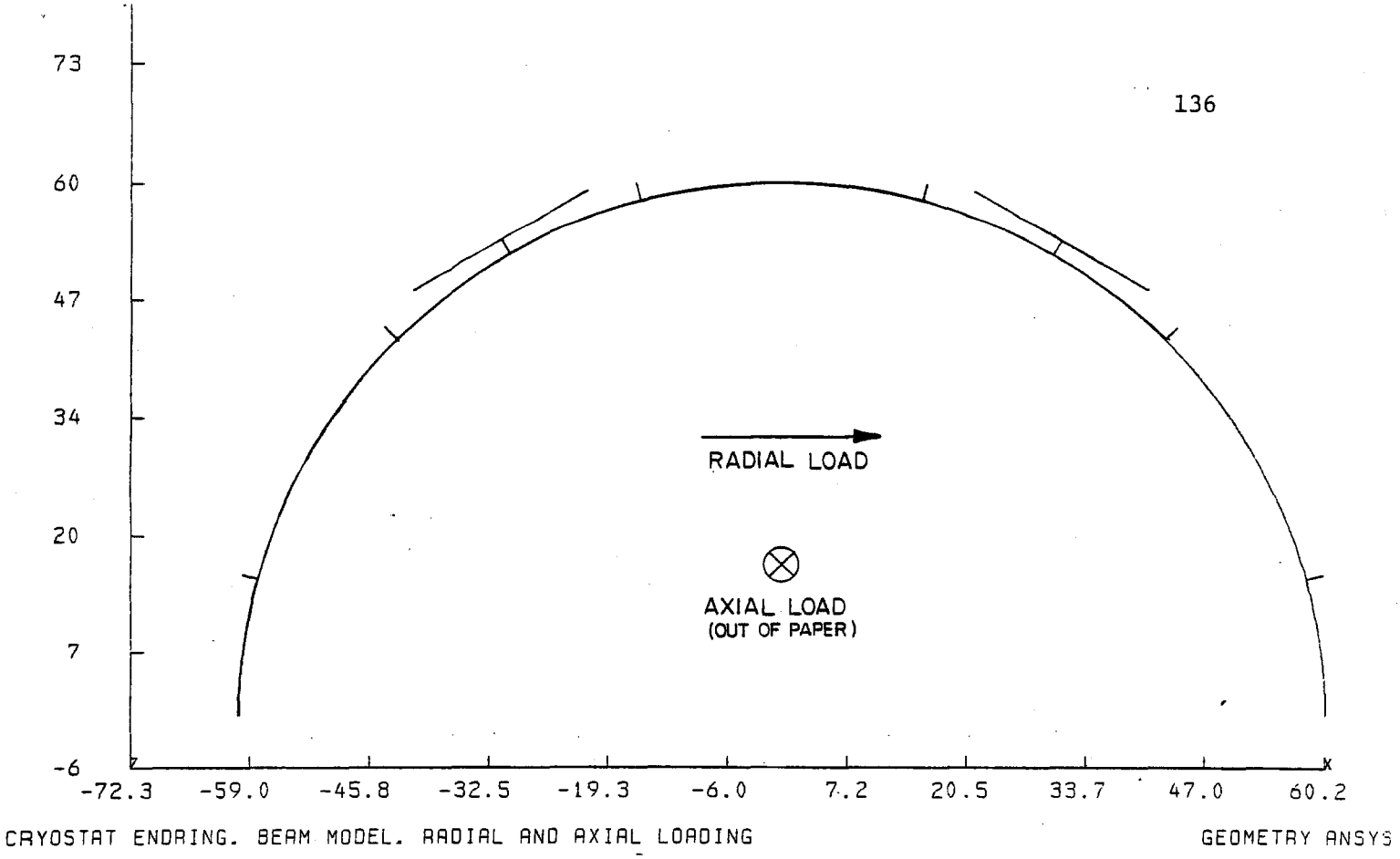

Fig. I(7). End ring beam model and loading direction

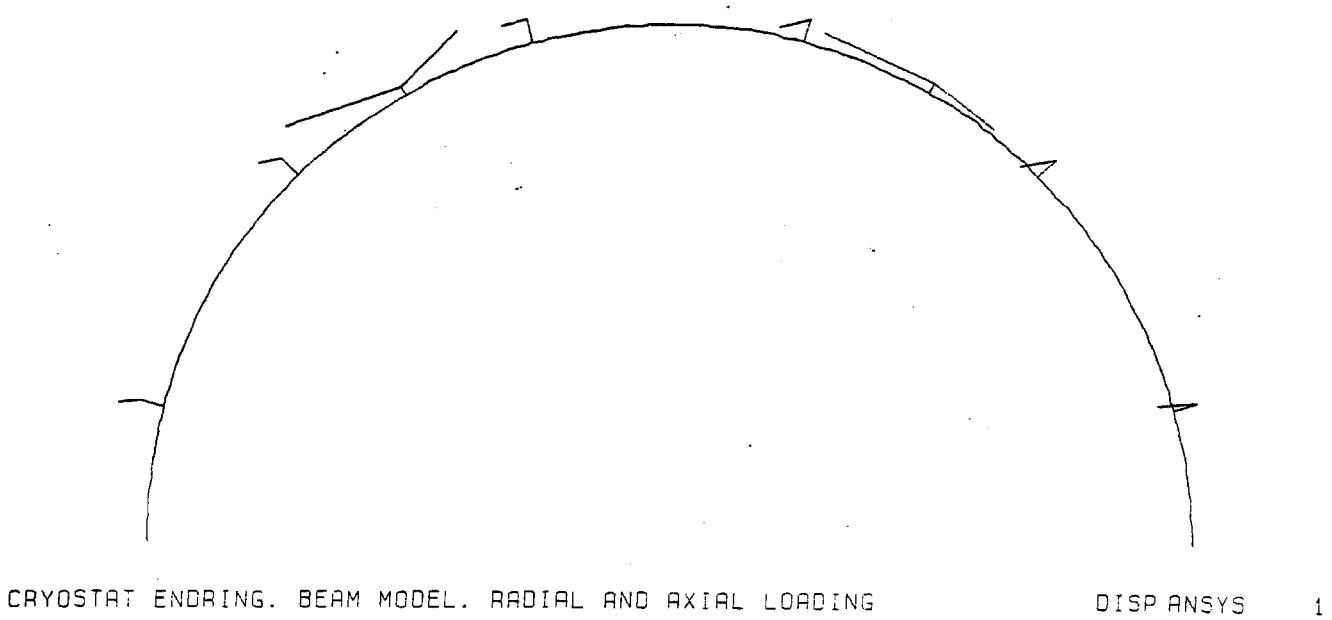

Fig. I(8). End ring distortion under radial and axial load

The outer shell radius change is beneficial in that it reduces the shell hoop stress by decreasing R in Eq. (3).

The curved inner surface of the end ring was shown to be an area of stress concentration for the pressure loading case. A decrease in the radius of this section should increase the stress concentrations. A small area of highly localized stress in excess of 14 ksi (96.5 MPa) may develop here. However, should future finite element work indicate this to be a problem, minor changes in this area should serve to relieve the concentration.

This analysis has made no attempt to determine accurate local stresses near the bolts in the flange area. However, increased flange area in the proposed design can only reduce stresses in this area.

Elastic Stability of the Bore Tube

The bore tube may have to withstand substantial external pressure if the He vessel is pressurized due to a magnet rapid discharge, loss of vacuum accident, etc. The required thickness of the tube under external pressure is determined by the critical pressure for elastic buckling failure. This is given by:

$$p_c = \frac{(0.807)\ E\ t^{2.5}}{L\ r^{1.5}} \left(\frac{1}{1-\nu^2} \right)^{3/4} \qquad \text{Southwall Equation} \qquad (5)$$

where

E = Young's modulus of aluminum = 11.6×10^6 psi for 5083 aluminum at 4 K

ν = Poisson's ration = 0.3

r = radius = 58.31"

t = thickness = 0.625"

L = length between end and center support ring = 95.5"

p_c = critical pressure for collapse

Assumptions

Ignore the effects of the conductor and banding on the bore tube stability (winding tension tends to lower the collapse pressure if field is off but conductor and banding increases substantially the effective thickness of the bore tube since they help hold it round.)

The critical pressure is

$$p_c = \frac{(0.807)(11.6 \times 10^6)(0.625)^{2.5}}{95.5\ (58.31)^{1.5}} \left(\frac{1}{1-(0.3)^2} \right)^{3/4}$$

$$p_c = 73 \text{ psi}$$

Roark recommends in a footnote that 0.8 P_c be used as a reasonable minimum collapse pressure for design purposes. 0.8 P_c = 58.4 psi. However, since we consider this calculation ultra-conservative, we picked 70 psia as the maximum operating pressure of the He vessel, and will verify this number with a more exact calculation at a later date.

APPENDIX J: MECHANICAL ANALYSIS OF SUPPORTS

In this appendix we calculate the stresses and deflections for the support system described in the text. For the purposes of clarity, we assume that all 12 axial and 24 radial supports are made of Inconel 718 which has the following material properties.

	300 K	4 K
σ_{yield}	157 ksi	199 ksi
$\sigma_{ultimate}$	190 ksi	268 ksi

Minimum elongation at 4 K ~ 14%

Young's modulus, E, at 300K ~ 3×10^7 psi

In addition we use magnetic spring rates of 1.3×10^5 lb/in axially and a maximum 7.0×10^4 lb/in radially.

Radial Supports

A schematic of the radial support system at one end of the coil is shown in Fig. J(1). The 12 identical supports are attached tangentially to the coil at 6 points. Each support is assumed to be preloaded so that it always remains in tension and since each support is attached via spherical bearings, stresses due to bending are assumed to be neglible.

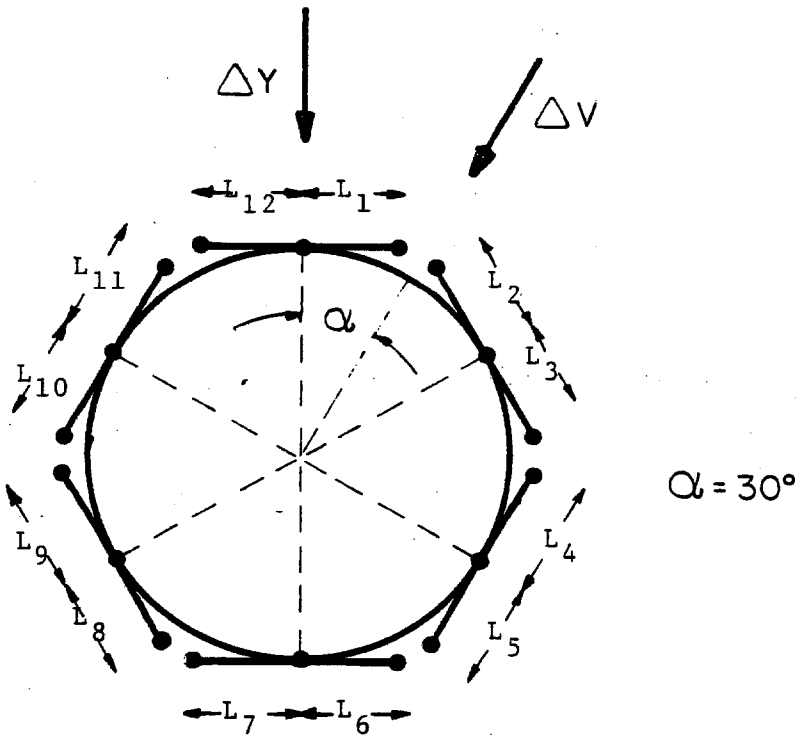

Fig. J(1). Radial Support System

We consider forces acting in two possible radial directions [Y and V in Fig. J(1)] but note that arbitrary azimuthal directions yield results intermediate to these two cases. For purposes of these calculations the coil itself is assumed to be perfectly rigid. Finite element analysis of the coil package with ANSYS indicate this to be a good asumption.

Magnetic force in the Y Direction. Consider a force F_Y that causes the coil to be displaced by a distance ΔY. Then each support changes its length ρ by an amount

$$\Delta L_1 = \Delta L_{12} = \sqrt{L_1^2 + \Delta Y^2} - L_1 \sim \frac{\Delta Y^2}{2L_1}$$

$$\Delta L_2 = \Delta L_{11} = \Delta Y \cos 30^\circ = (\sqrt{3}/2)\ \Delta Y$$

$$\Delta L_3 = \Delta L_{10} = -\Delta Y \cos 30^\circ$$

$$\Delta L_4 = \Delta L_9 = \Delta Y \cos 30^\circ$$

$$\Delta L_5 = \Delta L_8 = -\ \Delta Y \cos 30^\circ$$

$$\Delta L_6 = \Delta L_7 = \Delta L_1$$

$$\vdots$$

etc

The change in tension produced in each support by these deflections is given by

$$T = AE\ (\Delta L/L) \tag{1}$$

where

T = tension produced by displacement ΔL

E = Youngs modulus

A = Cross sectional area of the supports

thus

$$T_1 = \frac{AE}{L} \left(\frac{\Delta Y^2}{2L} \right)$$

$$T_2 = \frac{AE}{L} \quad \frac{\sqrt{3}}{2} \quad \Delta Y$$

$$T_3 = \frac{-AE}{L} \quad \frac{\sqrt{3}}{2} \quad \Delta Y$$

etc.

Noting that since ΔY is small the terms proportional to ΔY^2 are negligible and taking the components of these tensions in the Y direction gives

$$F_Y = 8\ T_2 \cos 30^\circ$$

$$= 8\ \frac{AE}{L} \left(\frac{3}{2}\right)^2 \quad \Delta Y$$

$$= 6\ \frac{AE}{L} \quad \Delta Y \tag{2}$$

We observe that the stiffness of the system in this direction is six times the stiffness of one radial support member.

Next we calculate the required cross sectional area of the supports. If we assume that the magnet is 1" from magnetic center so that a force of $F_Y = 7.0 \times 10^4$ lb acts upon it, then the supports with the highest tension

$$T = \frac{F_Y}{8\cos 30^\circ}$$

$$= \frac{7.0 \times 10^4}{8\left(\sqrt{\frac{3}{2}}\right)}$$

$$= 10100 \text{ lbs}$$

using a working stress of 67 ksi for Inconel 718 it follows that the required cross section area of a support is

$$A = T/\sigma = 10100/67000 = 0.151 \text{ in}^2$$

which corresponds to rods 7/16" in diameter (0.150 in^2). With this choice the spring constant of the support system in the Y direction can be calculated from equation (2) using L = 11.25" yields

$$K_Y = \frac{F_Y}{\Delta Y} = \frac{6AE}{L} = \frac{6(0.150 \text{ in}^2)(3.0 \times 10^7 \text{ lb/in}^2)}{11.25 \text{ in}}$$

$$= 2.4 \times 10^6 \text{ lb/in} \qquad (3)$$

clearly this is large compared to the radial magnetic spring of 7.0×10^4 lbs/in thus the system is stable.

Finally from (3) we can calculate the deflection of the coil assuming that it is 1" from magnetic center

$$\Delta Y = \frac{F_Y}{K_Y} = 0.029 \text{ in} \qquad (4)$$

<u>Magnetic force in the V direction.</u> Here we repeat the previous calculation for forces in the V direction

$$\Delta L_1 = \Delta L_2 = \Delta V \cos 60^\circ$$
$$\Delta L_3 = \Delta L_{12} = -\Delta V \cos 60^\circ$$
$$\Delta L_4 = \Delta L_{11} = \Delta V$$
$$\Delta L_5 = \Delta L_{10} = -\Delta V$$

etc.

thus

$$T_1 = T_2 = \frac{AE}{L} \Delta V \cos 60^\circ$$

$$T_3 = T_{12} = -\frac{AE}{L} \Delta V \cos 60^\circ$$

$$T_4 = T_{11} = \frac{AE}{L} \Delta V$$

$$T_5 = T_{10} = -\frac{AE}{L} \Delta V$$

Thus taking the components of these tensions in the V direction gives

$$F_V = 4\ T_4 + 8\ T_2 \cos 60^\circ = 8\ T_4$$

$$= 8 \frac{AE}{L} \Delta V \tag{5}$$

comparing equation (5) with (2) we see that the support system is even stiffer in this direction. (If the coil were off magnetic center by 1", the $\Delta V = 0.022"$,). The maximum tension that one support supplies is

$$T = \frac{AE}{L} \Delta V$$

which is 1/8 of the total force applied in the V direction. This tension corresponds to a maximum stress of

$$\sigma = \frac{T}{A} = \frac{7.0 \times 10^4}{(8)(0.150)} = 58 \text{ kpsi}$$

Axial Supports

Next we calculate the forces and deflections on the axial support members. If the coil is 1" off magnetic center in the axial direction and the magnetic spring constant is 8.7×10^4 lb/in. Then,

$$F_z = 8.7 \times 10^4 \text{ lb}$$

if this force is divided equally among the 12 axial supports, then

$$T = \frac{8.7 \times 10^4}{12} = 7250 \text{ lbs}$$

The force applied to the supports may be either compressive or tensile.

The required cross section of the supports is given by

$$A = \frac{T}{\sigma_A} = \frac{7250 \text{ lbs}}{6.7 \times 10^4 \text{ lb/in}^2} \simeq 0.11 \text{ in}^2$$

The deflection in the Z direction is

$$\Delta z = \frac{\sigma L}{E} = \frac{6.7 \times 10^4 \text{ psi}}{3 \times 10^7 \text{ psi}} (12.5 \text{ in})$$

$$= 0.028 \text{ in}$$

where we have used L = 12.5" as the length of the axial supports. The axial spring constant of this support system is

$$K_z = \frac{F_z}{\Delta z} = \frac{8.7 \times 10^4 \text{ lbs}}{0.028 \text{ in.}} = 3.1 \times 10^6 \text{ lb/in}$$

is 35 times stiffer than the magnetic spring constant.

Finally, since the axial support may operate in compression, we must consider elastic buckling of the supports. The critical stress in the support which would lead to elastic buckling is given by the Euler formula*

*Roark and Young, "Formulas for Stress and Strain," Fifth Edition, McGraw-Hill, New York (1975), p. 415.

$$\sigma_{crit} = \frac{c\ \pi^2 E}{(L/r)^2}$$

where L = length of the support

r = radius of gyration = I/A

I = moment of inertia

c = constant = 1 for free ends

Then for a support with the following cross section:

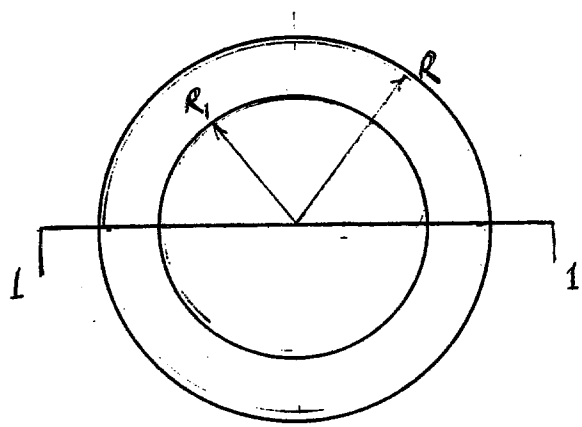

R = 0.44" (7/8" OD)

R_i = 0.395"

the cross sectional area is

$$A = \pi (R^2 - R_i^2) = 0.11 \text{ in}^2$$

thus the radius of gyration about axis 1-1 is

$$r = \frac{1}{2} \quad R^2 + R_i^2$$

$$r = 0.29 \text{ in}$$

using this value in equation (5) and L=11.5" for the effective length of the support

$$\sigma_{crit} = \frac{\pi^2 (3 \times 10^7 \text{ psi})}{(11.5/0.29)^2} = 188 \text{ kPsi}$$

which is above the yield point of the material, thus, the support would fail by yielding rather than elastic buckling in compression.

APPENDIX K: THERMAL ANALYSIS OF RADIATION SHIELDS AND INTERCEPTS

Performance Evaluation of Inner Shield

Heat Input from Shield Supports

$$Q = \frac{A}{L} \int_{77}^{300} K dT \qquad A = \pi r^2 = \pi (0.0047)^2 = 0.000071 \text{ m}^2$$

$$L = 0.111 \text{ m}$$

$$Q = \frac{0.000071 \text{ m}^2}{0.0111 \text{ m}} [141 \text{ W/m}] = 0.901 \text{ watts/support}$$

Number of supports for 30" separation is about 130.

Total Max Q = (130)(0.901) = 117.0 watts

NOTE: Triangular end of support ignored and contact resistance ignored. Both assumptions make analysis very conservative.

Heat Input from Radiation

Radiation losses are about 50 mW/ft^2.

Total area = $(\pi)(D)(L)$

$= (\pi)(9.8)(16.4) = 507 \text{ ft}^2$

Total radiation = 25 watts

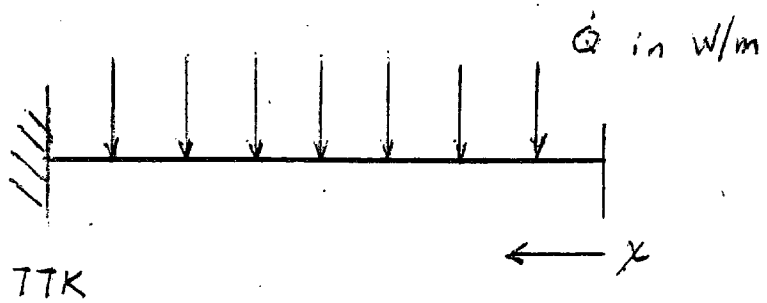

Maximum Center Temperature

$$\dot{Q} = KA \frac{dT}{dX}$$

Linear heat flux is $\frac{25 + 117}{5} = 28.5$ w/m

$$\dot{Q} = (28.5 \text{ W/m})(x) = KA\left(\frac{dT}{dx}\right)$$

$$\int_0^{2.5 \text{ m}} (28.5)(x)dx = \int_{T_{max}}^{77 \text{ K}} kA \, dT \qquad A = \pi(r_o^2 - r_i^2)$$

$$A = 0.030 \text{ m}^2$$

$$\left.\frac{(28.5)(x^2)}{2}\right|_0^{2.5 \text{ m}} = 250 \text{ W/m-K } (0.030 \text{ m}^2) \left.\right|_{T_{max}}^{77 \text{ K}} dT$$

$$T_{max} = 77 + 12 = 89 \text{ K}$$

Performance Evaluation of Outer Shield

Heat Input from G-10 Supports

$$Q = \frac{A}{L} \int_{77}^{300 \text{ K}} KdT = \frac{0.000113 \text{ m}^2}{0.014 \text{ m}} (141 \text{ W/m}) \qquad \text{where } A = \left(\frac{0.012}{2}\right)^2 \pi$$

Q = 1.14 watts/support

There are approximately 140 supports; if spacing is on equilateral triangles with 30" edges.

$$Q_{supports} = (140)(1.14) = 160 \text{ watts}$$

Heat Input From Thermal Radiation

Total area = (11 ft)(16.4 ft) = 566 ft^2

Total radiation at 50 mW/ft^2 is 28.3 watts

Linear Heat Flux

$$\frac{160 \text{ W} + 28.3 \text{ W}}{5 \text{ m}} = 37.7 \text{ W/m}$$

Integrating as before ... $A = \pi(r_o^2 - r_1^2)$

$$\frac{(37.7)(2.5 \text{ m})^2}{2} = 250 \text{ W/m-K } (0.033 \text{ m}^2) \quad \Delta T$$

$$T_{shield\ max} = 77 + 14.3$$

$$T_{max} = 91.3K$$

Thermal Analysis of Conduction Links for LN_2 Intercepts on Magnet Supports

The purpose of this section is to verify that it is reasonable to assume the nitrogen intercepts on the magnet supports operate at 80K. The intercepts on the radial supports are cooled by conduction from the LN_2 shield with flexible copper cable. The axial supports are cooled by the shroud on the

nitrogen shield at the chimney end. The method of analysis is to determine the necessary cross sectional area of the conduction link, and comment on its practicality.

Radial Supports

The nitrogen intercept must provide 3 watts of cooling. The conduction link is made of OFHC Cu braid. The distance from the extrusion is 10 cm.

$$3 \text{ watts} = (500 \text{ W/m-K})(A) \frac{(80-77)\text{K}}{(0.1 \text{ m})}$$

$$A = 2 \text{ cm}^2$$

The cross sectional area of the braid used for the 30" Bubble Chamber coil conversion is 0.42 cm^2. Five braids in parallel is satisfactory, although a single larger braid of sufficient area is readily available.

Axial Supports

The nitrogen intercept must provide 4 watts of cooling. The shield is made of 1100-F aluminum. The distance from the extrusion is about 4.5 cm.

$$2.5 \text{ watts} = (250 \text{ W/m-K})(A) \frac{(80-77)\text{K}}{(0.045 \text{ m})}$$

$$A = 1.5 \text{ cm}^2$$

The shield shroud is 0.32 cm thick, therefore, the most practical solution is to add an aluminum conduction bar to it at each

intercept. A practical bar size is 1" wide by 1/4" thick. The bar can be welded to the shroud before installation.

APPENDIX L: CODE* DESIGN OF VACUUM SHELLS

Inner Vacuum Shell

Shell under external pressure i.e, vacuum annulus at a pressure greater than one atmosphere. Code Paragraph UG-28.

$t = 0.25$ in (6.4 mm), $D = OD = 113$ in (2870 mm)

$L = 198$ in. (5029 mm)

$L/D = 1.75 \sim 1.8$ $D/t = 452 \sim 450$

From Fig. L(1) and L(2), which are Code Fig. UGO-28.0,

A factor = 0.0000775

and

$$P_a = \text{maximum allowable pressure differential}$$
$$= \frac{2\ AE}{3(D/t)}$$

for 6061-T6 aluminum alloy $E = 10.2 \times 10^6$ psi (70.3 GPa) so

$$P_a = 1.17 \text{ psi } (8.09 \text{ kPa}).$$

Shell under internal pressure i.e., vacuum annulus evacuated. Code Paragraph UG-27

$$t_{min} = \text{minimum allowable thickness}$$
$$= \frac{PR}{SE-0.6\ P}$$

where

P = design pressure = 15 psi (103.4 kPa), vacuum load

R = inner radius of shell = 56.25" (1429 mm).

*ASME Boiler and Pressure Vessel Code, Sect. VIII, Div. 1.

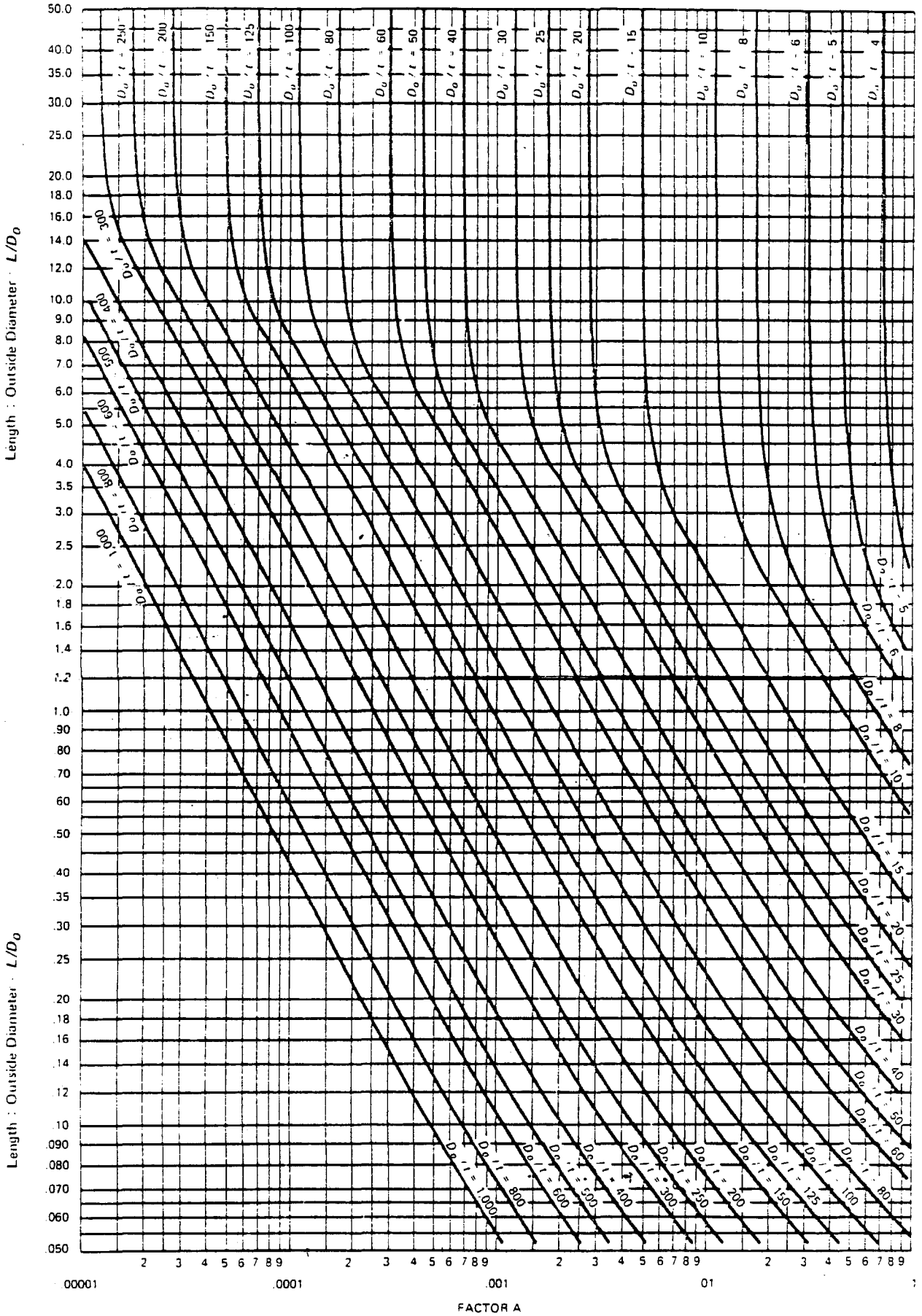

Fig. L(1) From ASME Code

FIG. UGO-28.0 GEOMETRIC CHART FOR CYLINDRICAL VESSELS UNDER EXTERNAL OR COMPRESSIVE LOADING (FOR ALL MATERIALS)

46 0780

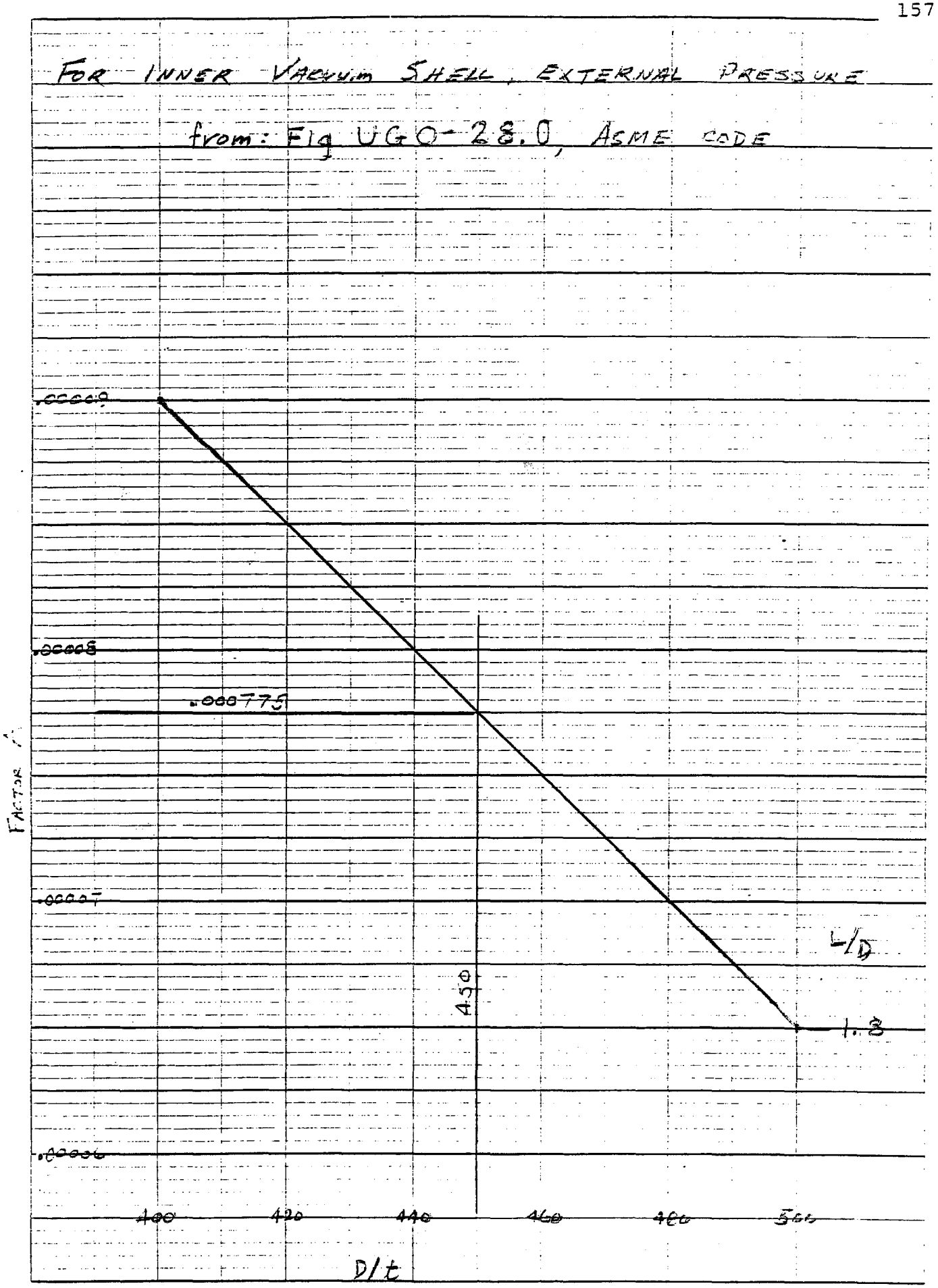

Fig L(2). From ASME Code

S = maximum allowable stress

= 6000 psi (41.4 MPa) for 6061-T6, welded

E = joint efficiency at = 0.80

and

t = 0.177 in (4.48 mm)

from which it is seen that the external pressure criteria dominates the design.

Outer Vacuum Shell

Shell under external pressure , vacuum annulus evacuated. Code Paragraph UG-28.

t = 0.750 in. (19.0 mm)

D = OD = 132 in. (3353 mm)

L = 188 in. (4775 mm)

L/D = 1.42 ~ 1.5, D/t = 176

From Fig. L(1) and L(3), which are Code Fig. UGO-28.0,

A factor = 0.000380

From Fig. L(4) and L(5), which is Code Fig. UNF-28.31, for 6061-T6, welded

B factor = 1900

and

P_a = maximum allowable pressure differential

$$= \frac{4B}{3(D/t)} = 14.4 \text{ psi } (99.29 \text{ kPa})$$

46 0780

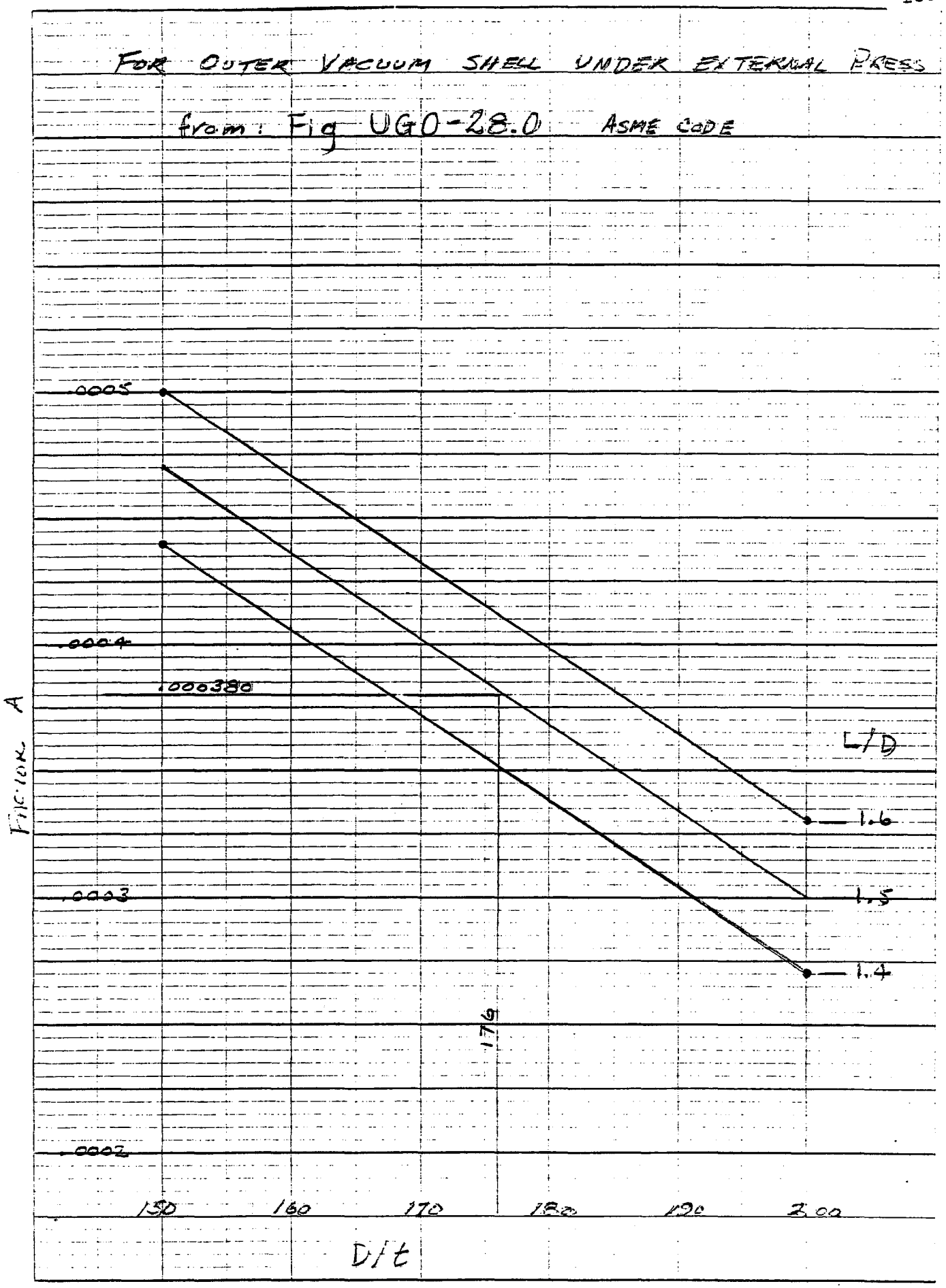

Fig. L(3). From ASME Code

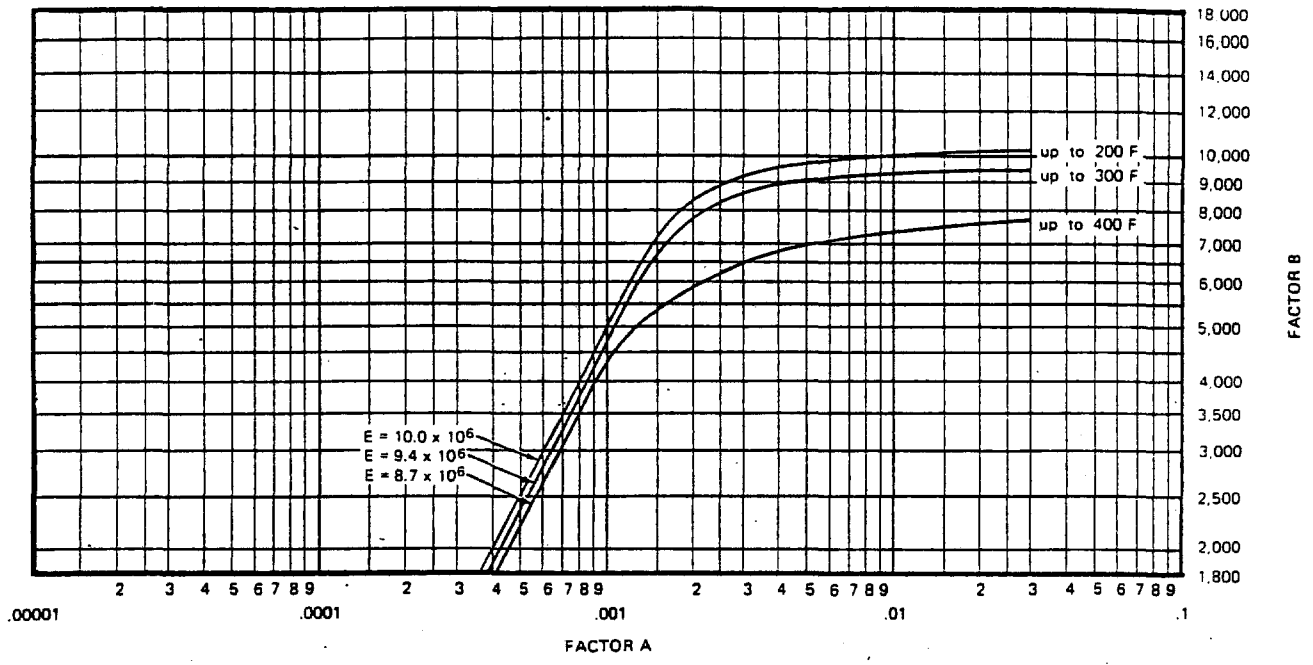

FIG. UNF-28.30 CHART FOR DETERMINING SHELL THICKNESS OF CYLINDRICAL AND SPHERICAL VESSELS UNDER EXTERNAL PRESSURE WHEN CONSTRUCTED OF WELDED ALUMINUM ALLOY 6061-T6 WHEN WELDED WITH: 5356 or 5556 FILLER METAL, ALL THICKNESSES; 4043 OR 5554 FILLER METAL, THICKNESS ≤ 3/8 IN. (NOTE 4)

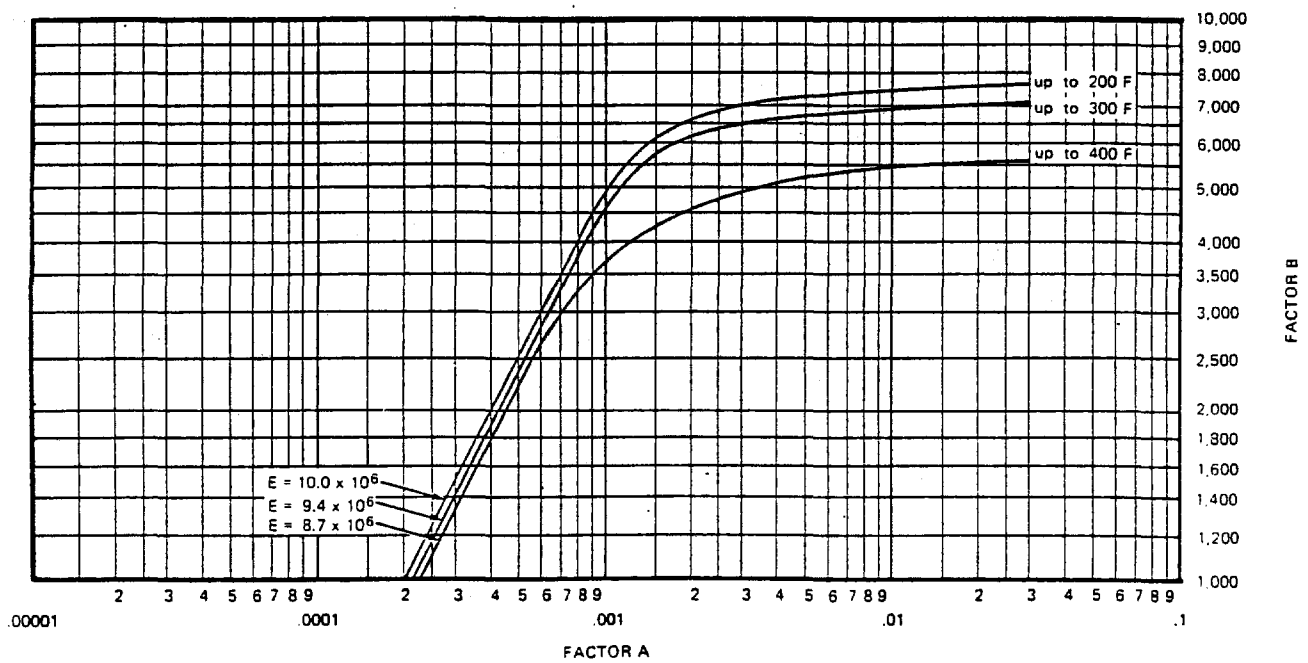

FIG. UNF-28.31 CHART FOR DETERMINING SHELL THICKNESS OF CYLINDRICAL AND SPHERICAL VESSELS UNDER EXTERNAL PRESSURE WHEN CONSTRUCTED OF WELDED ALUMINUM ALLOY 6061-T6 WHEN WELDED WITH 4043 OR 5554 FILLER METAL, THICKNESS > 3/8 IN. (NOTE 4)

Fig. L(4). From ASME Code

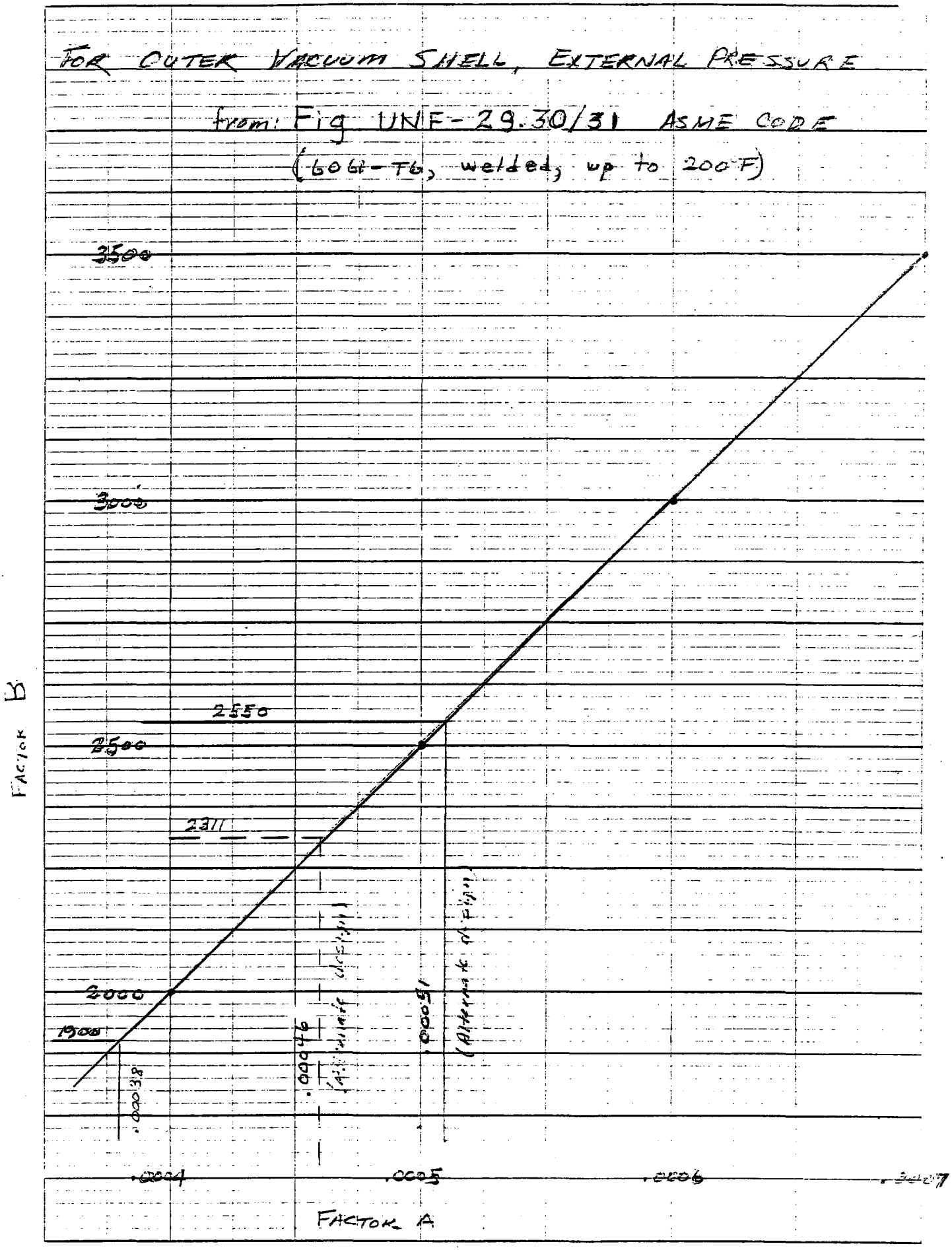

Fig. L(5). From ASME Code

Since the operating pressure differential across the shell is atmospheric pressure, which at the Fermilab elevation of 767 ft (233.8 m) above sea level is 29.2 in Hg or 14.35 psi (98.94 kPa), this shell is in accordance with the Code.

Shell under internal pressure , i.e., vacuum annulus at a pressure greater than one atmosphere. Code Paragraph UG-27.

$$p = \text{pressure rating of shell}$$

$$= \frac{SE\ t}{R + 0.6\ t}$$

where

S = max. allowable stress = 6000 psi (41.4 MPa)

E = weld efficiency = 0.80

t = shell thickness = 0.750 in. (19.0 mm)

R = inner radius of shell = 65.25 in. (1657 mm)

and p = 54.8 psi (0.378 MPa)

Permissible out-of-roundness of shells, Code Paragraph, UG-80,

$$\text{Maximum ID} - \text{Minimum ID} \leq 1\%\ D_{nominal}$$

For the inner shell,

$$\text{Maximum ID} - \text{Minimum ID} \leq 1.12 \text{ in. } (28.4 \text{ mm})$$

and for the outer shell,

$$\text{Maximum ID} - \text{Minimum ID} \leq 1.30 \text{ in. } (33.0 \text{ mm})$$

The maximum radial deviation from circular for $L/D = 1.50$, $D/t = 176$ (the outer shell) is $0.7\ t = 0.394$ in. (10.0 mm) and for $L/D = 1.8$, $D/t = 450$ (the inner shell) is ~ 1.4

t = 0.350 in. (8.9 mm). This deviation is measured with a template which has a chord length of at least 30".

Penetrations into Outer Shell , Code Paragraph UG-37. The penetration reinforcement is considered in section on power chimney.

Annular end flanges , Code Paragraph UG-34

t_{min} = minimum thickness of flat circular head required by Code

$$= d \sqrt{\frac{Cp}{SE}}$$

where

d = span between shells = 10 in. (254 mm)

c = geometry factor = 0.5

p = design pressure = 15 psi (103.4 kPa)

S = maximum permissible stress

= 6000 psi (41.4 MPa)

E = weld efficiency = 0.8

so t_{min} = 0.395 in. (10.0 mm)

and the flange thickness is greatly in excess of this minimum thickness.

Outer Vacuum Shell (Alternate Design)

Summary. The dimensions of shell and stiffening for an alternate design are given in the tables:

Outer Shell Dimensions
Alternate Design With Stiffening Rings

Inner diameter	130.875 in.	(3324 mm)
Outer diameter	132.000 in.	(3353 mm)
Wall thickness	9/16 inch	(0.5625 in.) (14.3 mm)
Length of Shell	188 inch	(4775 mm)
Length between stiffening rings	94 inch	(2388 mm)

Stiffening Ring Dimensions

Inner diameter of ring (Outer diameter of shell)	132.000 inch	(3353 mm)
Outer diameter of ring	148.000 inch	(3759 mm)
Radial thickness of ring	8.000 inch	(203 mm)
Axial length of ring	1.000 inch	(25.4 mm)

Shell Under External Pressure. vacuum annulus evacuated.

Code Paragraph UG-28.

$t = 0.5625$ in. (14.3 mm), $D = OD = 132$ in. (3353 mm)

$L = 94$ in. (2388 mm)

$L/D = 0.75$, $D/t = 235$

From Fig. L(6)

A factor = 0.00051

From Fig. L(4) and L(5), for 6061-T6, welded

B factor = 2550

and

P_a = maximum allowable pressure differential

$$= \frac{4B}{3(D/t)} = 14.5 \text{ psi } (99.97 \text{ kPa})$$

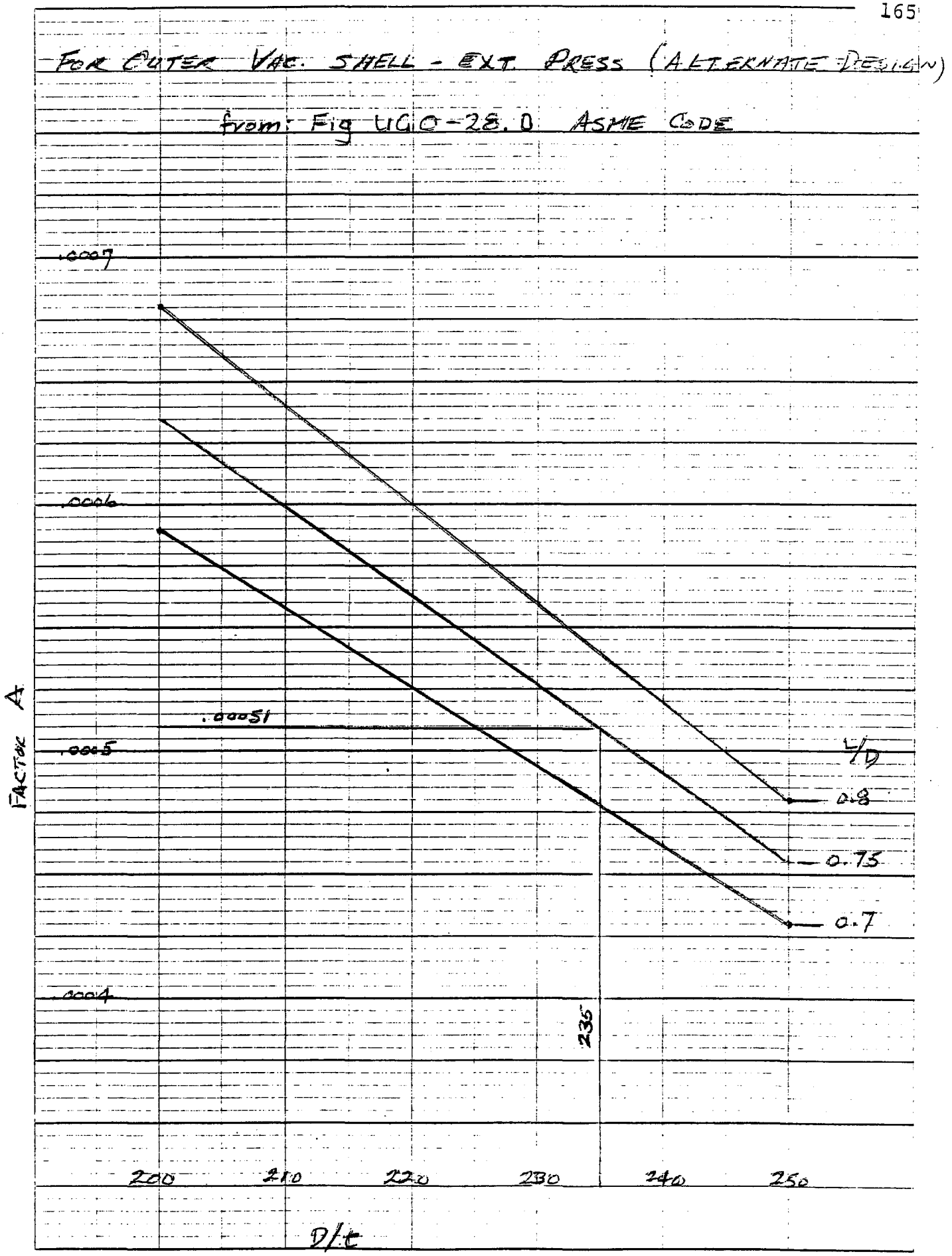

Fig. L(6). From ASME Code

Since the operating pressure of the shell is atmospheric pressure, which at the Fermilab elevation of 767 ft (233.8 m) above sea level is 29.2 in Hg or 14.35 psi (98.94 kPa), this shell is in accordance with the Code.

Shell Under Internal Pressure, i.e., vacuum annulus at a pressure greater than one atmosphere. Code Paragraph UG-27.

p = pressure rating of shell

$$= \frac{SE\ t}{R + 0.6\ t}$$

where

S = max. allowable stress

= 6000 psi (41.4 MPa)

E = weld efficiency = 0.80

t = shell thickness = 0.5625 in. (14.3 mm)

R = inner radius of shell

= 65.4375 in. (1662 mm)

and p = 41 psi (283 kPa)

Outer Shell Stiffening Ring, Code Paragraph UG-29, UG-30.

A_s = cross section area of ring

= 8 in^2 (5156 mm^2)

D = OD of shell = 132 in. (3353 mm)

L = length between rings = 94 in. (2388 mm)

t = shell thickness = 0.5625 in. (14.3 mm)

p = shell pressure = 15 psi (103.4 kPa)

then the B factor = $\dfrac{0.75\ pD}{t + \dfrac{A_s}{L}}$ = 2311

From Fig. L(4), and L(5), for 6061-T6

A factor = 0.00046

then I_s = required moment of inertia of ring about its neutral axis parallel to the shell axis

$$= \frac{D^2\ LA\ (t + \frac{A_s}{L})}{14}$$

$$= 34.57\ in^4\ (1.440 \times 10^3\ cm^4)$$

but

I = actual amount of inertia of ring

$= (1/12)(1)(8)^3 = 42.67\ in^4\ (1.775 \times 10^3\ cm^4)$

so the 1 in. x 8 in. ring satisfies the requirements of the Code.

The Code requires that the ring be attached to the shell by welding on both sides of the ring such that the welds occupy at least one half the shell circumference. The maximum spacing between weld areas is 8 t or 4.5 in. (114.3 mm). or 4.5 in. (114.3 mm).

APPENDIX M: DESIGN OF THE POWER CHIMNEY

Objective

To size the wall thicknesses for the components of the power chimney in accordance with the ASME Pressure Vessel Code ("Code") where applicable. To determine the reinforcement needed at the interface between the chimney and the magnet cryostat.

Vessel Design

Pressure Ratings. The vacuum shell is designed for an external pressure differential of 20 psi (0.14 MPa). The helium shell is designed for an internal pressure differential of 75 psi (0.52 MPa).

Vacuum Shell. Under external pressure code, Section VIII, Div. 1, Paragraph UG-28.

L = length of vessel = 115 (2932 mm)

D_o = diameter of vessel ~ 16" (406 mm)

t = required thickness of the vessel wall

P_a = allowable working pressure

assume $t = 0.188"$ (4.8 mm)

$L/D_o = 7.2$

$D_o/t = 85$

Figure UGO-28.0 then generates a value of the factor $A = 0.00022$. Using Fig. UHA-28.1 for material AISI stainless

steel 304

factor B = 3100

From Section UG-28

P_a = Maximum allowable pressure differential

$$= \frac{4B}{3(D_o/t)}$$

$$= \frac{4(3100)}{3(85)}$$

$$= 48.6 \text{ psi}$$

$$> P_{design} = 20 \text{ psi}$$

So 3/16" is acceptable.

<u>Helium Vessel.</u> Under internal pressure, with

L = length of helium shell = 115"

D = diameter of helium shell = 8"

P = design pressure differential = 75 psi

E = welding efficiency = 0.95

t = required thickness

S = maximum allowable stress value per stress limitations specified in UG-24, Paragraph WU-12 of Code

$S = 10$ Ksi at $100^{o}F$

Part of cryostat might be warm, so use S for calculation.

Following section UG-27 of Code

$$t = \frac{PR}{SE - 0.6P}$$

For $P = 75$ psi

$$t = \frac{75(4)}{(10,000)(0.95)-0.6(75)}$$

$$= 0.032" \ (0.8 \text{ mm})$$

For ease in handling, welding and construction, select

$$t = 1/8" \ (3.2 \text{ mm})$$

<u>Reinforcement Calculations,</u>

We have examined the requirements for the reinforcing rings necessary where the chimney joins the cryostat. We see no difficulty designing these reinforcements in accordance with Paragraph UG-37 of the Code.

APPENDIX N: DESIGN OF THE LOCAL LHE STORAGE DEWAR

Objective

To size the wall thicknesses for the LHe local storage dewar per ASME Pressure Vessel Code where applicable, and calculate reinforcement requirements for openings when required.

Description

1. The helium vessel is supported from a 304 stainless steel neck, which has a LN_2 intercept to reduce the heat leak.
2. It has a LN_2 cooled radiation shield.
3. It has 4 G-10 transport bumpers.
4. It has bellows or flexible hoses to allow contraction of connecting lines to the magnet power chimney.
5. It will have a 1" (25.4 mm) magnet cooldown and dewar fill line, a 4" (102 mm) OD rupture disk and LN_2 inlets.
6. The LN_2 system is forced flow, entering the magnet system through this dewar, cooling the radiation shield, and intercepting heat down the support neck. The LN_2 passes through the annular spaces on the connecting LHe transfer lines and enters the magnet power chimney.

Vessel Calculations

Assumptions

1. Internal pressure differential for the LHe vessel of 75 psi.
2. External pressure differential for the vacuum vessel of 20 psi.
3. Both vessels fabricated of 304 stainless steel.

Vacuum Shell. In accordance with Code, for shell.s under external pressure with

$L = 62"$ (1575 mm)

$D_o = 66"$ (1676 mm)

Let $t = 1/4"$ (6.4 mm)

$L/D_o = 0.84$, $D_o/t = 264$

From Fig. UGO-28.0 of the Code

$A = 0.0003$

From Fig. UCS-28.1 of the Code

$B = 4500$

and

$$p_a = \frac{4B}{3(D_o/t)}$$

$$= \frac{4(4500)}{3(264)}$$

$$= 22.7 \text{ psig } (0.15 \text{ MPa})$$

$$\geq p_{design}$$

So $t = 1/4"$ is satisfactory.

Vacuum Vessel Head. Under internal pressure, using Section UG-33(e) and a Brighton* standard head 66" OD, dish radius R = 62" with

*Brighton Corp., Cincinnati, Ohio, Engineering Data TE-14R.

$t = 1/4"$

$$A_{factor} = \frac{0.125}{(62")(1/4)}$$

$$= 0.005$$

From Fig. UCS-28.1

$B = 7200$

$$P_a = \frac{B}{(R/t)} = \frac{7200 \times 1/4}{62}$$

$= 29.0$ psi, which is acceptable

<u>LHe Vessel Shell.</u> Under internal pressure, with

$L = 46"$

$D = 60"$

$R=D/2 = 30"$

$P = 75$ psia

E = welding efficiency = 0.85

S = allowable stress at 300K per Code

= 18.8 Ksi for stainless steel

σ = yield strength at 300K for 304SS (Appendix B)

= 30 Ksi

$\sigma_{4.2K}$ = yield strength at 4.2K for 304SS

= 60 Ksi

Let $S_{4.2K}$ = allowable stress at 4.2K

$$= \frac{60}{30} \times 18.8 = 37.6 \text{ Ksi}$$

then $t = \dfrac{PR}{S_{4.2K}\ E - 0.6\ P}$

$$= \frac{(75)(30)}{(37600 \times 0.85) - 0.6(75)}$$

$= 0.063"$ (1.6 mm)

Choose $t = 0.125"$ (3.2 mm) for ease of fabrication.

<u>LHe Vessel Dished Head.</u> Under internal pressure, using section UA-4 Appendix I

Let

L = diameter of torispherical head

D_o = diameter of vessel = 60"

P = max. design pressure = 75 psia

E = welding efficiency = 0.85

S = max. allowable working stress at 4.2K for SS304 = 37.6 Ksi

$$M_{factor} = \frac{1}{4}\left(3 + \sqrt{\frac{L}{r}}\right)$$

r = knuckle radius = 3/4"

Using a Brighton 80-10 head,

$L = 62"$

$$M_{factor} = (0.25)(d + \sqrt{0.75})$$

$$= 3.02$$

$$t = \frac{PLM}{2\,SE - 0.2P} = \frac{(75)(43.2)(3.02)}{2(37600)(0.85) - (0.2)(90)}$$

$$= 0.153''$$

Because of space limitation, a Brighton standard head with a small knuckle radius can be used instead of a Brighton 80-10 or an ASME head. The thickness should be 3/16" = 0.1875" (4.8 mm).

Summary of Dimensions

Vacuum Vessel	- Shell:	1/4" (6.4 mm),	304 stainless steel
	- Heads:	1/4" (6.4 mm),	304 stainless steel
LHe Vessel	- Shell:	1/8" (3.2 mm),	304 stainless steel
	- Heads:	3/16" (4.8 mm),	304 stainless steel

Structural Considerations

Cold Mass of Dewar

= mass of dished leads + mass of cylinder

$= [200 \times 2 + \pi(60)(3/16)(42) \times (0.3)]$ lbs

= 845 lbs

Wt. of neck ~ $3/32\ (\pi)(4)(16) \times 0.3$ ~ 6 lbs.

Volume of liquid helium held inside dewar ~ 2200 ℓ

Weight of liquid helium

$$= \frac{2200 \times 125}{453.6} \text{ lbs}$$

$$= 606 \text{ lbs}$$

Max. vacuum load

$$= \frac{\pi (4)^2}{4} \times 15$$

$$= 188 \text{ lbs}$$

Total weight to be supported by neck in tension

$$= (845 + 6 + 606 + 188)$$

$$= 1645 \text{ lbs.}$$

The neck with a cross sectional area of 0.55 in^2, will offer a safety factor of

$$\frac{0.55 \times 30{,}000}{1645} = 10$$

Thermal Considerations:

Let t = wall thickness of neck ~ 0.045"

D = diameter of neck = 4" OD (102 mm)

L = length of neck = 16" (406.4 mm)

A = area of cross section for conduction = 0.55 in^2 (3.55 cm^2)

thermal conductivity integral for SS3304,

$$\int_{4.2K}^{300K} k(t)\,dt = 30.68 \text{ W/cm}$$

$$Q_{conduction} = \frac{A}{L} \int_{4.2K}^{300K} k(t)\,dt$$

$$= \frac{(3.55 \text{ cm}^2)(30.68 \text{ W/cm})}{40.64 \text{ cm}}$$

$$= 2.68 \text{ W}$$

With a nitrogen intercept half-way up the tube, with

$$\int_{4.2K}^{80K} k(t)\,dt \doteq 3.18 \text{ W/cm for stainless steel 304}$$

And $L = 8''$ (203.2 cm)

$$Q_{conduction} = \frac{(3.55)(3.18)}{20.32}$$

$$= 0.56 \text{ W}$$

We can reduce this heat load further by cooling the neck with exiting gas. From p. 241 of Cryogenic Engineering by Scott, with a gas flow rate of 11 mg/s

and for $L/A = \frac{20.32 \text{ cm}}{3.55 \text{ cm}^2} = 5.72 \text{ cm}^{-1}$, the heat delivered to the LHe bath,

$$Q < 10^{-4} \text{ W}$$

The neck design is therefore thermally acceptable.

APPENDIX O: HEAT LOAD INTO THE CRYOGENIC SYSTEMS

HEAT LOAD TO 4K

Axial Supports. The axial supports are intercepted with straps connected to LN_2. If we assume the intercepts are at 80K (see LN_2 shield appendix) then the heat leak for one support to 4K is

$$\dot{Q} = \frac{A_q \int_4^{80} k(t)dt}{L_1}$$

where A_q = cross sectional area of support = 0.71 cm^2

L_1 = length between 80K intercept and 4K = 10 cm

$\int_4^{80} K(t)dt$ = 3.61 W/cm for Inconel 718

thus for one support

$$\dot{Q} = \frac{(3.61)(0.71)}{10} = 0.26 \text{ W}$$

for 12 supports

$$\dot{Q} = 3.1 \text{ W to 4 K}$$

Radial Supports. The radial supports are also intercepted with a strap to the LN_2 shield. Assuming an 80 K intercept

L_1 = 11 cm, and A_r = 0.97 cm^2 then for one support

$$\dot{Q} = \frac{(3.61\ W/cm)(0.97\ cm^2)}{11\ cm} = 0.32\ W$$

for 24 radial supports

$$\dot{Q} = 7.64\ W \text{ to } 4\ K$$

Thermal Radiation (80K → 4.2K) Using 12 layers of NRC-2 and 3M aluminum tape #425 as in the CCM; with a surface heat transfer rate ~ 2 mW/ft^2 (21.5 mW/m^2) the heat leak into the shells is:

$$\dot{Q}_r = 4\ mW/ft^2 \times 1100\ ft^2 = 4.4\ W$$

Using at heat transfer rate of 50 mW/ft^2 for the end flanges gives

$$\dot{Q}_R = 50\ mW/ft^2 \times 40\ ft^2 = 2\ W$$

Heat Leak Into LHe Storage Dewar (Conduction & Radiation)

for the 1650 L dewar we use 1.5%/day

$$\dot{Q} = 1\ W$$

Conductor Joints (15)

0.5 W

Current Leads (6600A) Our experience with the CCM indicates that current leads are not free; to be conservative we include the full heat load. From American Magnetics Inc. data sheet for an optimum current lead

$$\dot{q}_{CL} = 2.8 \frac{L}{h\text{-}kA\text{-}pr} \times 6.6\ kA \times \frac{1\ W}{1.42\ L/h} \simeq 13\ W$$

<u>Heat Leak by Radiation and Conduction Down Power Chimney.</u> Assume 1#W (must be calculated later).

<u>Heat Leak Into Transfer Line</u>

$$\dot{Q} = (0.033\ W/m) \times 40\ m = 1.3\ W$$

(from Energy Doubler estimates ... may be optimistic)

<u>Heat Leak From U-Tubes</u>

~ 5 W

<u>Total Heat Load Into LHe System</u>

Axial supports	3.1 W
Radial supports	7.6 W
Radiation to coil vessel	6.4 W
Storage dewar	1.0 W
Conductor joints	0.5 W
Current leads	13.0 W
Power chimney	1.0 W
Transfer line & U-tubes	6.3 W
Miscellaneous	1.0 W
	39.9 W

Thus

$$\dot{q}_T = 40 \text{ W (56 liters of He/hr)}$$

The local storage dewar can supply the magnet for about 30 hrs of operation.

HEAT LOAD ON THE LN_2 SYSTEM

Axial Supports

The heat load to the 80K support from 300K is

$$\dot{Q} = \frac{A_q \int_{80}^{300} k(t)dt}{L_2}$$

where L_2 = length between 80 K intercept and 300K = 7 cm

$$\int_{80}^{300} k(t)dt = 18.4 \text{ W/cm for Inconel 718}$$

thus for one support

$$Q = \frac{(18.4)(0.71)}{7} = 1.81 \text{ W}$$

for 12 supports

$$\dot{Q} = 22.4 \text{ W to 80 K}$$

Radial Supports

Similarly, for L_2 = 6 cm, the heat load on one 80K support is

$$\dot{Q} = \frac{(18.4)(0.97)}{6} = 2.98 \text{ W}$$

or for 24 radial supports

$$\dot{Q} = 71.4 \text{ watts}$$

<u>LN_2 Shield Supports</u> (see Appendix K)

<u>Inner Shield</u>	117 W
<u>Outer Shield</u>	160 W
<u>Dewar Shield</u>	25 W
<u>Transfer Line Shield</u>	10 W
TOTAL CONDUCTION	312 W

<u>Thermal Radiation (300 → 80K).</u> Using 40 layers of NRC-2, with a heat transfer rate of 50 mW/ft^2 we expect (see Appendix K):

Inner shield	25 W
Outer shield	29 W
Storage dewar	5 W
120' transfer line	10 W
Misc (u-tubes, etc)	21 W
TOTAL RADIATION LOAD	80 W

LN_2 Intercept on Chimney	3 W
LN_2 Intercept on Dewar	8 W
U-tube Conduction	21 W

Total LN_2 Load. A good estimate for the total heat load is 425 W. A more conservative number used for design purposes 500 W which corresponds to 11 liters of LN_2/hr consumption.

APPENDIX P: MAGNET COOLDOWN

Objective of Calculation

To establish a magnet cooldown scenario for the CDF magnet.

Assumptions

With respect to the cold mass,

1. Neglect weight of the chimney
2. Neglect weight of the local storage dewar
3. Include mass of NbTi/Cu in calculating weight of conductor but assume enthalpy of aluminum
4. Neglect the minor contribution from support structures

Calculations

Cold Mass: Weight of the inner and outer helium vessel walls:

$$= [(188.5\text{in})(2\pi \times 58.25 \times 0.625\text{in}^2) + (164.5\text{in})(2\pi \times 60.84 \times 0.3125\ \text{in}^2)$$

$$+ (24\ \text{in})(2\pi \times 60.84 \times 1.0\ \text{in}^2)]\ (0.1\ \text{lb/in}^3)$$

$$= 7200\ \text{lbs}$$

Weight of the end caps of the helium vessel

$$= 2\pi(59.5")(3")(2") \times 2 \times 0.1\ \text{lb/in}^3$$

$$= 450\ \text{lbs}$$

Weight of the aluminum conductor

= 4940 lb (see Appendix A)

Weight of the aluminum banding

$= (0.167 \times 0.55\ in^2)(27000\ ft)(0.1\ lb/in^3)$

= 2973 lbs

Weight of stiffening rings and gas manifold ~ 200 lbs

Weight of the G-10 spacers

$= (1.3 \times 0.05\ in^2)(27000\ ft)(0.067\ lb/in^3)(0.5)$

= 720 lbs

Weight of the G-10 bore tube insulator

$= 2\pi \times 58.5" \times 0.16 \times 188.5" \times 0.067\ lb/in^3$

= 731 lbs

Total cold mass

$\simeq$ 15800 lbs of aluminum & 1450 lbs of G-10

Enthalpy $H_{4.2K}^{300K}$ for aluminum = 170.4 J/g

$= 77.3 \times 10^3$ J/lb

$H_{4.2K}^{300K}$ for G-10 = 91.1 J/g

$= 41.3 \times 10^3$ J/lb

$$H_{4.2K}^{80K} \text{ for aluminum} = 9.37 \text{ J/g}$$

$$= 4.25 \times 10^3 \text{ J/lb}$$

$$H_{4.2K}^{80K} \text{ for G-10} = 10.2 \text{ J/g}$$

$$= 4.63 \times 10^3 \text{ J/lb}$$

Thermal Energy:

Amount of thermal U energy required to be removed in cooling down from 300K to 80K

$$U(300 \rightarrow 80K) = 15800 \text{ lbx}(77.3-4.25) \frac{kJ}{lb} + 1450 \text{ lbsx}(41.3-4.63) \frac{kJ}{lb}$$

$$= 1.20$$

Amount of thermal energy required to be removed in cooling down from 80K to 4.2K:

$$U(80 \rightarrow 4.2K) = 15800 \text{ lbsx}4.25 \frac{kJ}{lb} + 1450 \text{ lbs} \times 4.63 \frac{kJ}{lb}$$

$$= 73.8 \text{ MJ}$$

Cryogen Requirements-LN_2: The heat of vaporization of LN_2,

L_v = 160 kJ/liquid liter (85.86 BTU/lb) ,

where the density of LN_2 is 0.8 kg/liquid liter.

The increase in the enthalpy, h, of nitrogen gas from 77K to 300K at 1 atm,

$$h(77 \rightarrow 300K) = h(300K) - h(77K)$$

$= 314 \text{ kJ/kg} - 81 \text{ kJ/kg}$

$= 233 \text{ kJ/kg}$

$= 186 \text{ kJ/liquid liter}$

If we assume that one-half of the total sensible heat is used in cooling the magnet, the specific energy removal capacity, Q is

$$Q = (160 + \frac{186}{2}) \text{ kJ/liquid liter}$$

$$\sim 250 \text{ kJ/liquid liter}$$

Since $U(300 \rightarrow 80K) = 1.20 \times 10^9$ J

V = volume of LN_2 required, using half the sensible heat

$$= \frac{1.20 \times 10^9 \text{ J}}{2.5 \times 10^5 \text{ J/liquid liter}}$$

$$= 4800 \text{ liquid liters}$$

<u>Cryogen Requirements - LHe:</u> For helium

$L_v = 20.5 \text{ kJ/kg} = 2.56 \text{ kJ/liquid liter}$

$h(4.2 \rightarrow 80K) = h(80K) - h(4.2K)$

$= 430.3 \text{ kJ/kg} - 30.1 \text{ kJ/kg}$ *

$= 400 \text{ kJ/kg} = 50 \text{ kJ/liquid liter}$

*Thermophysical Properties of Helium-4 from 2 to 1500K with Pressures to 1000 Atmospheres, National Bureau of Standards Technical Note NBS-631 (1972).

Assuming that 50% of this sensible heat is used in cooling the magnet

$$Q = (2.56 + \frac{50}{2})\ \text{kJ/liquid liter}$$

$$= 27.5\ \text{kJ/liquid liter}$$

Since $U(80 \rightarrow 4.2K) = 7.38 \times 10^7$ J

V = volume of LHe required, using half the sensible heat

$$= \frac{7.38 \times 10^7\ \text{J}}{2.7 \times 10^4\ \text{J/liquid liter}}$$

$$= 2.7 \times 10^3\ \text{liquid liters}$$

$$= 2700\ \text{liquid liters}$$

<u>Cooldown Rate:</u> The 15' Bubble Chamber has a maximum cool down rate of 20 kW; while the average cooldown rate for the Chicago Cyclotron Magnet (CCM) is ~ 1.5 KW. Because it is a horizontal solenoid, the coil can be cooled quite uniformly and the thermal stress problem no worse than for the CCM.*

Select cooldown rate = 2 KW

Duration required for cooldown from 300 to 80K

$$= \frac{1.2 \times 10^9\ \text{J}}{2 \times 10^3\ \text{kw}}$$

$$= 6\ \text{days}$$

*E.M.W. Leung, "CCM Operations Manual," Fermilab Internal Report, (unpublished).

Cooldown from 80K to 4.2K is almost limited only by how fast we can flow in the LHe since 90% of the thermal contraction (thermal stress) is gone.

It is hence recommended to cooldown

CDF from 300K to 80K in 6 days

80K to 4.2K in 2 days.

If the helium vessel is filled with liquid nitrogen, the subcooling technique we employed in CCM to reduce the nitrogen boiling point can also be used here to reduce the amount of LHe required for cooldown.

If the cooldown from 300 to 80K proceeds via cold helium gas the amount of gas which must be flowed through the systeem can be calculated assuming that half the sensible heat (enthalpy) from 300 → 80K is used.

$$H = \frac{1}{2}\,[h(300K) - h(80K)]$$

$$= \frac{1}{2}\,(1573 - 430)\ kJ/kg \quad *$$

$$= 572\ kJ/kg$$

*Thermophysical Properties of Helium-4 from 2 to 1500K with Pressures to 1000 Atmospheres, National Bureau of Standards Technical Note NBS-631 (1972).

Since,

$$U(300 \rightarrow 80K) = 1.20 \times 10^9 \text{ J}$$

$$M = \text{mass of GHe required} = \frac{1.20 \times 10^9 \text{ J}}{5.72 \times 10^5 \text{ J/kg}}$$

$$= 2100 \text{ kg}$$

With a compressor flow of

$$\dot{m} = 5 \text{ g/s} = 18 \text{ kg/h}$$

the time required

$$t = 2100 \text{ kg}/18 \text{ kg/h} = 116 \text{ h} \sim 5 \text{ days.}$$

APPENDIX Q: VENTING OF HELIUM VESSEL UNDER FAULT CONDITIONS

The superconducting coil and LHe storage dewar have a common vacuum system. Therefore a sudden loss of vacuum or an electrical fault in the coil could cause the He vessel to be overpressurized. To avoid damage to the system and/or protect personnel the LHe vessel must be protected from such overpressure. We have designed the LHe vessel to withstand a pressure of 70 psia. We will use standard relief valves to protect the vessel from overpressure conditions that occur slowly (e.q., eddy current heating due to a rapid superconducting discharge of the coil). In the event of a catastrophic failure (such as rupturing the vacuum vessel) the system is protected by an 8" burst disc on the power chimney and a 4" burst disc on the storage dewar.*

To size these bursts discs and the rest of the relief system, we have used the catastrophic loss of vacuum failure as a guide. We calculate below the expected heat flux into the LHe and the resultant pressure rise in the vessel. Since the

*An alternative suggestion to use Anderson Greenwood constant pressure relief value is being investigated. Under such a scheme, one can ensure supercritical condition inside the magnet upon a quench or sudden loss of vacuum. It is hoped that it can add additional protection to the coil during such a mishap. This scheme is employed on the U-25 MHD magnet built at Argonne National Laboratory.

results of calculations concerning possible catastrophic electrical faults depend very strongly on the type of fault assumed, we believe it is more useful to present the pressure rise in the LHe vessel as a function of the total power deposited in the magnet.

Maximum Heat Flux for Catastrophic Loss of Vacuum Failure

To calculate the maximum heat flux which the LHe system can experience, we consider the sudden and complete loss of the insulating vacuum as a worst case. Assuming that the LHe system is insulated with 12 layers of 500 A NRC-2 between the 78K and 4.2K surfaces, we can arrive at a heat transfer coefficient per unit area due to air condensation following loss of vacuum. From "Technology of Liquid Helium", NBS Monograph 111 (1968), p. 270 we expect this factor to be:

$$\frac{\dot{q}}{A} \simeq 0.47 \text{ W/cm}^2$$

The 4.2K surface area of the helium coil vessel, A_m, is

$$\begin{aligned} A_m &\sim (2\pi)(58 \text{ in})(194 \text{ in})+(2\pi)(61 \text{ in})(194 \text{ in})+2(2\pi)(59.5 \text{ in})(3 \text{ in}) \\ &= 1020 \text{ ft}^2 = 9.5 \times 10^5 \text{ cm}^2 \\ &= 1.47 \times 10^5 \text{ in}^2 \end{aligned}$$

The heat flux, Q_m, into the helium coil vessel following a sudden loss of vacuum is

$$\begin{aligned} \dot{Q}_m &= (9.5 \times 10^5 \text{ cm}^2)(0.47 \text{ W/cm}^2) \\ &= 447 \text{ kW} \end{aligned}$$

The 4.2K surface area of the local helium dewar, A_d, is:

$$A_d = 2\pi(30\text{ in})(60\text{ in}) + 2\pi(30\text{ in})^2$$
$$= 1.70 \times 10^4\text{ in}^2 = 1.09 \times 10^5\text{ cm}^2$$

and the heat flux, Q_d, into the local storage dewar is $Q_d = 51.2$ kW.

The total heat flux into both the helium vessels, Q_T, is:

$$\dot{Q}_T \simeq 500\text{ kW}$$

We note from Appendix D that eddy currents in the cryostat helium vessel cause a heat flux of 20 kW during a $\tau = 45$ s discharge.

We will therefore size the relief system for a heat flux of 600 kW.

Pressure Differential in Chimney Vent

We assume that the pressure rise in the magnet is completely determined by the pressure differential created by the exhaust flow line. The flow pattern is shown schematically in Fig. Q(1). The cryostat pressure vs. power deposition is determined for two cases a) the He gas exits at 5K and b) the exiting gas is heated by condensing air on the exhaust lines. The vacuum insulated helium chimney is 8" in diameter and 10' long. The chimney pipe empties into a box with blunt edges, then enters another 8" pipe, makes a 180° turn and travels another 3 m before exhausting into the outside vent. The outside vent is 12" in diameter and approximately 150' long. The burst disk is before the 180° turn and adds an effective length of 10 m.

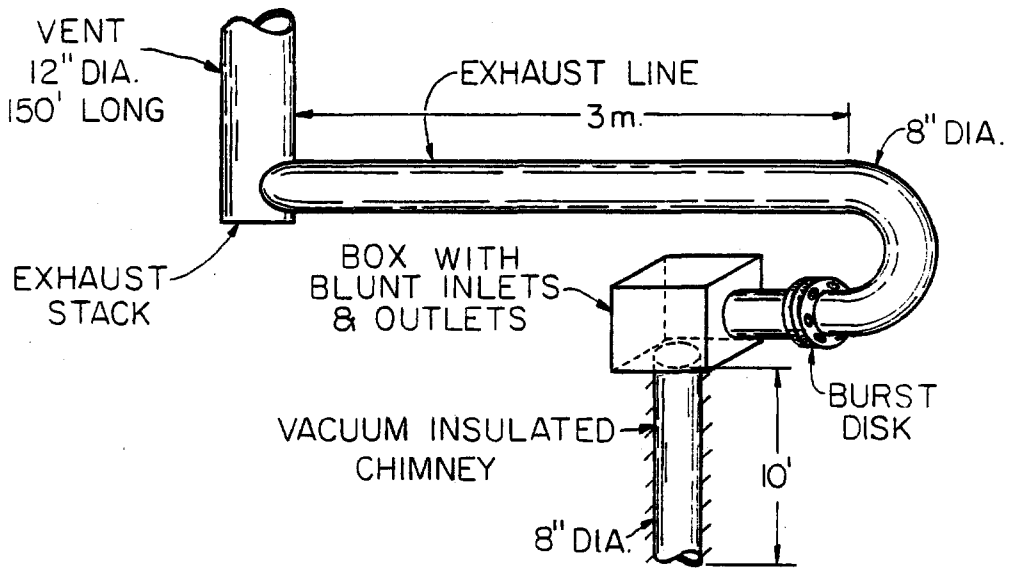

Fig. Q(1). Cryogen flow schematic

CASE a

1) $\frac{\Delta P}{\rho} = h_\ell \qquad h_\ell = f \frac{L}{D} \frac{V^2}{2}$

ρ Gaseous Helium at 1 atm, 5k = 11.94 kg

$L = L_1 + L_2 + L_3 + L_4$

where

L_1 = 3.05 m (length of chimney)

L_2 = 10 m (effective length of an 8" dia. burst disc*)

L_3 = 3 m (length of pipe to exhaust stack)

L_4 = 4.87 m (effective length of two 90° turns with R/D = 2.5)

D = 0.2032 m

Next determine expression for gas velocity as a function of input power in Watts.

Enthalpy change from liquid to gas at 1 atm is

30.13 J/G - 9.711 J/g = 20.42 J/g = 20,420 J/kg.

Mass of helium vaporized is therefore

$$\dot{M}\ \text{kg/sec} = \frac{P\ \text{J/sec}}{20{,}420\ \text{J/kg}}$$

All gas exits through chimney, therefore

$$\dot{M}\ \text{kg/sec} = \frac{P\ \text{watts}}{20{,}420\ \text{J/kg}} = \rho AV = \left(11.94\ \frac{\text{kg}}{\text{m}^3}\right)(\pi)\left(\frac{0.2032}{2}\right)^2 V$$

or

$$V = \frac{P\ (\text{watts})}{7906.7}$$

Then using

*Fike Metal Products Corp., Cat. 7378.

μ = absolute viscosity = 13.9×10^{-7} kg/m-sec

$\rho = 11.94$ kg/m^3

D = 0.2032 M

we can calculate the Reynolds number

$$R_e = \frac{\rho V D}{\mu}$$

From this number we can get the friction factor f* assuming the pipe is smooth. Using this friction factor we can then calculate the pressure differential ΔP_1 created by the chimney, burst disc, 180° bend and the exhaust line using Eq. (1). Values of V, R_e, f, and ΔP_1 are given below for various heat fluxes. In addition we calculate the contributions ΔP_2 of the following minor losses.

P (watts)	V (m/sec)	R_e	f	8" Pipe losses ΔP_1 (pascals)
100	0.0126	2.199×10^4	0.0255	0.00252
1,000	0.1264	2.206×10^5	0.015	0.144
10,000	1.264	2.206×10^6	0.010	9.94
100,000	12.64	2.206×10^7	0.008	795.0
1,000,000	126.4	2.206×10^8	0.007	69,573

*Reference "Intro. Fluid Mechanics", Fox & McDonald, 2nd Ed., pp. 361-363.

Blunt Inlet from Cryostat to Pipe

Minor loss coefficient k = 0.5 (op cit p. 368)

$$h_{em} = (0.5)\frac{V^2}{2}$$

Expansion loss to box on top of chimney

$$\text{Area Ratio} = \frac{A_1}{A_2} = \frac{\pi(4")^2}{\pi(7")^2} = 0.326$$

Expansion Loss Coefficient is 0.5

$$h_{\ell m} = 0.5\,\frac{V^2}{2}$$

Contraction Loss to Exhaust Line From Box on Chimney

Area Ratio = 0.326

Contraction loss Coefficient is 0.35

$$h_{\ell m} = 0.35\,\frac{V^2}{2}$$

Expansion Loss to Exhaust Stack From Exhaust Line

Square edged transition loss coefficient is 1.0

$$h_{\ell m} = 1.0\,\frac{V^2}{2}$$

Total Minor Head Loss

$$\frac{\Delta\rho_2}{\rho} = (0.5 + 0.5 + 0.35 + 1.0)\ \frac{V^2}{2}$$

Power (watts)	Velocity	Minor Losses ΔP_2 (pascals)
100	0.0126	0.000186
1,000	0.1264	0.0188
10,000	1.264	1.88
100,000	12.64	187.7
1,000,000	126.4	18,772.0

The final pressure differential ΔP_3 is created by the 150' long, 12" diameter exhaust stack.

P (watts)	V (m/sec)	R_e	f	12" Pipe Loss ΔP_3
100	0.0056	1.47×10^4	0.028	0.000786
1,000	0.056	1.47×10^5	0.0167	0.0468
10,000	0.56	1.47×10^6	0.011	3.08
100,000	5.6	1.47×10^7	0.008	224.6
1,000,000	56.0	1.47×10^8	0.007	19,649.00

Total Pressure Drop

$$\Delta P = \Delta P_1 + \Delta P_2 + \Delta P_3$$

Power (watts)	ΔP (pascals)	ΔP (psi)
100	0.00349	5.13×10^{-7}
1,000	0.2096	3.08×10^{-5}
10,000	14.9	2.19×10^{-3}
100,000	1,207.3	0.177
1,000,000	1.08×10^{5}	16.0

Case b

The exhausting helium gas is initially at 4.2K. It is warmed by heat flowing into the 150' vent pipe during its exit. The maximum steady state heat flux which condensing air can provide is 0.47 W/cm^2. Using the pipe's surface area, we calculate the maximum heat flux to the gas, and therefore its exit temperature. Calculations are made to show the pressure drop is still small.

The total area of the pipe for heat transfer is

$$\text{Pipe area} = (\pi)(0.2032\ m)(3\ m)+(\pi)(0.3048\ m)(45.7\ m)$$

$$\text{Pipe area} = 45.6\ m^2$$

The total heat flux is

$$\dot{Q} = (4700\ W/m^2)(45.6\ m^2) = 2.14 \times 10^5 \text{ watts}$$

The resulting rise in temperature of the helium gas is summarized in the following table:

Power Dumped in Cryostat (watts)	Helium Mass Flow (kg/sec)	Heating Power (watts)	Exhaust Temperature (K)	Approximate Total Pressure Drop (psi)
10,000	0.489	2.14×10^5	85 K	0.048
100,000	4.89	2.14×10^5	12 K	0.511
1,000,000	48.9	2.14×10^5	5 K	16.0

The exhaust temperature was calculated by using the equation

$$\ddot{Q} = \dot{m}(h_{exit} - h_{4.2K})$$

The results indicate the low flow rate cases do have a higher exit temperature, however, the pressure drops for these cases are still negligible. The approximate total pressure drop is listed in the table.